Control and Power Management of Grid Connected Vented Oscillating Water Column Wave Energy Converter Arrays

By
Gimara Rajapakse
College of Science and Engineering

Submitted in fulfilment of the requirements for the degree of Doctor of Philosophy

University of Tasmania

March 2021

DECLARATION OF ORIGINALITY

This thesis contains no material which has been accepted for a degree or diploma by the University or any other institution, except by way of background information and duly acknowledged in the thesis, and to the best of my knowledge and belief no material previously published or written by another person except where due acknowledgement is made in the text of the thesis, nor does the thesis contain any material that infringes copyright.

Signed:

Mrs. Gimara Rajapakse
Candidate
College of Science and Engineering
University of Tasmania

Date: 11/11/2020

AUTHORITY OF ACCESS

This thesis may be made available for loan and limited copying and communication in accordance with the Copyright Act 1968.

Signed:

Mrs. Gimara Rajapakse
Candidate
College of Science and Engineering
University of Tasmania

Date: 11/11/2020

STATEMENT REGARDING PUBLISHED WORK CONTAINED IN THESIS

The publisher of the paper comprising Chapter 5 holds the copyright for that content, and access to the material should be sought from the respective conference proceedings. The remaining published open access papers comprising Chapters 2, 3, 4, 6 and remaining non published content of the thesis may be made available for loan and limited copying and communication in accordance with the Copyright Act 1968.

Signed:

Mrs. Gimara Rajapakse
Candidate
College of Science and Engineering
University of Tasmania

Date: 11/11/2020

STATEMENT OF CO-AUTHORSHIP

The following people and institutions contributed to the publication of work undertaken as part of this thesis:

Candidate -- Mrs. Gimara Rajapakse, College of Science and Engineering, University of Tasmania

Author 1 -- Dr. Alan Fleming, College of Science and Engineering, University of Tasmania

Author 2 -- Dr. Shantha Jayasinghe, College of Science and Engineering, University of Tasmania

Author 3 -- Professor Michael Negnevitsky, College of Science and Engineering, University of Tasmania

Author 4 -- Professor Farhad Shahnia, School of Engineering and Information Technology, Murdoch University

Contribution of work by co-authors for each paper:

PAPER 1: Located in Chapter 2

G. Rajapakse, S. G. Jayasinghe, A. Fleming, and F. Shahnia, "Model Predictive Control-based Power take-off Control of an Oscillating Water Column Wave Energy Conversion System," In Proceedings of the 2017 International Conference on Substantial Energy Engineering (ICSEE 2017), Perth, Australia, 12–14 June 2017, *IOP Conf. Series: Earth and Environmental Science 73 (2017) 012010*, 2017.

Author contributions:
Conceived and designed the simulation study: Candidate, Author 1, Author 2
Performed the simulation study: Candidate, Author 2
Analysed the data: Candidate, Author 2
refinement and presentation: Author 1, Author 2, Author 4
Wrote the manuscript: Candidate.

PAPER 2: Located in Chapter 3

G. Rajapakse, S. G. Jayasinghe, A. Fleming, and Michael Negnevitsky, "A Model Predictive Control-Based Power Converter System for Oscillating Water Column Wave Energy Converters," *Energies 2017*, vol. 10, no. 10, 2017.

Author contributions:
Conceived and designed the simulation study: Candidate, Author 1, Author 2
Performed the simulation study: Candidate, Author 2
Analysed the data: Candidate, Author 2
Contributed reagents/materials/analysis tools/ refinement: Author 1, Author 2, Author 3
Wrote the manuscript: Candidate.

PAPER 3: Located in Chapter 4

G. Rajapakse, S. G. Jayasinghe, A. Fleming, and Michael Negnevitsky, "Grid Integration and Power Smoothing of an Oscillating Water Column Wave Energy Converter," *Energies 2018*, vol. 11, no. 07, 2018.

Author contributions:
Conceived and designed the simulation study: Candidate, Author 1, Author 2
Performed the simulation study: Candidate, Author 2
Analysed the data: Candidate, Author 2
Contributed reagents/materials/analysis tools/ refinement: Author 1, Author 2, Author 3
Wrote the manuscript: Candidate.

PAPER 4: Located in Chapter 5

G. Rajapakse, S. G. Jayasinghe, and A. Fleming, "Power Management of an Oscillating Water Column Wave Energy Converter with Battery/Supercapacitor Hybrid Energy Storage," In conference proceedings of the 2018 International Conference on Power and Energy System (ICPES2018), Colombo, Sri Lanka, 21–22 December 2018, *IEEE Xplore,* 2019.

Author contributions:

Conceived and designed the simulation study: Candidate, Author 1, Author 2
Performed the simulation study: Candidate, Author 2
Analysed the data: Candidate, Author 2
Contributed reagents/materials/analysis tools/ refinement: Author 1, Author 2
Wrote the manuscript: Candidate.

PAPER 5: Located in Chapter 6

G. Rajapakse, S. G. Jayasinghe, and A. Fleming, " Power Smoothing and Energy Storage Sizing of Vented Oscillating Water Column Wave Energy Converter Arrays," *Energies 2020,* vol. 13, 1278, 2020.

Author contributions:
Conceived and designed the simulation study: Candidate, Author 1, Author 2
Performed the simulation study: Candidate, Author 2
Analysed the data: Candidate, Author 2
Contributed reagents/materials/analysis tools/ refinement: Author 1, Author 2
Wrote the manuscript: Candidate.

We, the undersigned, endorse the above stated contribution of work undertaken for each of the published (or submitted) peer-reviewed manuscripts contributing to this thesis:
Signed:

Signed:			
	Mrs. Gimara Rajapakse Candidate Candidate College of Science and Engineering University of Tasmania	Dr. Alan Fleming Primary Supervisor College of Science and Engineering University of Tasmania	Dr. Vikram Garaniya Director National Centre for Maritime Engineering and Hydrodynamics Australian Maritime College
Date:	11/11/2020	11/11/2020	11/11/2020

ACKNOWLEDGEMENTS

The author sincerely acknowledges the following people without whom this work will not have been accomplished.

First and foremost, I would like to express my sincere gratitude to my supervisory team of Dr. Alan Fleming and Dr. Shantha Jayasinghe. They provided their guidance and continuous support throughout this journey to all aspect of this work by providing facilities and hands-on support to carryout experiments. Their insightful comments on my research and writing brought greater clarity to the research articles and this thesis. Also, I extend my gratitude to Prof. Michael Negnevitsky and Prof. Farhad Shahnia, for their contributions during the research publication process.

I thank the graduate research coordinator, Dr. Roberto Ojeda Rabanal, for arranging the confirmation of candidature and yearly reviews and for giving pertinent advice over the years. Also, I thank Confirmation of Candidature (CoC) panel members, Assoc. Prof. Irene Penesis and Dr. Hung Nguyen, for providing valuable feedback on the COC report and presentation, Toby Davis and Michael Underhill for providing technical support during hardware experiments. Furthermore, I thank all my friends and colleagues at AMC/UTAS who supported me in numerous ways over the course of the candidature.

Last but not least, I thank my family. My parents Gemunu Rajapakse and Dulani Rajapakse; for the sacrifices they have made throughout my life. My husband Rumesh for his unwavering love and support in pursuing my dreams. And my children Raneili and Thiraj for their unconditional love and distractions. To them, I dedicate this thesis.

"It can scarcely be denied that the supreme goal of all theory is to make the irreducible basic elements as simple and as few as possible without having to surrender the adequate representation of a single datum of experience"

Albert Einstein (14 March 1879 – 18 April 1955)

ABSTRACT

Wave energy is a vast, sustainable, and low environmental impact renewable energy source with a high degree of predictability and availability at large scale. Over the last six decades, numerous studies have been conducted, and various technologies have been developed to convert wave energy into electricity. Nevertheless, Wave Energy Conversion (WEC) is still not a widespread technology, compared to other dominant renewable energy technologies such as wind and solar. One of the contributing factors for this is the large and periodic fluctuations present in the extracted power in WEC systems. Even though intermittencies are present in the extracted power in the wind and solar generation systems, the level of fluctuations present in those systems are much smaller compared to that in wave energy. Therefore, the direct connection of a WEC system to a power grid without any power conditioning could lead to instabilities.

The use of energy storage is a promising solution to absorb fluctuation and thereby ensure smooth power delivery to the grid. Battery energy storage is the most common solution recommended for similar issues in the wind and solar energy systems. Nevertheless, due to the short-term and periodic (10 -15 seconds) nature of the power pulses present in wave energy, a combination of battery and supercapacitor is recommended as the most suitable energy storage solution for WEC systems. Most studies reported in the literature on WEC systems with battery-supercapacitor hybrid energy storage have considered only a single WEC system. The effects of spatial and temporal averaging of extracted power in wave energy converter arrays on the sizing of energy storage systems have not been explored so far. Therefore, this study has attempted to fill this knowledge gap using vented oscillating water column (VOWC) wave energy converter arrays. VOWC is a novel WEC technology developed at the Australian Maritime College in collaboration with the Wave Swell Energy company in Australia. This technology produces energy only during the inhale stage resulting in large discrete power pulses. These characteristics of VOWC make control and power smoothing even more challenging compared to conventional bi-directional WEC technologies such as Wells turbines. As solutions, novel control and power management strategies have been developed to suit the characteristics of the VOWC. The efficacy of the developed control and power management solutions are validated through simulations carried out on the MATLAB/Simulink digital simulation

platform. The results verify the efficacy of the proposed control strategy in tracking the setpoints efficiently with minimal overshoots and oscillations. Furthermore, the findings confirm that the proposed PMS can reduce the mismatch between supply and demand, while maintaining smooth delivery of power to the grid in single and array configurations of VOWC WECs. Moreover, further findings reveal that the required ESS capacity drops when WEC systems are placed correctly in array configurations.

TABLE OF CONTENTS

LIST OF FIGURES

LIST OF TABLES

NOMENCLATURE

$\square^*$	reference
$\square^P$	predicted
ΔP	pressure difference
Ψ_{pm}	permanent magnet flux
Ψ_{sd}	d axes permanent magnet flux
Ψ_{sq}	q axes permanent magnet flux
ω_m	mechanical angular speed of PMSG
ωt	actual angle
A	battery exponential voltage
B	battery exponential capacity
C_{dc}	dc-link capacitor
C_{sc0}	initial capacitance of the supercapacitor
C_t	total equivalent capacitance
D	duty cycle
E_{sc}	supercapacitor energy
f_f	frequency
g_{boost}	cost function for boost operation
g_{buck}	cost function for buck operation
g_{rec}	cost function - rectifier
g_{inv}	cost function - inverter
I_{bat}	battery current
i_L / i_{ESS}	inductor current
i_s	source current
$\vec{i_s}$	source current vector
$i_{s\alpha}$	real axes source current
i_{sb}	imaginary axes source current
i_{sd}	d axes source current
i_{sq}	q axes source current
J	inertia of the air-turbine generator system
J_e	inertia of the generator
J_t	inertia of the turbine
k	sampling instance
K_b	battery polarization resistance
$k_{\square}$	scaling factor
L_d	d axes inductance of the PMSG
L_q	q axes inductance of the PMSG

n_g	gear ratio
n_p	number of pole pairs of PMSG
P_{base}	initial grid power reference
P_g	active power - grid
P_s	active power - source
$P_{sc\%}$	percentage of power difference (P_s-P_g)
Q	battery capacity
Q_0	initial charge of the supercapacitor
Q_g	reactive power - grid
Q_s	reactive power - source
R_s	stator resistance
R_{sc}	Supercapacitor inner resistance
$\vec{S}$	switching function vector
$\overrightarrow{S_a}, \overrightarrow{S_b}, \overrightarrow{S_c}$	three phase switching function vector
SOC_{bat}	SOC of the battery
SOC_{sc}	SOC of the supercapacitor
t	time
T_e	electromagnetic torque of the PMSG
T_m	mechanical torque of the air-turbine
T_s	sampling time
v_0	initial voltage across supercapacitor
$\overrightarrow{v_{AFE}}$	AFE rectifier voltage vector
$V_{b\ ch}$	battery charging voltage
$V_{b\ dc}$	battery discharging voltage
v_{dc}	dc-link voltage
v_{ESS}	Voltage across ESS
$\overrightarrow{v_s}$	source voltage vector
$v_{s\alpha}$	real axes source voltage
v_{sb}	imaginary axes source voltage
v_{sc}	supercapacitor voltage
v_{sd}	d axes source voltage
v_{sq}	q axes source voltage
$\overrightarrow{v_{VSI}}$	inverter voltage vector

ABBREVIATIONS

2L-VSI	Two Level Voltage Source Inverter
AC	Alternating Current
AFE	Active Front End
AMC	Australian Maritime College
BESS	Battery Energy Storage System
DC	Direct Current
DOD	Depth of Discharge
FCS	Finite Control Set
ESS	Energy Storage System
HESS	Hybrid Energy Storage System
MGSES	Multi-Generator Systems with Energy Storage
MPC	Model Predictive Control
MPPT	Maximum Power Point Tracking
PI	Proportional- Integral
PID	Proportional-Integral-Derivative
PMS	Power Management System
PMSG	Permanent Magnet Synchronous Generator
PPMS	Predictive Power Management System
PWM	Pulse Width Modulation
OWC	Oscillating Water Column
OWCDBW	Oscillating Water Column Detached Breakwater
SCES	Supercapacitor Energy Storage
SOC	State of Charge
THD	Total Harmonic Distortion
TSO	Transmission System Operators
VOWC	Vented Oscillating Water Column
VOWCDBW	Vented Oscillating Water Column Detached Breakwater
WEC	Wave Energy Converter
WSE	Wave Swell Energy

1
INTRODUCTION

1.1 Introduction

Oceans cover more than 70% of the earth offer a vast amount of renewable energy and have potential to make significant contributions towards renewable energy targets worldwide. Having recognized this potential, many nations have invested in research and development related to ocean energy. Out of the many forms, wave energy is the easily accessible and widely available form of ocean energy. Currently, there are many technologies developed to extract power from waves (Carson et al., 2010), (Carson et al., 2014).

Over the past 30-40 years, numerous offshore demonstrations on different types of WECs have taken place around the globe. Commonly used WECs in those studies can be categorised into three main groups based on variations around the working principle, namely: Oscillating bodies (Attenuator), Oscillating Water Column (OWC) and overtopping device (Carson et al., 2014), (Hong et al., 2014). The reproduced Figure 1.1, from (Falcao, 2010), illustrates the various classifications of WECs. The OWC wave energy converters offer the advantage of having all moving parts above the water level which makes it easy to install and maintain, reducing the overall cost.

Australian Wave Swell Energy Ltd. (WSE) has developed a new OWC technology which is an efficient and simple design to rectify air flow compared to many other concepts (Wave Swell Energy, 2017). The unidirectional air-turbine generates power only during the inhale stage, resulting in significantly large discrete pulses in the generated electrical power. This could lead to instabilities, especially in weak power grids, if the extracted power is delivered directly into the grid. Maintaining the turbine speed within the optimal range under changing wave conditions is another control challenge.

The conventional approach to achieve the above control objectives is to use pulse width modulation (PWM) techniques that linearize the power converters, while power converters and drive systems are controlled in cascade multi-loop systems with proportional integral (PI) regulators (Guerrero et al., 2011, Mehrasa et al., 2014, Mehrasa et al., 2015, Mehrasa et al., 2016). New strategies proposed in (Mehrasa et al., 2015), (Mehrasa et al., 2016), etc. improve

the performance of this controller in the presence of nonlinear loads. Nevertheless, in general, linear control methods with a modulation applied to nonlinear systems lead to uneven performance throughout the dynamic range (Rodriguez and Cort´es, 2012). The implication of this method has been identified as very challenging to modern power converters such as multi-level, matrix converters, etc. (Rodriguez and Cort´es, 2012). Moreover, system constraints and technical requirements cannot be directly included in the conventional control design. To overcome these issues, this study takes a novel approach to apply the model predictive control (MPC) to the power converter controllers.

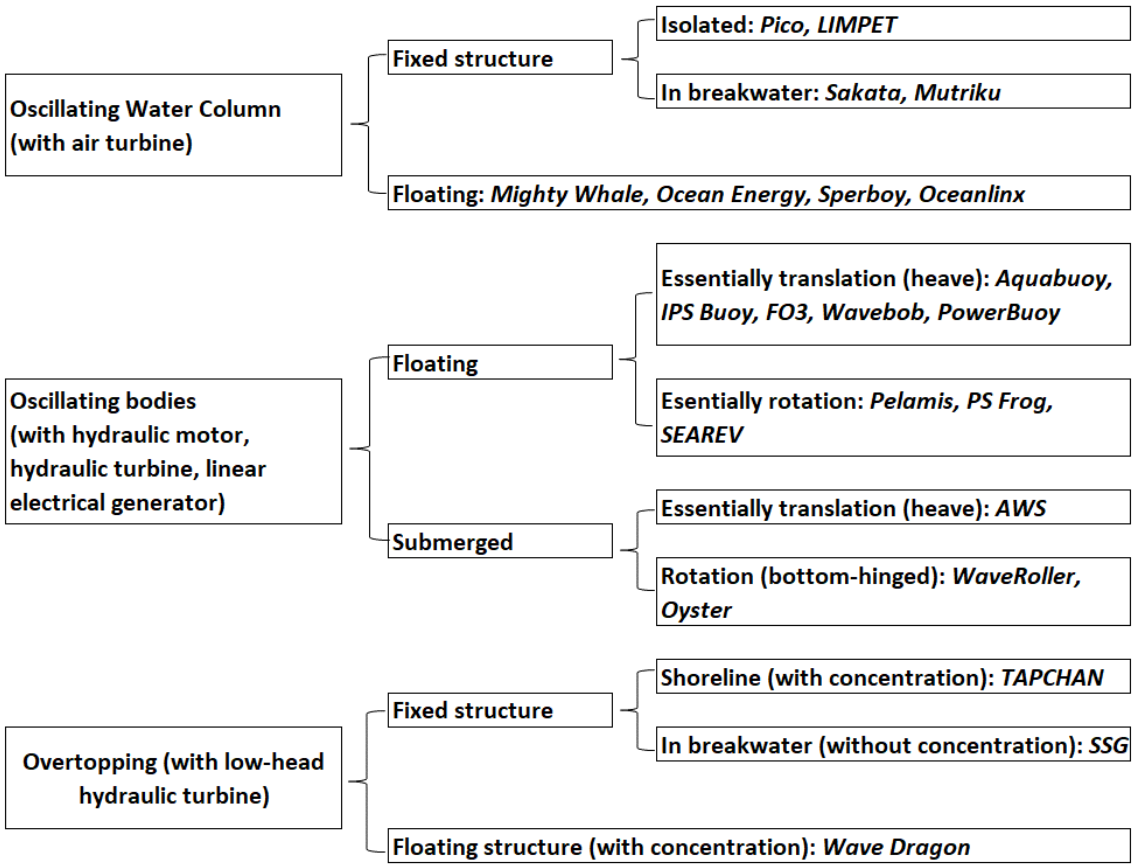

Figure 1. 1: Classification of wave energy converters (Falcao, 2010)

With the advancement of microprocessor technologies, model predictive control (MPC) has become popular as a simple and fast digital control technology for power electronic converter systems (Sultana et al., 2017). Moreover, the absence of tuning makes MPC more attractive over conventional PI controllers. In the field of renewable energy, finite control set (FCS) MPC has recently been proposed for variable speed wind energy conversion systems (Abdelrahem et al., 2016) with a model reference adaptive system observer to estimate the generator rotor speed

and position. Nevertheless, the applicability of FCS-MPC in OWC WECs has not been tested so far. The objective of the MPC proposed in (Abdelrahem et al., 2016) is to extract maximum power from the wind by controlling the generator speed according to the actual wind speed. Similar variable speed operations have been proposed for WECs to track the maximum power point (MPPT) using different control strategies other than MPC (Delmonte et al., 2016, Lekube et al., 2017). Nevertheless, the choice of variable or fixed speed operation of the turbine depends on its design and operating requirements. Therefore, the objective of the associated power take-off (PTO) controller should also vary accordingly. The particular turbine considered in this study targets to operate at a pre-designed operating speed range to achieve the optimum turbine efficiency regardless of the change in differential air pressures (Wave Swell Energy, 2017). Therefore, the objective of the proposed controller is to maintain the turbine speed within the optimum range under varying wave conditions.

Another important aspect of this research is the power management of multi-generator systems with energy storage (MGSES) to improve the system dynamics of a WEC system and deliver quality and constant amount of power to the grid regardless of the sea conditions. MGSES comprises of spatially distributed WEC systems with energy storage devices, aiming to compensate for power fluctuations. When there is more than one OWC system in question, there are array effects that affect the energy production of the turbine depending on their location within the array. It could result in magnifying or reducing the fluctuations in the generated power. Therefore, this study applies a common PMS to several arrays of OWC to optimize the quality of overall power output by integrating multi-devices to the common point of coupling of the grid.

The inclusion of energy storage to absorb power fluctuations in renewable energy systems is well explored and there are numerous publications proposing various topologies and control techniques (Hannan et al., 2017). In fact, the application of battery energy storage in WEC systems is also not new (Tedeschi et al., 2011, Ceballos et al., 2015, Vilathgamuwa et al., 2015). The novelty of this study comes in the development of MPC for the whole converter system, including the energy storage, and implementation of the power management and control of the MGSES with constraints.

1.2 Research Question

Thus, the specific research questions answered in this project are:

1) How to develop model predictive controllers for power converters to maintain the turbine speed within optimum speed range and to feed power to the grid while meeting grid code requirements?
2) What should be the power management strategy for a single generator system and multi-generator systems with energy storage?

1.3 Research Objectives

The research objectives to be achieved by answering the above research questions include:

1) Development of model predictive controllers for a grid interfacing converter system that meets relevant criterion in grid codes;
2) Propose power management system for single generator and multi-generator wave energy conversion systems with energy storage;

1.4 Research Methodology

To answer the research questions and to fulfil the research objectives while establishing the accuracy of the findings, this study was carried out in six phases.

Phase 1: Identify the grid codes relevant to the WEC system (discussed in Chapter 3)

Phase 2: Identify the system characteristics of the OWC air turbine-generator system (discussed in Chapters 2 and 3)

Phase 3: Software model of the Electrical power conversion system of the OWC WEC in MATLAB/Simulink (discussed in Chapters 2 and 3)

Phase 4: Develop grid code compliant MPC for interfacing power converters (discussed in Chapters 2 and 3)

Phase 5: Develop a power management strategy for grid-connected OWC air turbine generator system with energy storage (discussed in Chapter 4)

Phase 6: Confirm the accuracy of the developed power management strategy for grid-connected multi OWC air turbine generator systems with energy storage (discussed in Chapter 6)

1.5 Novel Aspects

The distinctive OWC air-turbine considered in this study has a unique characteristic and targets to operate at a pre-designed operating speed range to maintain the optimum turbine efficiency, regardless of the changes in differential air pressure. Therefore, it requires a novel control strategy which is customised to match with the characteristics. MPC has been chosen as the control approach as it response fast and does not require tuning. The presence of large periodic power pulses is unique to the vented OWC WEC systems compared to wind or tidal energy systems and thus, it requires special attention in developing suitable MPC strategy. Moreover, the development of a power management system for a single turbine-generator system and a multi-generator system (OWC array) with energy storage is another novel area that has been explored in this research.

1.6 Thesis Structure

This thesis comprises a collation of published and submitted refereed journal and refereed conference papers presented in chapters 2 to 6. The publishing details are clearly indicated at the beginning of each chapter. As the chapters consist of standalone publications, some content has been repeated although efforts have been taken to reduce such repetitions. This is especially true with regard to the introductions, modelling of the OWC turbine-generator grid integration system and the MATLAB/Simulink simulation setup. This thesis uses actual SI units and units derived from SI units. Chapter 2 to Chapter 6 are the most recent versions provided for publication. The structure of the thesis is as follows.

***Chapter 1*:** The introductory chapter, which provides the relevant background and problem definition leading to the research question, objectives, methodology of the project, and the novel contributions including an introduction to FCS-MPC and a brief description of the PMS proposed in this thesis.

***Chapter 2*:** Provides details on the power take-off control of a single stage unidirectional OWC air-turbine generator system and proposes a model predictive control-based speed controller for the turbine-generator assembly connected to a DC-grid.

***Chapter 3*:** Enhances Chapter 2 and develops model predictive controllers for a back-to-back converter system connected to an AC-grid aiming to maintain the turbine speed within its optimum range. Direct connection of a battery bank into the dc-link of the back-to-back power

converter system is used to smooth the power delivered to the grid. MPC controllers are designed to control the battery current in charging and discharging states.

***Chapter 4*:** Applies FCS-MPC for the power processing of an OWC system with a supercapacitor energy storage integrated into the dc-link of a back-to-back power converter through a bidirectional dc-dc converter to achieve smooth power delivery to an AC-grid.

***Chapter 5*:** Develops a PMS for a grid connected OWC with a battery/supercapacitor hybrid energy storage system. The power commitment to the grid is adjusted based on the deviation of battery SOC from the mid-point and its rate of change.

***Chapter 6*:** Expands the PMS developed in Chapter 5 on grid integrated single OWC to grid integrated array of OWC devices. The PMS is to optimize the overall efficiency of the array with no/minimal changes to the control system/s of the electrical power converters.

***Conclusion*:** The concluding chapter provides main conclusions, bringing together the findings of all the chapters. It also provides recommendations for future work.

***Appendices*:**

Appendix I: Describes the MATLAB/Simulink models used in Chapters 2, 3, 4, 5 and 6 to obtain simulation results aiming to confirm the validity of proposed control algorithms.

Appendix II: Provides parameters and FCS-MPC algorithms used for modelling and simulation of the OWC wave energy conversion with ESS and Power converters in MATLAB/Simulink.

2

MODEL PREDICTIVE CONTROL-BASED POWER TAKE-OFF CONTROL OF AN OSCILLATING WATER COLUMN WAVE ENERGY CONVERSION SYSTEM

This chapter was originally presented as a paper at the International Conference on Sustainable Energy Engineering (ICSEE 2017) at Perth, Australia on 12-14/06/2017 and published in the '*Journal of Earth and Environmental Science* (ISSN: 1755-1315)'. The citation for the research article is:

G. Rajapakse, S. G. Jayasinghe, A. Fleming, and F. Shahnia, "Model Predictive Control-based Power take-off Control of an Oscillating Water Column Wave Energy Conversion System," In Proceedings of the 2017 International Conference on Substantial Energy Engineering (ICSEE 2017), Perth, Australia, 12–14 June 2017, *IOP Conf. Series: Earth and Environmental Science 73 (2017) 012010*, 2017.

Abstract

Australia's extended coastline asserts abundance of wave and tidal power. The predictability of these energy sources and their proximity to cities and towns make them more desirable. Several tidal current turbine and ocean wave energy conversion projects have already been planned in the coastline of southern Australia. Some of these projects use air-turbine technology with air driven turbines to harvest the energy from an oscillating water column. This study focuses on the power take-off control of a single stage unidirectional oscillating water column air turbine generator system and proposes a model predictive control-based speed controller for the turbine-generator assembly. The proposed method is verified with simulation results that show the efficacy of the controller in extracting power from the turbine while maintaining the speed at the desired level.

2.1 Introduction

The climate change, pollution, scarcity and various other negative aspects of conventional fossil fuels advocate the growth of clean energy technologies such as solar, wind, ocean, bio-fuel, etc. Out of these, ocean energy has drawn much attention in recent years as one of the most promising renewable energy resources with high energy density and low cost (Carson et al., 2010)-(Hughes and Heap, 2009). More than 70% of the earth is covered by oceans that have a vast amount of renewable energy, stored as thermal, potential and kinetic energies. These ocean energies also consist of unique characteristics; vast, sustainable and almost zero environmental impact (Carson et al., 2010, Carson et al., 2014). It has been proven that tidal current is very predictable and the tidal charts are accurate for years to come and the wave energy can be predicted several days in advance (Hannon et al., 2016). These characteristics permit both of these energies to be used for supplying the base power demand mixed with other appropriate generation and/or storage systems (Carson et al., 2010). According to (Hannon et al., 2016), the ocean energy available in less than 80m depth from ocean connected coastlines is almost 5 times the world consumption which is approximately 15PWh per annum. However, at present, ocean energy supplies only 0.02% of the world energy consumption.

One challenge for wave and tidal energy is to generate electricity at a constant level. On average, tidal current speed drops to zero twice in every 12.4 hours (time varies according to the location) and the speed varies depending on the proximity of the moon and sun relative to earth, despite its independency from prevailing weather conditions (Carson et al., 2010, Benelghali et al., 2007). In contrast, wave swell depends on the wind speed, duration of wind, as well as the depth and topography of the sea floor (Carson et al., 2010). The length and strength of waves vary from one to the next, leading to time varying generation of power from the waves. Therefore, the inherent variability of marine kinetic energy requires some form of energy storage for smooth generation of electrical power.

Another main challenge is economic feasibility as the high production cost at present challenges the large-scale commercial applications. At this stage, in Australia, wave and tidal energies are at the pre-commercial state and their outlook depends on research, development, and demonstration (Carson et al., 2010, Hughes and Heap, 2009, Carson et al., 2014). According to (Carson et al., 2014), there are several ocean energy demonstration plants operating or under construction in the coastline of Southern Australia. Most of these projects are based on wave

energy conversion systems (WECs). The companies involved in these projects believe their nearshore shallow water ocean renewable energy projects could be cost competitive with other onshore renewables and fossil fuels in coming years (Hannon et al., 2016, Oceanlinx, 2017, Wave Swell Energy, 2017).

The WECs engaged in different projects employ different conversion principles. These systems could be categorized into three main groups; oscillating bodies (Attenuator), oscillating water column (OWC) and overtopping device (Carson et al., 2014, Hong et al., 2014). The principle of oscillating bodies converts the kinetic energy of the wave into mechanical energy by absorbing the wave energy to induce an alternating motion on a structure immersed in the ocean. This motion operates the hydraulic cylinder to extend and retract. The high-pressure oil produced as a result of this motion drives a generator. The project in Garden Island by Carnegie Wave Energy employs CETO wave converter; fully submerged buoy with CETO pod, comes under Oscillating bodies. The project by BioPower Systems in Port Fairy uses similar principle with BioWAVE concept and O-Drive module (Carson et al., 2014). The OWC principle is based on the oscillating motion of the water that is used to compress air inside a chamber and direct the air into an air turbine. The turbine is then coupled with a generator (Hannon et al., 2016, Oceanlinx, 2017 - Hong et al., 2014). The King Island project by Wave Swell energy uses the OWC principle. The overtopping principle is based on the use of a hydraulic head between a reservoir and the mean water level to drive turbines. This technology is not yet used in any project in Australia.

Irregular natural behavior of ocean waves creates irregular air flow inside the OWC chamber which is then passed onto the turbine. Consequently, the speed of the generator coupled to the turbine also varies, resulting in variable voltage and/or frequency at the output. Therefore, to interface this variable output of the generator into the ac grid, a rectifier-inverter combination is required. If the grid is dc only, a rectifier is required to extracts power from the turbine-generator assembly and feed into the grid. Therefore, irrespective of the grid type, speed control of the turbine is carried out by a rectifier, either to one or different speed levels to maintain the turbine speed at an optimum level to uphold maximum efficiency of the turbine.

This paper focuses on the speed control of the turbine through the control of the rectifier while feeding power to a dc grid. The traditional approach in generator speed control is to employ proportional-integral (PI) controllers which require careful tuning to achieve desired

performance. This paper takes a novel approach to use the model predictive control (MPC). The particular turbine considered in this study has a unidirectional airflow through it and produces power only during the air intake. Moreover, it does not essentially require variable speed operation and thus, a constant speed of 650rpm is set as the control objective while extracting power from the waves.

As the focus of this paper is on the electrical power take off from the turbine, modeling and analysis of airflow inside the OWC and torque generation of the turbine are not discussed. Instead, a typical torque profile produced by the turbine at 650rpm is considered as the mechanical input to the generator. As the torque varies, the input power to the generator varies and thus, the rectifier has to change its power extraction while maintaining the speed. This control objective is applied to the proposed controller which predicts the speed in the next sampling interval for all the switching combinations of the rectifier and selects the combination with the lowest speed error. As this particular controller is based on the system model and does not require tuning, it is fast and simple to use.

The rest of the paper is organized as follows. Section 2 explains the operation of the OWC air turbine. Section 3 presents the mathematical model of the generator assembly followed by the MPC of the rectifier in Section 4. Section 5 presents the simulations results to verify the operation of the proposed MPC strategy. Conclusions drawn from this study are presented in the Section 6.

2.2 OWC air turbine system

The majority of the WECs, which are based on offshore underwater locations, require the entire system to be lifted above the sea level or use divers to carry out maintenance and repairs which is very costly. Therefore, at present, much research is in progress to develop topologies to find the best solutions to maximize efficiency and robustness while minimizing the overall size of the turbine, generator, converters, repair and maintenance cost, etc. (Oceanlinx, 2017, Wave Swell Energy, 2017, Hong et al., 2014). The OWC air turbine system has relatively easy access particular to the energy conversion system since the turbine, generator and associated parts are

well above the water line. This design not only allows regular maintenance but is also a cost-effective power generation option.

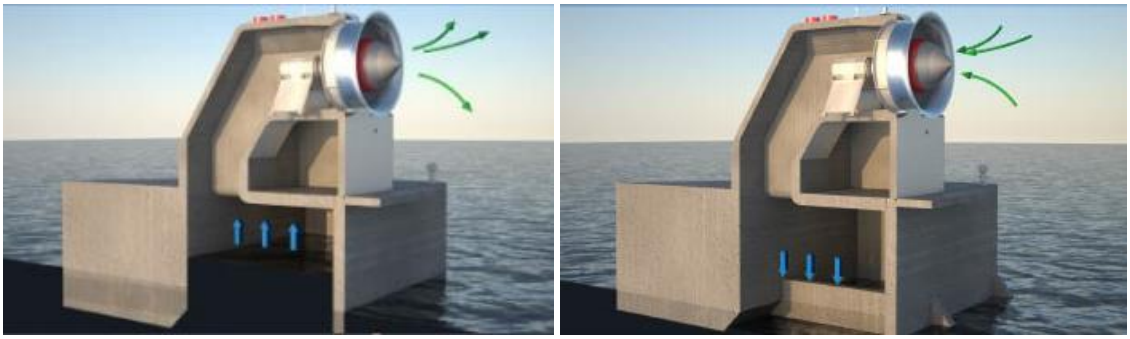

(a)

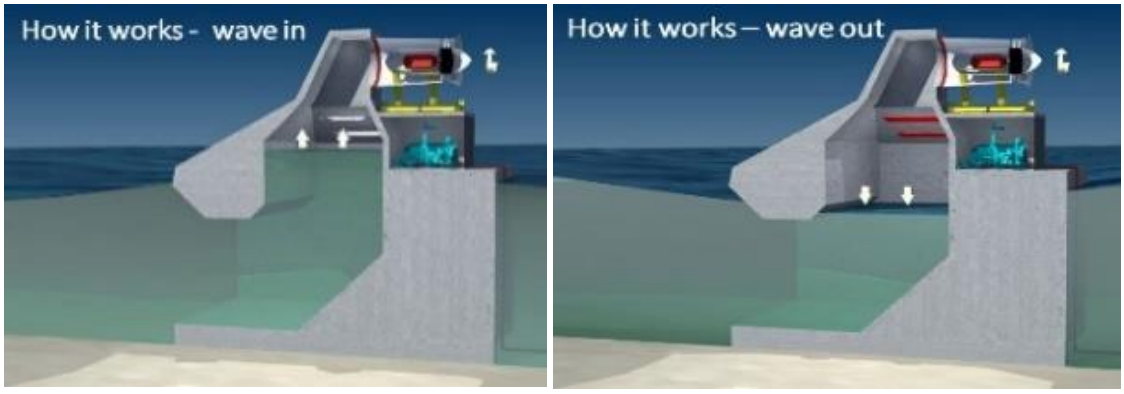

(b)

Figure 2. 1: a). OWC bidirectional air turbine (Oceanlinx, 2017), b). OWC Unidirectional air turbine (Wave Swell Energy, 2017)

The air turbine technologies such as Impulse, Radial, etc. are currently being researched to gain better overall performance at irregular flow conditions and avoid stall which is a drawback of the Wells turbine technology (Takao and Setoguchi, 2012). Regardless of the type of air turbine deployed, the overall design of OWC-based WECs are based on the rise and fall of the ocean wave in a partially submerged chamber. The arrangement is in a way that when the passing wave oscillates inside the WEC chamber oscillates the trapped air inside the chamber. The air pressure fluctuation inside the chamber forces the air to pass in/out through an air turbine at the top of the chamber. The turbine is coupled to a generator. The rotational speed of the turbine depends on the air pressure and the control system of the generator.

As shown in Figure 2. 1. a), the Oceanlinx's OWC turbine has employed the bidirectional reaction turbine for continuous electricity generation in varying flow conditions and flow directions of the waves (Oceanlinx, 2017). As shown in Figure 2. 1. b), the Wave Swell Energy

uses unidirectional air turbine with ingenious concept and allows to use simpler, robust and more reliable design targeting to achieve higher energy conversion efficiency (Wave Swell Energy, 2017). This study considers only the single stage unidirectional air turbine to model the drive system of the generator. The single stage unidirectional air turbines are designed to harness only omnidirectional airflow. These types of turbines are free from limitations due to stalling compared to bidirectional turbines. Moreover, they provide useful efficiencies over wide range of flow rates; thus, they are capable of operating over wide range of pressure drop conditions; increase the pressure drop with increasing flow rate till they become choked preventing further increase with increasing flow rate at much higher pressure drop away from range of interest (Setoguchi et al., 2001). In this study, a typical torque profile of the abovementioned turbine is used as the mechanical input to the generator .

2.3 Mathematical model of the generator

The proposed electrical power conversion system is designed to extract power from the turbine, exploiting the simple and most appropriate subsystems that suits to the OWC air turbine system. The system utilizes a three-phase permanent magnet synchronous generator (PMSG) and a two-level active front-end (AFE) rectifier built with insulated gate bipolar transistors (IGBTs). An MPC technique controls the rectifier. Figure 2. 2, illustrates the considered PMSG connected to the dc interface system.

Even though a multi-pole PMSG is a comparatively large and heavy machine, it has the advantage of using direct drive system avoiding gears. Moreover, it has the ability to use full speed range and requires no power converter or brushes to supply and control the field winding. Therefore, PMSGs are robust and require low maintenance. (Benelghali et al., 2012, O'Sullivan and Lewis, 2011, Abdelrahem et al., 2016, Hansen et al., 2011). Many researchers also believe that, this improved reliability of the system due to reduced mechanical stresses and low maintenance cost would compensate the initial cost (Benelghali et al., 2012, O'Sullivan and Lewis, 2011, Xie and Tang, 2012). Therefore, a PMSG is chosen as the generator in this study. The active and reactive power of the generator output in the αβ reference frame, assuming a balanced three-phase system, are given as (Rodriguez et al., 2013);

$$P = v_{s\alpha} i_{s\alpha} + v_{s\beta} i_{s\beta} \tag{2.1}$$

$$Q = v_{s\beta} i_{s\alpha} - v_{s\alpha} i_{s\beta} \tag{2.2}$$

where P and Q are the active and reactive power respectively, v_s and i_s are the source voltage and current respectively while subscripts α and β represent the real and imaginary axes. The space vector models of

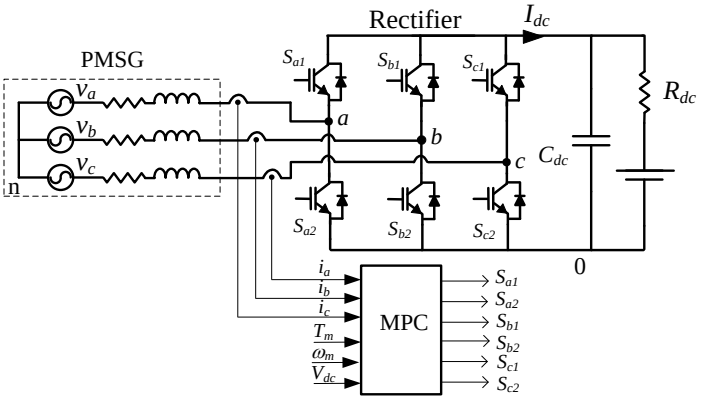

Figure 2. 2: OWC Air turbine generator – dc grid interface system.

the three-phase source voltage ($\vec{v_s}$) and source current ($\vec{i_s}$) derived from the phase voltages (v_{sa}, v_{sb}, v_{sc}), and currents (i_{sa}, i_{sb}, i_{sc}) can be represented as in (2.3) and (2.4) where $\vec{\omega} = e^{\frac{j2\pi}{3}}$ (Parvez et al., 2015).

$$\vec{v}_s = \frac{2}{3}\left(v_{sa} + \vec{\omega} v_{sb} + \overrightarrow{\omega^2} v_{sc}\right) \tag{2.3}$$

$$\vec{i}_s = \frac{2}{3}\left(i_{sa} + \vec{\omega} i_{sb} + \overrightarrow{\omega^2} i_{sc}\right) \tag{2.4}$$

The mathematical model of the variable speed multi-pole PMSG in the dq synchronous rotating reference frame, assuming symmetrical stator windings, negligible stator slots' effect on the rotor inductances with rotor position, negligible magnetic hysteresis and saturation effects, and constant power losses in windings can be given by (Krishnan, 2010, Hughes and Heap, 2009).

$$v_{sd} = R_s i_{sd} + L_d \frac{di_{sd}}{dt} - \omega_e L_q i_{sq} \tag{2.5}$$

$$v_{sq} = R_s i_{sq} + L_q \frac{di_{sq}}{dt} + \omega_e L_d i_{sd} + \omega_e \Psi_{pm} \tag{2.6}$$

while the PMSG's flux and electromagnetic torque are

$$\Psi_{sd} = L_d i_{sd} + \Psi_{pm}; \quad \Psi_{sq} = L_q i_{sq} + 0 \tag{2.7}$$

$$T_e = 1.5 n_p\left[\left(L_d - L_q\right) i_{sd} i_{sq} + \Psi_{pm} i_{sq}\right] = 1.5 n_p \Psi_{pm} i_q \tag{2.8}$$

Rewriting (2.1) and (2.2) in the dq synchronous rotating reference frame, one gets

$$P = T_e\omega_m = 1.5\,(v_{sd}i_{sd} + v_{sq}i_{sq}) \quad (2.9)$$

$$Q = 1.5\,(v_{sq}i_{sd} - v_{sd}i_{sq}) \quad (2.10)$$

where i_{sd} and i_{sq} are the physical current quantities transformed into the dq frame, v_{sd} and v_{sq} are the physical voltage quantities transformed into the dq frame, R_s is the stator's resistance, $L_d = L_q$ are the inductances of the PMSG on the dq axis, Ψ_{pm} is the permanent magnet flux, Ψ_{sd} and Ψ_{sq} are the flux components respectively in the d and q axes, T_e is the generator's electromagnetic torque, and ω_m is the mechanical angular speed of the generator.

The formulas associated with the turbine and generator rotor, considering the direct drive system of the turbine generator and zero rotational damping coefficient can be written as;

$$J\,\frac{d\omega_m}{dt} = T_m - T_e \quad (2.11)$$

Where $J = J_e + \frac{J_t}{n_g}$

The generator rotor electrical angular speed (ω_e)can be written as

$$\omega_e = n_p\,\omega_m = 2\pi f_e \quad (2.12)$$

where J_e, J_t and J are the inertia of the generator, turbine and the air turbine system respectively, T_m is the mechanical torque of the turbine, $n_g$is the gear ratio, n_p is the number of pole pairs, and f_e is the electric frequency.

2.4 AFE rectifier and MPC of the converter

2.4.1 AFE Converter Model

The rectifier consists of 6 IGBT-diode switches. The circuit is fed by the ac voltage (v_s), generated by the PMSG, through combination of source and line filter inductances $L_s = [(L_{sa} + L_{fa}), (L_{sb} + L_{fb}), (L_{sc} + L_{fc})]^T$ and resistances $R_s = [(R_{sa} + R_{fa}), (R_{sb} + R_{fb}), (R_{sc} + R_{fc})]^T$. A dc-link capacitor ($C_{dc}$) reduces the voltage ripples. The IGBT switches operate in such a manner that two IGBTs connected to the same phase are operated in contrary mode to avoid short circuits (e.g., when S_{a1} is ON, S_{a2} is OFF, and vice versa). The rectifier's switching state is determined by the gating signals S_a, S_b and S_c. These three switching signals can produce eight consequent switching states resulting in eight possible voltage vectors as presented in Table 2.1, and Figure 2. 3.

Table 2. 1: Switching states and voltage space vectors (Abdelrahem et al., 2016, Parvez et al., 2015)

Switching states			Voltage space vector
S_a	S_b	S_c	$\overrightarrow{v_{AFE}}$
0	0	0	$\overrightarrow{v_0} = 0$
1	0	0	$\overrightarrow{v_1} = 2v_{dc}/3$
1	1	0	$\overrightarrow{v_2} = v_{dc}/3 + j\, v_{dc}/\sqrt{3}$
0	1	0	$\overrightarrow{v_3} = -v_{dc}/3 + j\, v_{dc}/\sqrt{3}$
0	1	1	$\overrightarrow{v_4} = -2v_{dc}/3$
0	0	1	$\overrightarrow{v_5} = -v_{dc}/3 - j\, v_{dc}/\sqrt{3}$
1	0	1	$\overrightarrow{v_6} = v_{dc}/3 - j\, v_{dc}/\sqrt{3}$
1	1	1	$\overrightarrow{v_7} = 0$

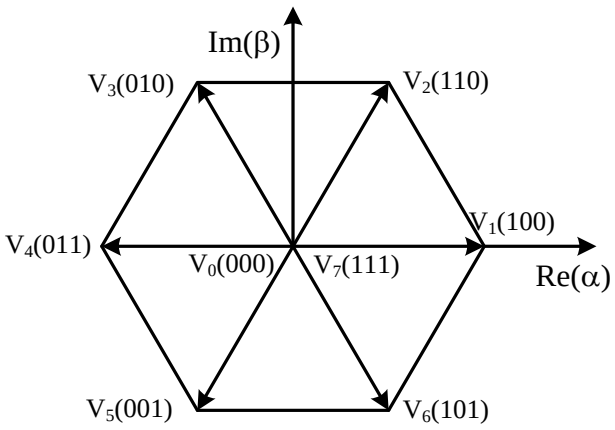

Figure 2. 3: Space vector diagram.

The switching function vector ($\overrightarrow{S}$) can then be written as

$$\vec{S} = \frac{2}{3}\left(S_a + \vec{\omega}S_b + \overrightarrow{\omega^2}S_c\right) \tag{2.13}$$

while the rectifier's space vector ($\overrightarrow{v_{AFE}}$) related to phase to neutral voltages (v_{a0}, v_{b0}, v_{c0}) and dc bus voltage (v_{dc}) can be written as (Parvez et al., 2015, Liu et al., 2016)

$$\overrightarrow{v_{AFE}} = \frac{2}{3}\left(v_{a0} + \vec{\omega}v_{b0} + \overrightarrow{\omega^2}v_{c0}\right) \tag{2.14}$$

$$\overrightarrow{v_{AFE}} = \vec{S} \cdot v_{dc} \tag{2.15}$$

The relationship between the generated three-phase voltage vectors and the rectifier's input voltage vectors can be obtained by applying Kirchhoff's voltage law to the input side of the rectifier as

$$\vec{v}_s = L_s \frac{\overrightarrow{di_s}}{dt} + R\vec{i}_s + \frac{2}{3}\left(v_{a0} + \vec{\omega}v_{b0} + \overrightarrow{\omega^2}v_{c0}\right) - \frac{2}{3}\left(v_{n0} + \vec{\omega}v_{n0} + \overrightarrow{\omega^2}v_{n0}\right) \tag{2.16}$$

The input current dynamics of the rectifier, derived from (2.14), (2.16) and assuming $\frac{2}{3}\left(v_{n0} + \vec{\omega}v_{n0} + \overrightarrow{\omega^2}v_{n0}\right) = v_{n0}\frac{2}{3}\left(1 + \vec{\omega} + \overrightarrow{\omega^2}\right) = 0$, can be written as (Parvez et al., 2015)

$$\frac{\overrightarrow{di_s}}{dt} = -\frac{R_s}{L_s}\vec{i}_s + \frac{1}{L_s}\vec{v}_s - \frac{1}{L_s}\overrightarrow{v_{AFE}} \tag{2.17}$$

The MPC is formulated in the discrete-time domain and thus, the rectifier's input current and rectified voltage are derived in a discrete-time model as in (18), using Euler's approximation in one switching period where T_s is the sampling time ($T_s > 0;\ kT_s \le t \le (k+1)T_s$) and k is the sampling instance.

$$\frac{\overrightarrow{di_s}}{dt} \approx \frac{\vec{i}_s\,(k+1) - \vec{i}_s\,(k)}{T_s} \tag{2.18}$$

For the $(k+1)$sampling instance the input current can be written as in (2.19) (Rodriguez et al., 2013, Parvez et al., 2015, Liu et al., 2016)

$$\vec{i}_s\,(k+1) = \left(1 - \frac{R_s T_s}{L_s}\right)\vec{i}_s(k) + \frac{T_s}{L_s}\left(\vec{v}_s(k) - \vec{v}_{AFE}(k)\right) \tag{2.19}$$

2.4.2 Finite Control Set MPC (FCS-MPC)

FCS-MPC with short prediction horizon is a promising control technology for achieving accurate control of the turbine speed through the control of the rectifier. MPC is used over many other control schemes for power converters such as PI, fuzzy, adaptive, sliding mode, etc. due to its simplicity and fast response. In this control scheme, a model of the system is considered in order to predict the future behavior of the variables (Rodriguez et al., 2013). According to (Parvez et al., 2015), the MPC controllers is not only simpler than voltage oriented control based pulse width modulators but also accurately track the reference value by generating the optimum switching signal. Also, the MPC algorithm is easy to configure with constraints and non-linearity (Parvez et al., 2015, Rodriguez et al., 2013). The FCS-MPC requires high

processing power and high accuracy of model parameters. At present, powerful processors overcome this issue at high speed and reduced cost (Vazquez et al., 2014).

The proposed control structure is designed to maintain the turbine speed at 650rpm. The FCS-MPC algorithm minimizes the error between reference and predicted angular speeds, denoted respectively by ω^* and ω^pwhich is calculated from

$$\omega^p = \omega_m(k+1) = \omega_m(k) + \frac{T_s}{J}\ (T_m - T_e) \tag{2.20}$$

In the control system, the future value of current, $i_s(k+1) = i_s^p$ is calculated from measured $v_s(k)$, $i_s(k)$ and $V_{dc}(k)$ by MPC controller using (19) for each one of eight possible switching vectors ($\vec{S}$). Then, i_s^p is converted into dq frame (i.e., i_d^p and i_q^p) to calculate ω^p of the turbine rotor, before it is compared to ω^* using the cost function of (g) from (2.21) to select the switching state which minimizes the cost function. The error between d axis current reference ($i_d^* = i_{d\_ref}\ (k+1)$) and predicted d axis current ($i_q^p = i_q(k+1)$) is added to the cost function with an arbitrary constant K to reduce the d-axis current in the generator and thereby avoid flux weakening. Figure 2. 4, illustrates the proposed FCS-MPC control algorithm for the rectifier. The arbitrary constant K is decided based on the generator system, reference current and simulation results. This study is taken the value of K as $2e^{-4}$.

$$g = |\omega^* - \omega^p| + K.|i_d^* - i_d^p| \tag{2.21}$$

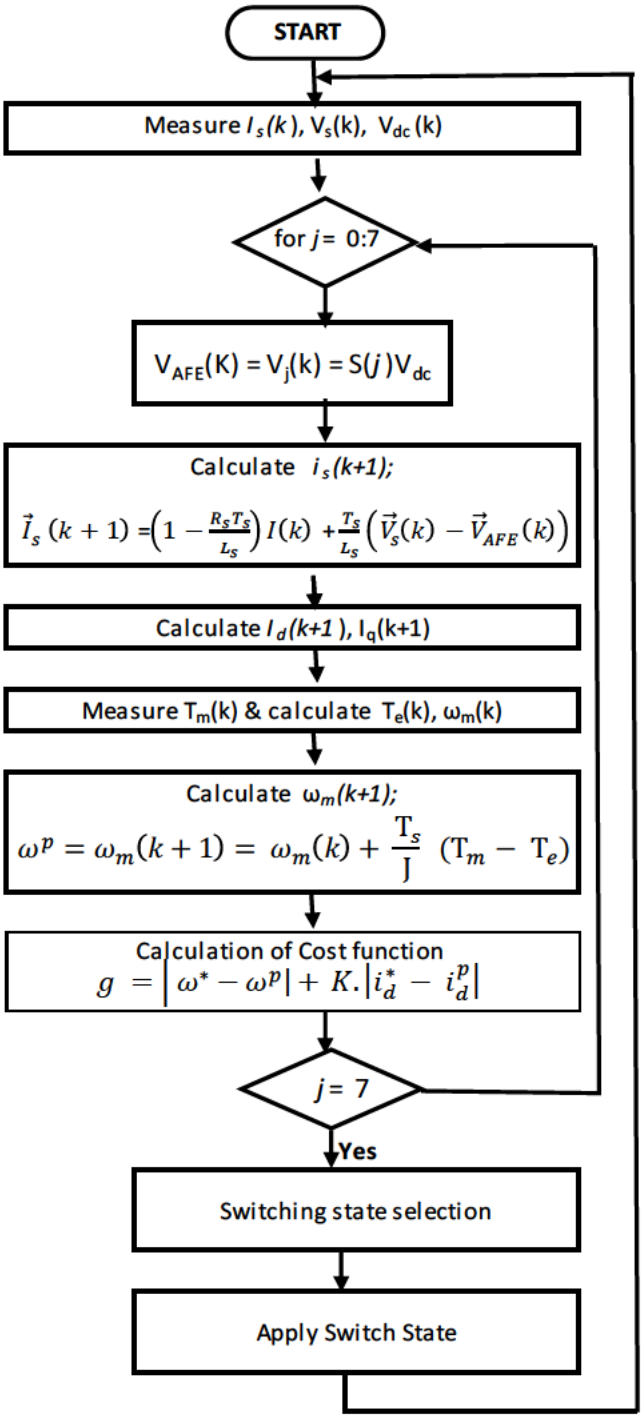

Figure 2. 4: Proposed FCS-MPC algorithm flowchart for the rectifier.

2.5 Simulation Results

A simulation study was carried out in MATLAB/Simulink to verify the operation of the proposed FCS-MPC based controller. Figure 2. 2, illustrates the simulation model of proposed air turbine generator-dc grid integration system. The simulation results are shown in Figure 2. 6. a)-2. 6. h), which are used to verify the operation of the proposed controller.

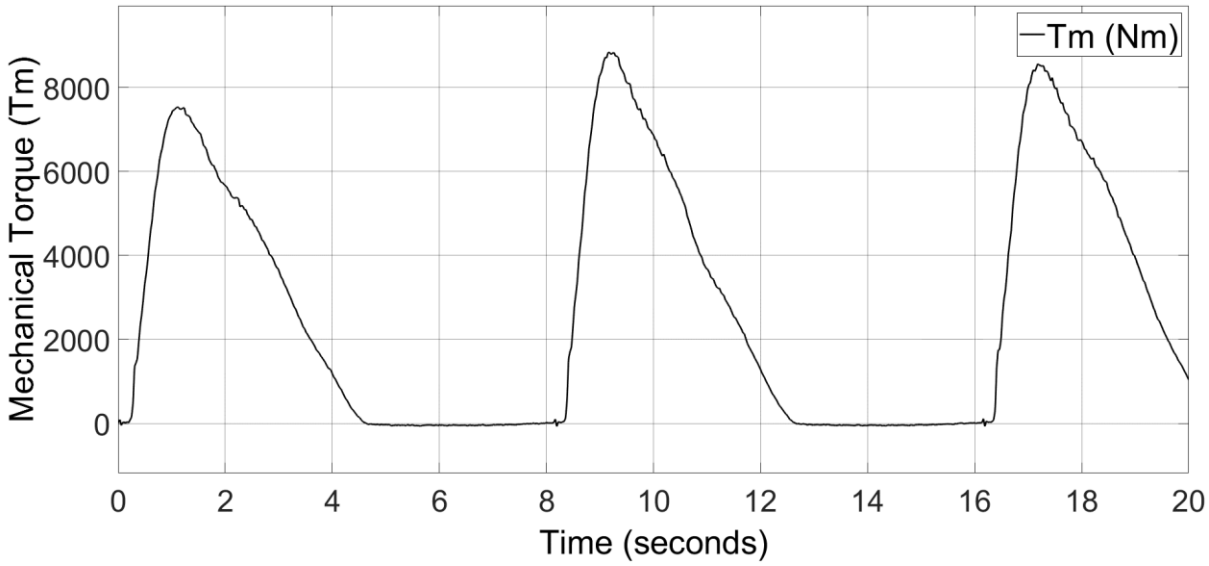

(a)

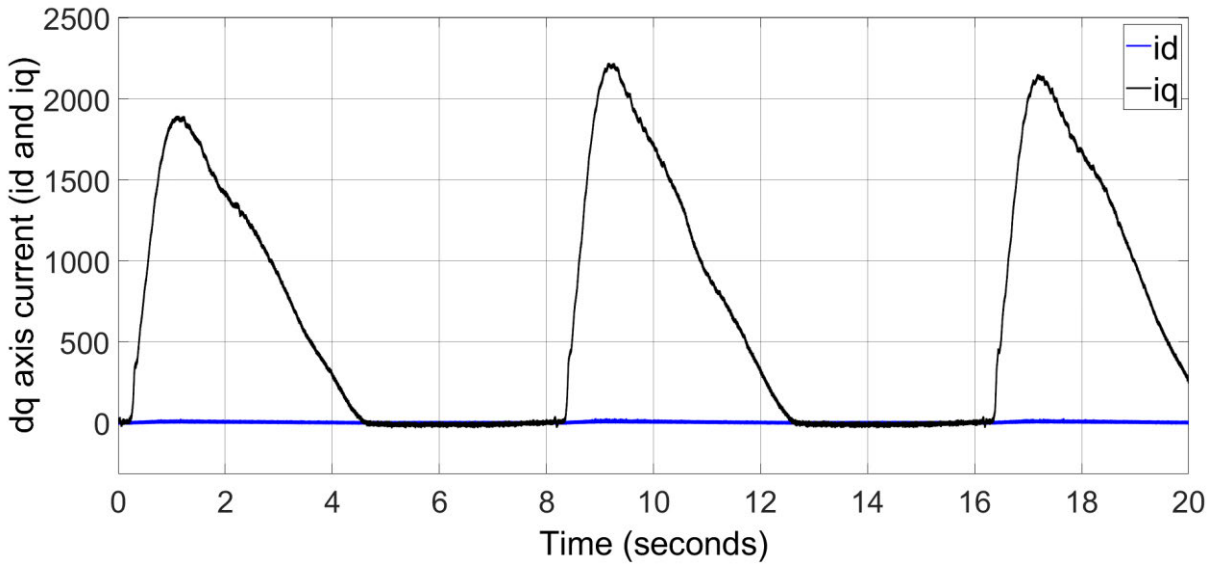

(b)

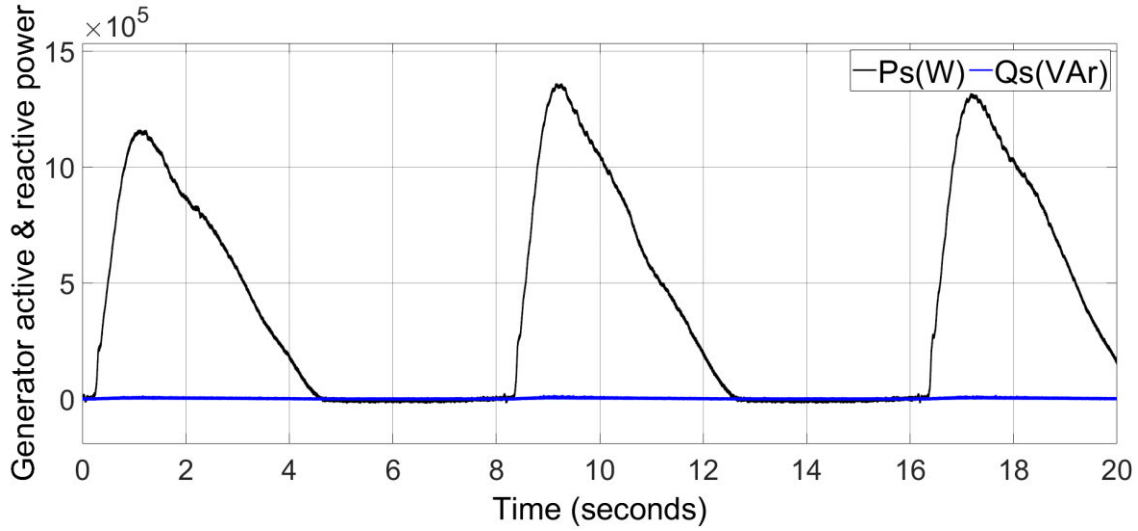
×10^5
15
10
5
0
Generator active & reactive power
Ps(W)
Qs(VAr)
0
2
4
6
8
10
12
14
16
18
20
Time (seconds)

(c)

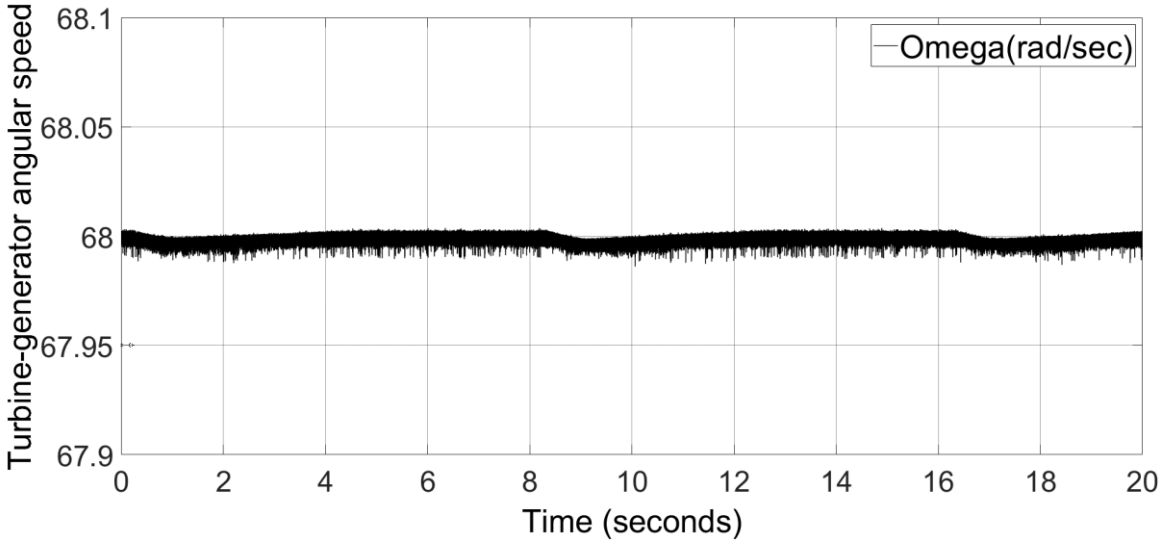
68.1
68.05
68
67.95
67.9
Turbine-generator angular speed
Omega(rad/sec)
0
2
4
6
8
10
12
14
16
18
20
Time (seconds)

(d)

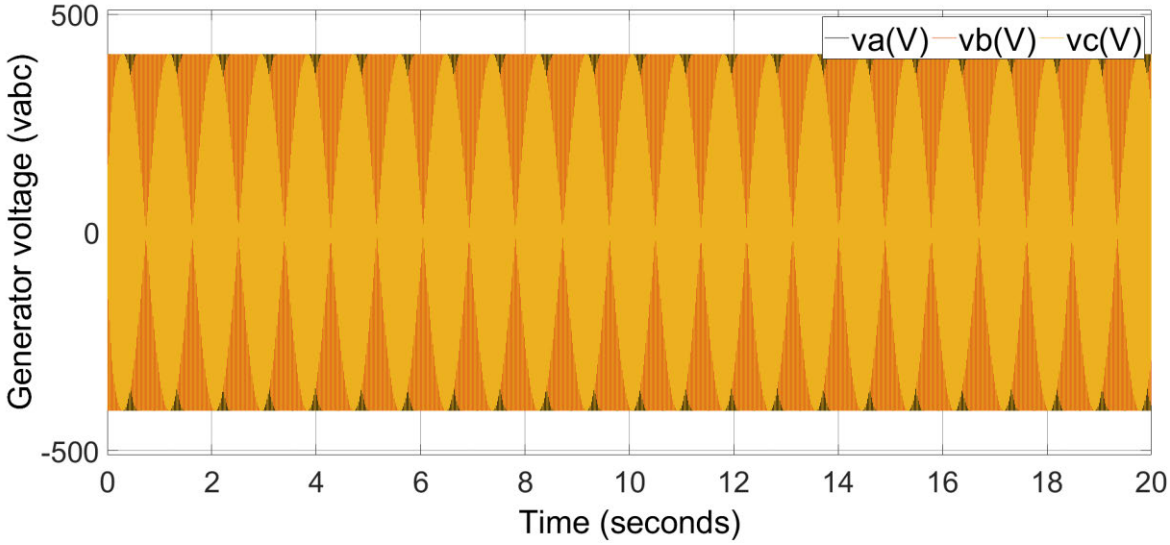
500
0
-500
Generator voltage (vabc)
va(V)
vb(V)
vc(V)
0
2
4
6
8
10
12
14
16
18
20
Time (seconds)

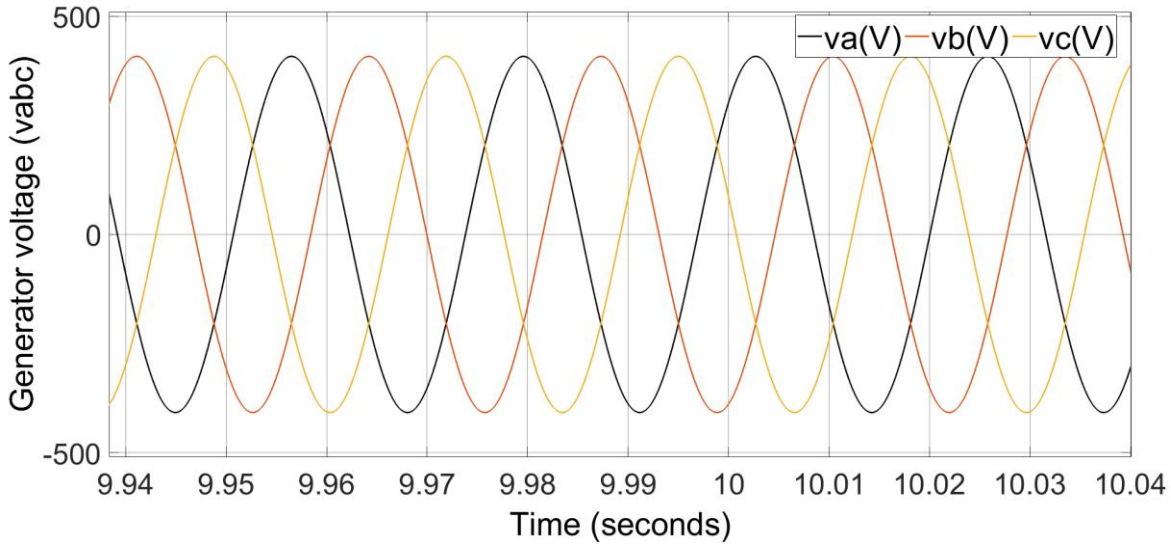
va(V)
vb(V)
vc(V)
Generator voltage (vabc)
500
0
-500
9.94
9.95
9.96
9.97
9.98
9.99
10
10.01
10.02
10.03
10.04
Time (seconds)

(e)

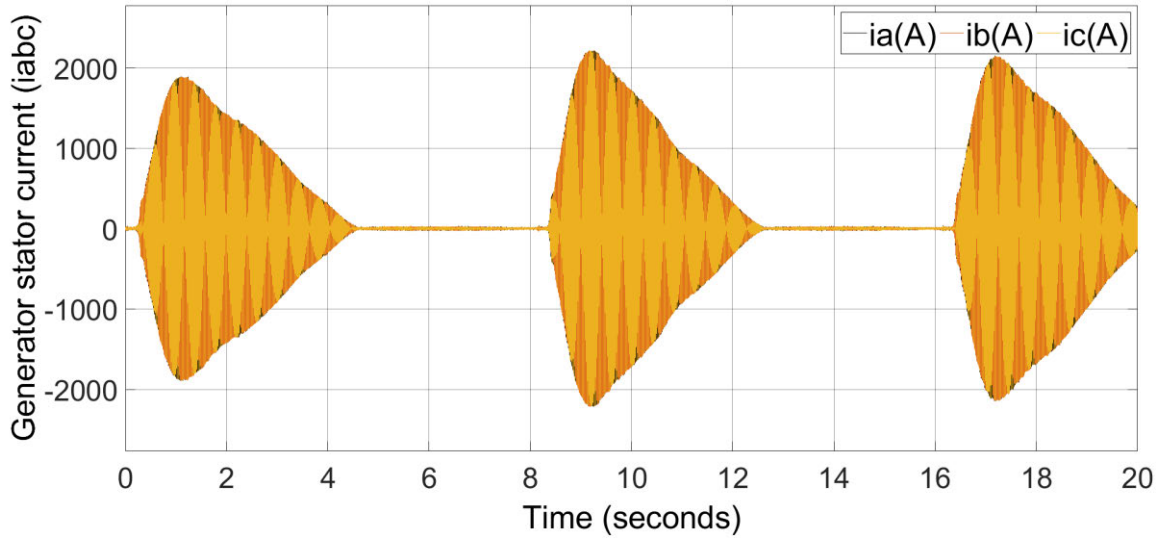
ia(A)
ib(A)
ic(A)
Generator stator current (iabc)
2000
1000
0
-1000
-2000
0
2
4
6
8
10
12
14
16
18
20
Time (seconds)

(f)

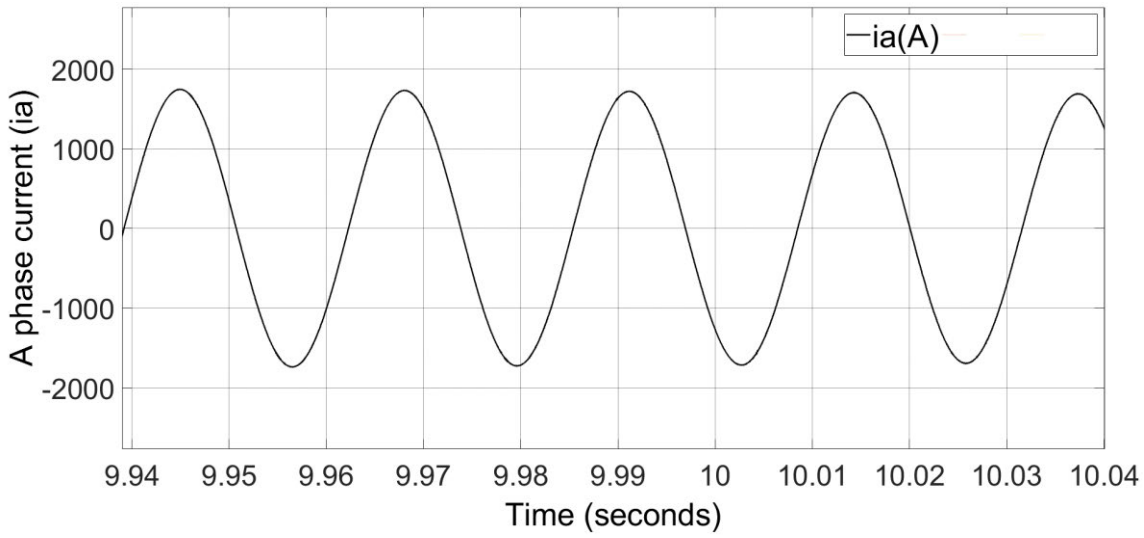
ia(A)
A phase current (ia)
2000
1000
0
-1000
-2000
9.94
9.95
9.96
9.97
9.98
9.99
10
10.01
10.02
10.03
10.04
Time (seconds)

(g)

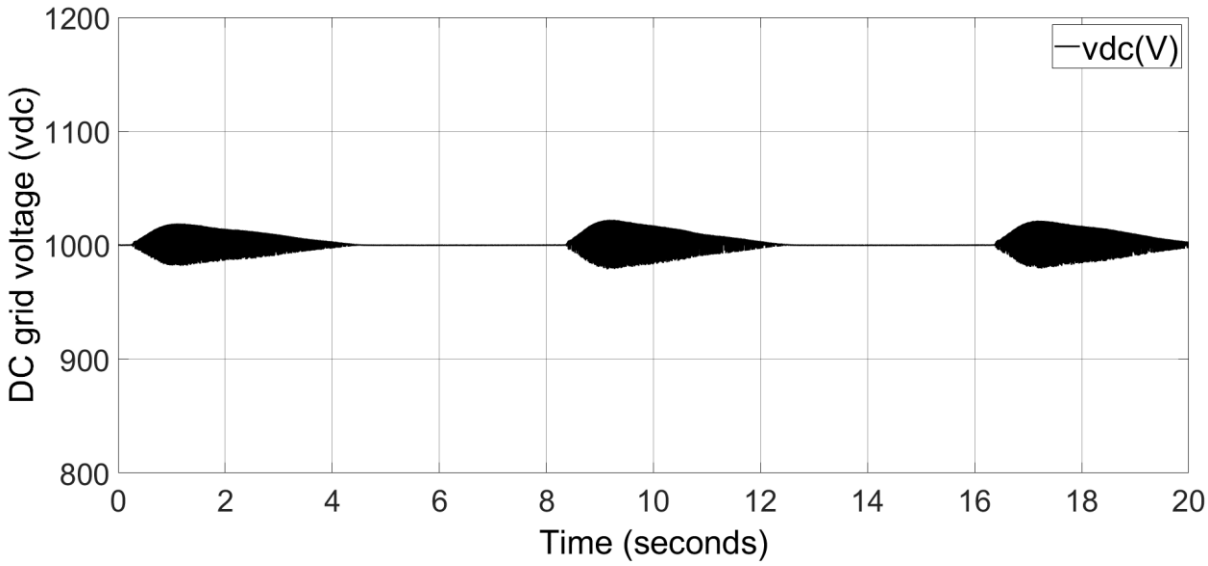

(h)

Figure 2. 5: Performance of the proposed FCS-MPC for the PMSG of an OWC unidirectional air turbine: a). Mechanical torque T_m(Nm), b). id and i_q(A) components of stator current in the d_q(A) frame, c). Active power P(W) and reactive power Q(Var) of the PMSG, d). Rotor angular speed Omega$_m$(rad/s), e). Generator output voltage v_{abc}(V), f). Stator current – i_{abc}(A), g). Stator current i_a(A), h). dc link voltage v_{dc}(V).

Figure 2. 6. a), shows the torque profile applied to the generator. In this study, even though the torque given as a direct input to the controller, in real WEC systems currents and voltages of the generator are measured to calculate the torque. Figure 2. 6. b), depicts the q axis stator current which varies in proportion to the torque. Figure 2. 6. c), shows the active power and reactive power output of the generator. The active power also varies in proportion to the torque which confirms the ability of the proposed controller to extract power from OWC air turbine with varying input torque. Figure 2. 6. d), shows the rotor angular speed is following the reference value 68rad/s which is set at target operating conditions of the air turbine. This particular value was chosen based on the efficiency curve shown in Fig. 3.3(a). As shown in Figures 2. 6. e)-2. 6. f), the PMSG's output voltage and current are nearly sinusoidal. As shown in Figure 2. 6. g), the total harmonic distortion (THD) of the a-phase current (i_a) is less than 5% which complies with the IEEE standards (2014). Figure 2. 6. h), illustrates the dc bus voltage which has only 2% variation. Sampling time the simulations was set to 100ms which gives a 200:1 ratio with the fundamental frequency of the output is 50Hz. This ratio is large enough to minimize the errors that could arise due to the Euler approximation used in the discrete time models of the variables.

2.6 Conclusion

This paper presents an MPC-based speed controller for an air turbine-connected PMSG of an oscillating water column WEC system. Simulation results verify that the proposed controller extracts power from the turbine at varying input torque conditions while maintaining the speed at the set point. The proposed controller does not require tuning and thus, it is easy to implement. The discrete nature of the controller makes it easy to realize in modern digital controllers.

3

A MODEL PREDICTIVE CONTROL-BASED POWER CONVERTER SYSTEM FOR OSCILLATING WATER COLUMN WAVE ENERGY CONVERTERS

This chapter was published in the special issue on Marine Energy of the 'Energies' journal. The citation for the research article is:

G. Rajapakse, S. G. Jayasinghe, A. Fleming, and Michael Negnevitsky, "A Model Predictive Control-Based Power Converter System for Oscillating Water Column Wave Energy Converters," *Energies 2017*, vol. 10, no. 10, 2017.

Some (less than 20%) of the content of chapter 2 has been repeated in this chapter.

Abstract

Despite the predictability and availability at large scales, wave energy conversion (WEC) has still not become a mainstream renewable energy technology. One of the main reasons is the large variations present in the extracted power which could lead to instabilities in the power grid. In addition, maintaining an optimal speed of the turbine under changing wave conditions is another control challenge, especially in oscillating water column type WEC systems. As a solution to the first issue, this paper proposes the direct connection of a battery bank into the dc-link of the back-to-back power converter system and thereby smoothening the power delivered to the grid. For the second issue, model predictive controllers are developed for the rectifier and the inverter of the back-to-back converter system aiming to maintain the turbine speed within its optimum range. In addition, MPC controllers are designed to control the battery current as well in both charging and discharging. Operations of the proposed battery direct integration scheme and control solution are verified through computer simulations. Simulation results show that the proposed integrated energy storage solution and control techniques are capable of delivering smooth power to the grid while maintaining the turbine speed within its optimum range under varying wave conditions.

Keywords: Active front end rectifier, finite control set-model predictive control, two-level voltage source inverter, wave energy conversion.

3.1 Introduction

Wave energy is a vast, sustainable and low environmental impact renewable energy source which is gaining popularity among the research community (Carson et al., 2010, Carson et al., 2014, Rajapakse et al., 2017a, Stegman et al., 2017). Numerous researches have been conducted and various technologies have been developed to convert wave energy into electricity since mid of the twentieth century (Delmonte et al., 2016). Nevertheless, practical implementations of these technologies have always been challenging with varying degrees of success (Delmonte et al., 2016). According to (Hannon et al., 2016), only four countries have fully operational wave energy conversion (WEC) systems so far while few other countries, including Australia, are rapidly progressing towards commercial deployments. As reported in (Carson et al., 2014), there are several WEC projects in progress at various stages in the southern Australian coast line aiming to increase the renewable share in the grid. These projects use different WEC technologies, out of which the project at the King Island conducted by Wave Swell Energy (WSE) uses the oscillating water column (OWC) technology which is simple, cost effective and easy to maintain (Wave Swell Energy, 2017).

This particular WEC system employs a bottom standing OWC plant which is positioned about 700m from the shoreline of the King Island at mean sea level depth of 10m (Fleming et al., 2017). This design concept focuses on oscillation of the ocean wave inside a fixed and partially submerged hollow concrete structure, known as OWC chamber. The passing ocean waves which rise and fall inside the OWC chamber make the trapped air inside the chamber to compress and decompress. This makes a varying differential pressure in the OWC chamber with respect to the atmosphere. When the pressure inside the OWC chamber is low, atmospheric air is drawn into the chamber through a unidirectional air turbine which is coupled to a generator to generate electricity. When the air chamber pressure is above atmospheric pressure, the trapped air is passed through passive non-return air flow valves built into the OWC chamber (Fleming et al., 2017). Therefore, this turbine generates power only during the inhale stage resulting in pulses in the generated electrical power. The characteristics of the particular air turbine are different to those of the traditional turbines such as Wells turbine and impulse turbine, and thus its control objective is different to what has been reported in the literature (Falcao and Henriques, 2015, Wave Swell Energy, 2017).

Amidst the drawback of power pulses, WSE and other companies commissioning similar type of commercial scale projects believe that the OWC system will be reliable, require less maintenance and cost effective compared to other onshore renewables and fossil fuels in coming years (Rajapakse et al., 2017a, Hannon et al., 2016, Wave Swell Energy, 2017, Oceanlinx, 2017). To achieve these objectives and promote WEC as a competitive renewable energy technology, it is essential to gain maximum overall efficiency from wave to wire and comply with the grid codes applicable to the WEC system. This involves maintaining the turbine within its optimum speed range and delivering smooth power to the grid.

Similar to wind energy electrical conversion systems, the back-to-back converter arrangement is the popular grid integration technology for WEC systems as it decouples the generator dynamics from the grid and allows the turbine to run at different speeds to optimise the energy capture (Tedeschi et al., 2011, Heier, 2014). Nevertheless, aforementioned power pulses still propagate into the power grid through the power converter which could lead into instabilities in the grid (Tedeschi et al., 2011, Heier, 2014, Wu et al., 2010). Therefore, energy storage systems (ESS) that can absorb power fluctuation and thereby ensure smooth power delivery to the grid are becoming an integral part of WEC systems.

The inclusion of energy storage to absorb power fluctuations in renewable energy systems is well explored and there are numerous publications proposing various topologies and control techniques. In fact, the application of battery energy storage in WEC systems is also not new (Zou and Cheng, 2017). The common approach of integrating an ESS, in the form of a battery bank and/or supercapacitor bank , is the use of an interfacing dc-dc or dc-ac converter (Tedeschi et al., 2011, Ceballos et al., 2015, Vilathgamuwa et al., 2015). This enables direct control over the charge/discharge current on the energy storage system. Nevertheless, as shown in Figure 1, this paper proposes to connect a battery ESS (BESS) directly into the dc-link of the WEC system without an interfacing converter. The problem with this approach is the absence of direct control over the battery current. Neither the rectifier nor the inverter shown in Figure. 1 can directly control the battery current. In addition, the dc-link voltage, V_{dc}, is also not controlled and allowed to vary depending on the battery SoC and its current. In the proposed system, inverter controller regulates the current (in other words power) injected into the grid while the rectifier controller controls the generator current (to regulate the speed). Since the battery is directly connected to the dc-link, battery current is the difference between the current supplied by the rectifier and the current taken out by the inverter (the capacitor is there to absorb high

frequency components). Both of these currents are controllable. Therefore, this paper proves that the battery current is also controllable, which is one of the novel aspect presented in this paper. As this is an indirect control of the battery the system is designed and the grid power reference is chosen in a way that the battery current in both charging and discharging states will not exceed safe operating limits.

The conventional control techniques use pulse width modulation (PWM) methods which linearize power converters while power converters and drive systems are controlled in cascade multi loop systems with Proportional Integral (PI) regulators (Guerrero et al., 2011, Mehrasa et al., 2014, Mehrasa et al., 2015, Mehrasa et al., 2016). New strategies proposed in (Mehrasa et al., 2015), (Mehrasa et al., 2016), etc. improve the performance of this controller in the presence of nonlinear loads. Nevertheless, in general, linear control methods with a modulation applied to nonlinear systems lead to uneven performance throughout the dynamic range (Rodriguez and Cort´es, 2012). Implication of this method has been identified as very challenging to modern power converters such as multi-level, matrix converters, etc. (Rodriguez and Cort´es, 2012). Moreover, system constraints and technical requirements cannot be directly included into the conventional control designs. To overcome these issues, modern digital control methods are introduced for the power converters. The recent developments of microcontrollers and fast powerful digital signal processors make these digital control methods a reality.

Apart from the direct connection of the battery into the dc-link, this paper proposes a finite control set model predictive controller (FCS-MPC) for the rectifier and inverter. With the advancement of microprocessor technologies, model predictive control (MPC) has become popular as a simple and fast digital control technology for power electronic converter systems (Sultana et al., 2017). Moreover, the absence of tuning makes MPC more attractive over conventional PI controllers. In (Tarisciotti et al., 2015), a current control scheme for a three phase rectifier has been introduced using modulated MPC (M^2PC) to reduce switching frequency and total harmonic distortion (THD) in phase currents, by three times compared to conventional MPC. In (Nguyen and Kim, 2017), a similar control scheme for a three phase grid connected inverter has been introduced using M^2PC with a moving average filter-phase lock loop considering distorted grid conditions. Apart from improving the THD, the other main concern of (Tarisciotti et al., 2015) and (Nguyen and Kim, 2017) is the large computational effort required in the controller. In the field of renewable energy, FCS-MPC has recently been proposed for variable speed wind energy conversion systems (Abdelrahem et al., 2016) with a

model reference adaptive system observer to estimate the generator rotor speed and position. Nevertheless, the applicability of FCS-MPC in OWC WESs has not been tested so far.

The objective of the MPC proposed in (Abdelrahem et al., 2016) is to extract maximum power from the wind by controlling the generator speed according to the actual wind speed. Similar variable speed operations have been proposed for WECs to track the maximum power point (MPPT) using different control strategies other than MPC (Delmonte et al., 2016, Lekube et al., 2017). Nevertheless, the choice of variable or fixed speed operation of the turbine depends on its design and operating requirements. Therefore, the objective of the associated power take-off (PTO) controller should also vary accordingly. The particular turbine considered in this study targets to operate at a pre-designed operating speed range to achieve the optimum turbine efficiency regardless of the change in differential air pressures (Wave Swell Energy, 2017). Therefore, the objective of the proposed controller is to maintain the turbine speed within the optimum range under varying wave conditions.

The operation of the proposed battery energy storage integration system and effectiveness of the model predictive controllers are verified through MATLAB/Simulink software simulations. The paper is organized as follows. Section 3.2 reviews the electrical grid and grid codes requirements applied to the King Island WEC system in Australia. Section 3.3 presents the overall system modelling of OWC. The model predictive control for both the power converters presented in Section 3.4. Section 3.5 presents simulation results and discusses the implications of the results. Conclusions derived from the discussion are presented in Section 3.6.

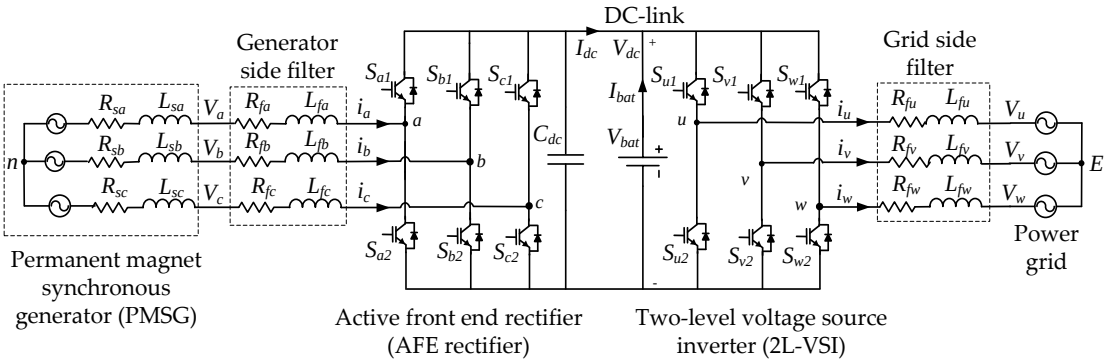

Figure 3. 1: Schematic Diagram of the proposed OWC Air Turbine Generator - Grid interface system

3.2 Electrical Grid and Grid Codes in Australia- King Island

In Australia, all grid connected inverters should comply with the requirements of 'AS4777 - Australian guidelines for grid connection of energy systems through inverters' and 'AS3100 – Approval and test specification general requirements for electrical equipment'. These guidelines are based on IEC61000-6-3:2006 and IEEE1547 standards. The same standards apply to the grid connected wind turbine generators and solar inverters (Carson et al., 2014, CleanEnergyCouncil, Tasnetworks, 2016). According to (CleanEnergyCouncil) which is an Australian body that administers the accreditation of renewable energy installers and grid connected inverters in Australia, fewer Australian policies and standards have been published for renewable energies except for solar PV industry to date. Therefore, most of the small scale renewable energy system interconnections are assessed on a case by case basis (CleanEnergyCouncil, Tasnetworks, 2016). The power grid where the WEC system considered in this paper is going to be connected is a standalone hybrid off-grid transmission network of 11kV, isolated from both mainland Australia and Tasmania. (2014 to present).

Australian transmission system operators (TSOs) require all grid-connected power plants to be compliant with the grid codes. This means that the WEC system should have adequate capability to act as conventional power plants. The important steady state operation conditions required by the TSO are identified as (Lekube et al., 2017, Wu et al., 2010):

- The power plant should be able to control its active power output according to the limits set by TSO to maintain system security and reliability.
- The power factor is required to be maintained as $PF_{inductance}$ equal to 1.0 and $PF_{capacitance}$ equal to 0.95 at both 100% and 50% power.

- The frequency should be maintained between 47 Hz and 52 Hz.
- The operating voltage should be kept at ±10% of the rated voltage at the point of connection (POC).
- The voltage quality standards such as rapid voltage changes, harmonic voltages, voltage variations and flicker should comply with the standards of IEC 61000-3-2 and IEEE1547.

The grid connected converter of the OWC WEC system should adhere to all these grid codes. Therefore, the proposed back-to-back full scale power converter should be able to ensure the quality of the power supply to the grid regardless the intermittentancy present in the output of the air turbine generator system. Therefore, energy storage is essential to absorb power fluctuations, maintain a smooth dc-link voltage and ensure a smooth power delivery to the grid (Ceballos et al., 2015).

3.3 Overall System Modelling

3.3.1 Wave, OWC and Air Turbine model

A prototype of the single stage unidirectional air turbine, which is used in this study, is shown in Figure 3. 2. Compared to conventional bi-directional air turbines used in WECs, this particular turbine is expected to achieve higher energy conversion efficiency (Wave Swell Energy, 2017). Preliminary tests of the turbine model have been carried out in the model test basin at the Australian Maritime College.

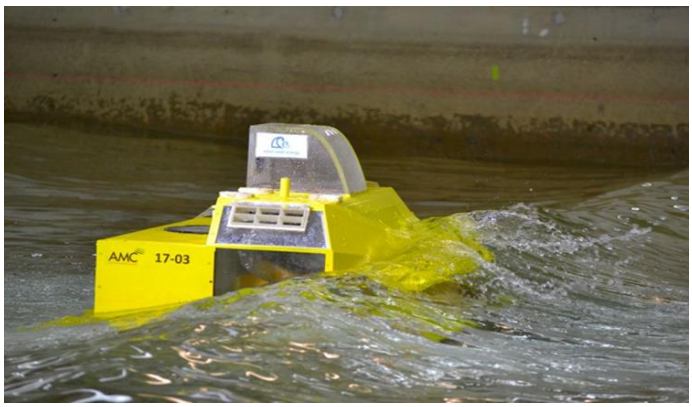

Figure 3. 2: Model Scale experiments performed in the Australian Maritime College's Model Test Basin (Wave Swell Energy, 2017).

As mentioned above, this turbine produces power only during the air intake. The graph in Figure 3. 3. a), depicts the predicted efficiency curve of the air turbine which peaks around 650rpm. As this particular turbine does not necessarily require variable speed operation (Wave Swell

Energy, 2017, Fleming et al., 2017) 650rpm is set as the control objective for this study. Figure 3. 3. b), illustrates a distinctive pressure profile experienced by the turbine at the point of its design speed which was obtained from the tests carried out with the prototype mentioned above. The torque generated by the pressure drop profile is taken as the mechanical input to the generator. The empirical relationship between the pressure drop and the torque was obtained as

$$T_m = 30.815\Delta P^2 - 653\Delta P \tag{3.1}$$

where T_m is the mechanical torque produced by the turbine in Nm and ΔP is the pressure drop dynamics through the turbine in kPa**.** This mechanical torque has been used as the input to the generator for the simulation purposes.

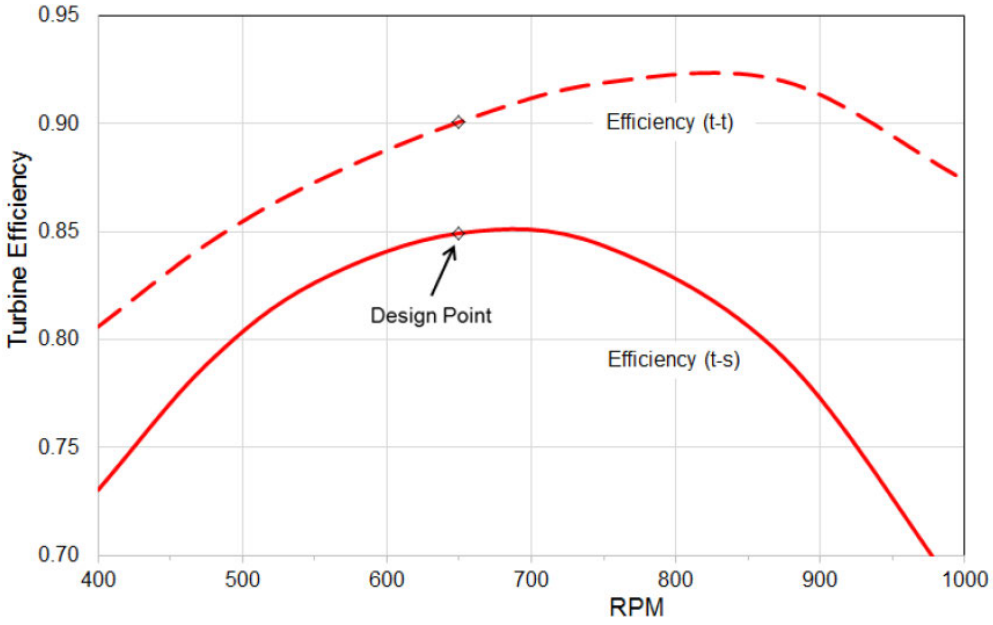

(a)

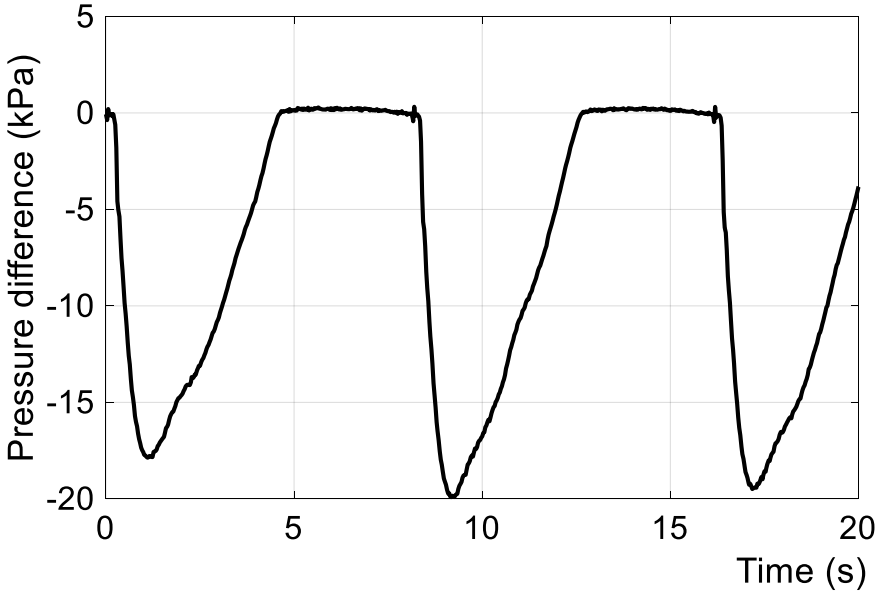

(b)

Figure 3. 3: (a). Predicted efficiency curve for the unidirectional air turbine designed for OWC project extracted from Turbine design report by PerAero Turbine Designs LLC, (b). Pressure drop ΔP(kPa) vs Time (sec) at 650rpm (Fleming et al., 2017).

3.4 PMSG and Grid model

The behaviour of three-phase machines is usually described by their voltage/current equations and inductances. The coefficients of the differential equations that describe their behaviour are time varying. The relationship between the generated three-phase voltages/currents can be illustrated as (Bimbhra, 1992)

$$\begin{bmatrix} f_a \\ f_b \\ f_c \end{bmatrix} = f \begin{bmatrix} \cos(\omega t) \\ \cos(\omega t - \frac{2\pi}{3}) \\ \cos(\omega t - \frac{4\pi}{3}) \end{bmatrix} \tag{3.2}$$

where f represents sinusoidal quantity of voltage, current, flux linkages, or electric charge in balanced circuit. ωt is the actual angle.

To reduce the complexity of the algorithm three-phase quantities are converted to the dq rotating reference frame. Firstly, three-phase quantities are converted into an orthogonal component system (αb stationary reference frame) by taking the projections of the three-phase quantities on an orthogonal axis using Clark's Transformation. Then the results are converted into dq rotating reference frame using Park's transformation to obtain the desired results. The

three-phase to dq rotating reference frame, when the rotating frame is aligned 90^o behind three-phase's A axis (Bimbhra, 1992)

$$\begin{bmatrix} f_d \\ f_q \\ f_0 \end{bmatrix} = \frac{2}{3} \begin{bmatrix} \sin(\omega t) & \sin\left(\omega t - \frac{2\pi}{3}\right) & \sin\left(\omega t - \frac{4\pi}{3}\right) \\ \cos(\omega t) & \cos\left(\omega t - \frac{2\pi}{3}\right) & \cos\left(\omega t - \frac{4\pi}{3}\right) \\ \frac{1}{2} & \frac{1}{2} & \frac{1}{2} \end{bmatrix} \begin{bmatrix} f_a \\ f_b \\ f_c \end{bmatrix} \tag{3.3}$$

The active and reactive power of the generator output in the αβ reference frame, assuming a balanced three-phase system are given as (Rodriguez et al., 2013, Rajapakse et al., 2017a):

$$P = v_{s\alpha} i_{s\alpha} + v_{s\beta} i_{s\beta} \tag{3.4}$$

$$Q = v_{s\beta} i_{s\alpha} - v_{s\alpha} i_{s\beta} \tag{3.5}$$

where P and Q are active and reactive power respectively, v_s and i_s are the source voltage and current respectively while subscripts α and β represent the real and imaginary axes respectively. The space vector models of the three-phase source voltage ($\vec{v}$) and source current ($\vec{i}$) derived from the phase voltages (v_{sa}, v_{sb}, v_{sc}), and currents (i_{sa}, i_{sb}, i_{sc}) can be represented by (Parvez et al., 2015, Rajapakse et al., 2017a):

$$\vec{v}_s = \frac{2}{3} \left(v_{sa} + \vec{\omega} v_{sb} + \overrightarrow{\omega^2} v_{sc}\right) \tag{3.6}$$

$$\vec{i}_s = \frac{2}{3} \left(i_{sa} + \vec{\omega} i_{sb} + \overrightarrow{\omega^2} i_{sc}\right) \tag{3.7}$$

where $\vec{\omega} = e^{\frac{j2\pi}{3}}$. The mathematical model of the variable speed multi-pole PMSG in the dq synchronous rotating reference frame, assuming symmetrical stator windings, negligible stator slots' effect on the rotor inductances with rotor position, negligible magnetic hysteresis and saturation effects, and constant power losses in windings can be given by (Krishnan, 2010, 2009, Rajapakse et al., 2017a, Hughes and Heap, 2009)

$$v_{sd} = R_s i_{sd} + L_d \frac{di_{sd}}{dt} - \omega_e L_q i_{sq} \tag{8}$$

$$v_{sq} = R_s i_{sq} + L_q \frac{di_{sq}}{dt} + \omega_e L_d i_{sd} + \omega_e \Psi_{pm} \tag{9}$$

while the PMSG's flux and electromagnetic torque are

$$\Psi_{sd} = L_d i_{sd} + \Psi_{pm} \; ; \Psi_{sq} = L_q i_{sq} + 0 \tag{3.10}$$

$$T_e = 1.5 n_p \left[\left(L_d - L_q \right) i_{sd} i_{sq} + \Psi_{pm} i_{sq} \right] = 1.5 n_p \Psi_{pm} i_q \tag{3.11}$$

Rewriting (3.4) and (3.5) in the dq synchronous rotating reference frame one gets

$$P = T_e \omega_m = 1.5 \left(v_{sd} i_{sd} + v_{sq} i_{sq} \right) \tag{3.12}$$

$$Q = 1.5 \left(v_{sq} i_{sd} - v_{sd} i_{sq} \right) \tag{3.13}$$

where i_{sd} and i_{sq} are the physical current quantities transformed into the dq frame, v_{sd} and v_{sq} are the physical voltage quantities transformed into the dq frame, R_s is the stator's resistance, $L_d = L_q$ are the inductances of the PMSG on the dq axis, Ψ_{pm} is the permanent magnet flux, Ψ_{sd} and Ψ_{sq} are the flux components respectively in the d and q axes, T_e is the generator's electromagnetic torque, and ω_m is the mechanical angular speed of the generator.

The formulas associated with the turbine and generator rotor, considering the direct drive system of the turbine generator and zero rotational damping coefficient can be written as (2009, Rajapakse et al., 2017a, Lekube et al., 2017)

$$J . \frac{d\omega_m}{dt} = T_m - T_e \tag{3.14}$$

where $J = J_e + \frac{J_t}{n_g}$; J_e , J_t and J are the inertia of the generator, turbine and the combined system respectively, T_m is the mechanical torque of the turbine, $n_g$is the gear ratio which is 1. The generator rotor electrical angular speed (ω_e) can be written with reference to the number of pole pairs (n_p) and the electric frequency(f_e) as

$$\omega_e = n_p . \omega_m = 2\pi f_e \tag{3.15}$$

Both PMSG and power grid models have been designed using equations (3.2) – (3.15). AC grid has been modelled by a constant voltage source in the study assuming a strong grid.

3.5 Li-Ion battery model

As mentioned above, energy storage is becoming an integral part of WEC systems which improves the dynamic behaviour of the overall system, allowing stable operation regardless of the variations in waves. The storage system stores the excess electricity production making wave energy more dispatchable; with continuous supply shifts (Kempener and Borden, 2015, Leuchter, 2011). Even though supercapacitor or superconductive magnetic energy storage has advantages of long life, continuous power and attractive temperature range, batteries found to be more suitable for this project due to the requirement of the storage system to supply shifts which demand long charge/ discharge periods (Kempener and Borden, 2015). Li-Ion batteries were selected among all the other commercially available battery types in the market due to its advantages over others explained in (Kim et al., 2017b). According to (2017a) and (2015) The Li-Ion batteries have been significantly improved in recent years and readily available in the market. Some of the advantages using these batteries are desirable charging efficiency (~98%), high energy density (J/m^3), high volume density (W/m^3), satisfactory specific power (W/kg) with continuous power supply and relatively cheaper value per usable kWh per cycle (Kempener and Borden, 2015, Leuchter, 2011, 2017a). All these desirable characteristics also permit the storage system to use the least amount of space while providing high energy and power (Kempener and Borden, 2015). According to (2015), up to 255 modules of 12V Li-Ion battery could be connected to achieve required voltages and capacity for the proposed BESS. The battery specification sheet (2017a), confirms that the industrial Lithium-ion battery single modules with 88.8 VDC can be connected in unrestricted series and unlimited parallel configurations and provide up to 15000 charge/discharge cycles at 80% depth of discharge (DoD). Since the DoD percentage used in this study's BESS is much less in normal sea conditions the batteries can last for maximum engineered design life which is about 10 years. The state of charge (SoC) control and energy management of the battery is not discussed in this paper. In the proposed system, the battery current is the difference between the current supplied by the rectifier and the current taken out by the inverter. The battery current is not directly controlled in this design. Instead, both of the other currents are controlled using MPC to control the battery current indirectly. The design sets the grid power reference as not to exceed safe operating limits of the battery current in both charging and discharging states.

The mathematical equations for the Li-Ion battery charging ($I_{bat} < 0$) and discharging ($I_{bat} > 0$) could be illustrate as neglecting RC circuits and effect of the change of temperature (Thirugnanam et al., 2014, Rahmoun and Biechl, 2012)

$$V_{b\,dc} = V_0 - K_b \cdot \frac{Q}{Q - it} \cdot I_{bat} - K_b \cdot \frac{Q}{Q - it} \cdot it + A \cdot e^{(-B.it)} \tag{3.16}$$

$$V_{b\,ch} = V_0 - K_b \cdot \frac{Q}{it + 0.1 \cdot Q} \cdot I_{bat} - K_b \cdot \frac{Q}{Q - it} \cdot it + A \cdot e^{(-B.it)} \tag{3.17}$$

Where $V_{b\,dc}$ and $V_{b\,ch}$ are nonlinear voltages of the battery during discharging and charging conditions respectively. V_0 is the constant voltage, I_{bat} is the battery's low frequency current dynamics, K_b is the polarization resistance, it is the extracted capacity, Q is the maximum battery capacity, A is the exponential voltage and B is the exponential capacity. The electrical power conversion system is designed to maintain the I_{bat} in desired current limits for normal sea conditions.

3.6 MPC for the Power Conversion Systems

The finite control set (FCS) MPC with short prediction horizon has been proposed for the OWC power converters over many other modern control schemes such as fuzzy logic control, neural networks, sliding mode control, etc. due to its simplicity and fast response (Rajapakse et al., 2017a). The FCS-MPC fulfils the function of the PWM block and cascade multi loop PI control (Rodriguez and Cort´es, 2012). This facilitates the software based optimal solutions with industry flexibility and simplicity. These software based solutions also permit to address several objectives simultaneously.

As mentioned in (Rajapakse et al., 2017a), in this control scheme, a model of the system is considered to predict the future behaviour of the variables (Rodriguez et al., 2013, Vazquez et al., 2014). According to (Parvez et al., 2015) and (Rodriguez and Cort´es, 2012), MPC controllers are not only simpler than voltage oriented control (VOC) based pulse width modulator (PWM) but also accurately track the reference value by generating the optimum switching signal. Also, the MPC algorithm is easy to configure with constraints and non-linearity (Parvez et al., 2015, Vazquez et al., 2014, Rodriguez et al., 2013). The FCS-MPC requires high processing power and high accuracy of model parameters. At present powerful microprocessors overcome the issue of computational complexity with their high speed and

reduced cost (Vazquez et al., 2014). The inaccuracy or variations of parameters could be addressed with adaptive technologies which observe the behaviour of the system for given inputs and update the parameters accordingly.

The fast microcontrollers such as TMS320F28377S (200MHz) (Texas Instruments, 2017) with high speed calculations enable fast sampling which permit online implementation of MPC, to simplify system optimisation problems with the aid of the discrete nature of power converters. To design an MPC for the control of a power converter, first the power converter should be modelled identifying all possible switching states and its relation to the input and output parameters such as current, voltage, etc. Then the discrete time models should be obtained to predict the future behaviour of the variables that are to be controlled. The last step is to define the cost function to gain the desired outcome (Rodriguez and Cort´es, 2012, Rodriguez et al., 2013). In 2016, M. Abdelrahem, C. Hackl and R. Kannel (Abdelrahem et al., 2016) proposed a similar sensor-less FCS-MPC for a variable speed wind turbine system with model reference adaptive system (MRAS) observer to estimate the generator rotor speed and position. According to (Abdelrahem et al., 2016),(Rodriguez and Cort´es, 2012) and (Rodriguez et al., 2013) this sensor-less FCS-MPC with short prediction horizon control strategy is a promising control technology for achieving accurate control of the converters. As these calculations are based on the generator model it is simple, acts fast and does not require tuning.

In an OWC system, as the torque varies, input power to the generator varies and thus the AFE rectifier has to control the speed of the turbine to either a set speed, or different speed levels to maintain the turbine speed at an optimum level to achieve the maximum efficiency of the turbine. The project that this research is based on requires its turbine speed to be maintained at 650rpm (Wave Swell Energy, 2017, Fleming et al., 2017). This control objective is given to the proposed MPC which predicts the speed in the next sampling interval for all the switching combinations of the rectifier and selects the combination which has the lowest speed error. Figure 3. 4, shows the bloc diagram of the proposed control system.

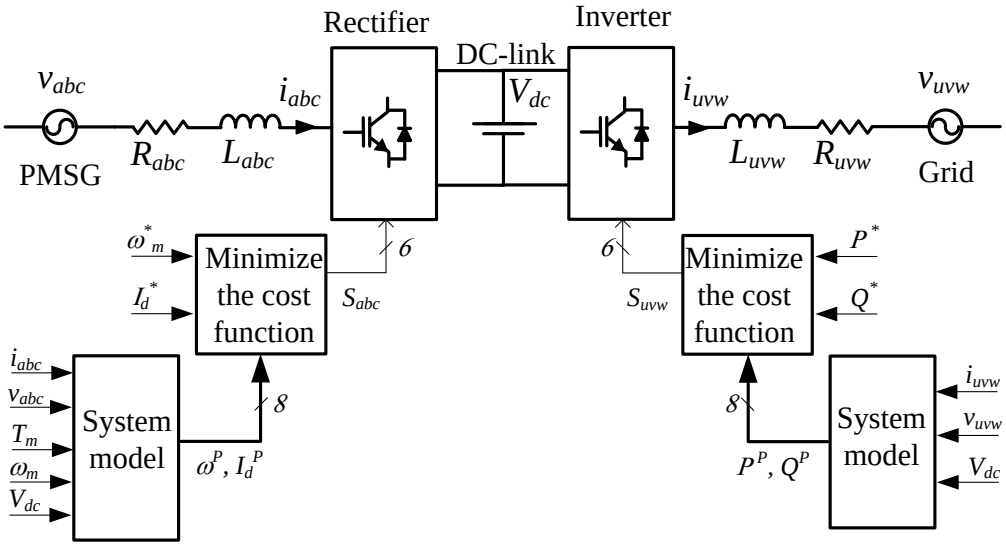

Figure 3. 4: MPC for Active Front End Rectifier and Two-Level Voltage Source Inverter.

The control objective of 2L-VSI controller is to control active and reactive power electrical variables to pre-set values. The 2L-VSI MPC predicts the active and reactive power in the next sampling interval for all the switching combinations of the inverter and selects the combination which has the lowest power error.

3.6.1 Active Front End Rectifier (AFE rectifier) Model

The rectifier consists of 6 IGBT-diode switches. The circuit is fed by the ac voltage (v_s), generated by the PMSG, through combination of source and line filter inductances $L_s = [(L_{sa} + L_{fa}), (L_{sb} + L_{fb}), (L_{sc} + L_{fc})]^T$ and resistances $R_s = [(R_{sa} + R_{fa}), (R_{sb} + R_{fb}), (R_{sc} + R_{fc})]^T$. A dc-link capacitor ($C_{dc}$) reduces the voltage ripples. The IGBT switches operate in such a manner that two IGBTs connected to the same phase are operated as a contrary pair to avoid short circuits (e.g., when S_{a1} is ON, S_{a2} is OFF, and vice versa). The rectifier's switching state is determined by the gating signals S_a, S_b and S_c. These three switching signals can produce eight consequent switching states resulting in eight possible voltage vectors as presented in Table 1 (Rajapakse et al., 2017a, Abdelrahem et al., 2016, Parvez et al., 2015).

Table 3.1: Switching states and voltage space vectors of three phase voltage source.

Switching states			Voltage space vector
S_a	S_b	S_c	$\overrightarrow{v_{AFE}}$
0	0	0	$\overrightarrow{v_0} = 0$
1	0	0	$\overrightarrow{v_1} = 2v_{dc}/3$
1	1	0	$\overrightarrow{v_2} = v_{dc}/3 + j\, v_{dc}/\sqrt{3}$
0	1	0	$\overrightarrow{v_3} = -v_{dc}/3 + j\, v_{dc}/\sqrt{3}$
0	1	1	$\overrightarrow{v_4} = -2v_{dc}/3$
0	0	1	$\overrightarrow{v_5} = -v_{dc}/3 - j\, v_{dc}/\sqrt{3}$
1	0	1	$\overrightarrow{v_6} = v_{dc}/3 - j\, v_{dc}/\sqrt{3}$
1	1	1	$\overrightarrow{v_7} = 0$

The switching function vector ($\overrightarrow{S}$) can then be written as

$$\vec{S} = \frac{2}{3}\left(S_a + \vec{\omega}S_b + \overrightarrow{\omega^2}S_c\right) \tag{3.18}$$

while the rectifier's space vector ($\vec{v}_{AFE}$) related to phase to neutral voltages (v_{a0}, v_{b0}, v_{c0}) and dc bus voltage (V_{dc}) can be written as (Parvez et al., 2015, Liu et al., 2016, Rajapakse et al., 2017a)

$$\vec{v}_{AFE} = \frac{2}{3}\left(v_{a0} + \vec{\omega}v_{b0} + \overrightarrow{\omega^2}v_{c0}\right) \tag{3.19}$$

$$\vec{v}_{AFE} = \vec{S} \cdot v_{dc} \tag{3.20}$$

The relationship between the generated three-phase voltage vectors and the rectifier's input voltage vectors can be obtained by applying Kirchhoff's voltage law to the input side of the rectifier as (Rajapakse et al., 2017a)

$$\vec{v}_s = L_s \frac{\overrightarrow{di_s}}{dt} + R_s\vec{i}_s + \frac{2}{3}\left(v_{a0} + \vec{\omega}v_{b0} + \overrightarrow{\omega^2}v_{c0}\right) - \frac{2}{3}\left(v_{n0} + \vec{\omega}v_{n0} + \overrightarrow{\omega^2}v_{n0}\right) \tag{3.21}$$

The input current dynamics of the rectifier, derived from (3.19), (3.21) and assuming

$\frac{2}{3}\left(v_{n0} + \vec{\omega}v_{n0} + \overrightarrow{\omega^2}v_{n0}\right) = -v_{n0}\ \frac{2}{3}\left(1 + \vec{\omega} + \overrightarrow{\omega^2}\right) = 0$, can be written as (Parvez et al., 2015, Rajapakse et al., 2017a)

$$\frac{\overrightarrow{di_s}}{dt} = -\frac{R_s}{L_s}\vec{i}_s + \frac{1}{L_s}\vec{v}_s - \frac{1}{L_s}\vec{v}_{AFE} \tag{3.22}$$

The MPC-based controller is formulated in the discrete-time domain. Therefore, the rectifier's input current and rectified voltage have to be derived in a discrete-time model, using Euler's approximation method with one switching period where T_s is the sampling time ($T_s > 0;\ kTs \leq t \leq (k+1)Ts$) and k is the sampling instant of (Rajapakse et al., 2017a)

$$\frac{\overrightarrow{di_s}}{dt} \approx \frac{\vec{i}_s\,(k+1) - \vec{i}_s\,(k)}{T_s} \tag{3.23}$$

for the $(k+1)$ sampling instant from (22) and (23) as (Rodriguez et al., 2013, Parvez et al., 2015, Liu et al., 2016, Quevedo et al., 2012, Rajapakse et al., 2017a)

$$\vec{i}_s\,(k+1) = \left(1 - \frac{R_s T_s}{L_s}\right)\vec{i}_s(k) + \frac{T_s}{L_s}\left(\vec{v}_s(k) - \vec{v}_{AFE}(k)\right) \tag{3.24}$$

3.6.2 FCS- MPC for AFE rectifier

The proposed control structure is designed to maintain the turbine speed at 650 rpm. The FCS-MPC algorithm minimizes the error between reference and predicted angular speeds, denoted respectively by ω^* and ω^p. The discrete time model for the (k+1) sampling time instant is (Rajapakse et al., 2017a)

$$\omega^p = \omega_m(k+1) = \omega_m(k) + \frac{T_s}{J}\ (T_m - T_e(k+1)) \tag{3.25}$$

In the control system, the future value of current, $i_s(k+1) = i_s^p$ is calculated from measured $v_s(k)$, $i_s(k)$ and $v_{dc}(k)$ by MPC controller using (19) for each one of eight possible switching vectors ($\vec{S}$). Then, i_s^p is converted into dq frame (i.e., i_d^p and i_q^p) to calculate ω^p of the turbine rotor, before it is compared to ω^* using the cost function of (g_{rec}) from (Rajapakse et al., 2017a)

$$g_{rec} = \left| \omega^{*} - \omega^{p} \right| + K. \left| i_d^{*} - i_d^{p} \right| \quad (3.26)$$

to select the switching state which minimizes the cost function. The error between d axis current reference ($i_d^{*} = i_{d\_ref}(k+1)$) and predicted d axis current ($i_d^{p} = i_d(k+1)$) is added to the cost function with an arbitrary constant K to reduce the d-axis current in the generator and thereby, avoid flux weakening. Figure 3. 5. a), illustrates the proposed FCS-MPC control algorithm for the AFE rectifier (Rajapakse et al., 2017a).

3.6.3 Two Level Voltage Source Inverter (2L-VSI) Model

As shown in Figure 3. 1, the 2L-VSI inverter connects the DC link to the AC grid through the line filter inductances $L_g = [(L_{gu} + L_{fu}), (L_{gv} + L_{fv}), (L_{gw} + L_{fw})]^T$ and resistances $R_g = [(R_{gu} + R_{fu}), (R_{gv} + R_{fv}), (R_{gw} + R_{fw})]^T$. This is designed to control the output active and reactive power as required by the grid code (Rodriguez et al., 2013, Liu et al., 2016, Parvez et al., 2016). 2L-VSI's IGBT switches are operated in a similar manner as the AFE rectifiers. The inverter switching state is determined by the gating signals S_u, S_v and S_w.

The relationship between the grid three phase AC voltage and inverter input voltage vectors are obtained by applying Kirchhoff's voltage law to the output side of the 2L-VSI as

$$\vec{v}_{VSI} = L_g \frac{\overrightarrow{di_g}}{dt} + R_g \vec{i}_g + \frac{2}{3}\left(v_{gu} + \vec{\omega} v_{gv} + \overrightarrow{\omega^2} v_{gw}\right) + \frac{2}{3}\left(v_{E0} + \vec{\omega} v_{E0} + \overrightarrow{\omega^2} v_{E0}\right) \quad (3.27)$$

where $v_g$is the grid voltage and i_g is the grid current. The input current dynamics of the 2L-VSI is written as (Parvez et al., 2015)

$$\frac{\overrightarrow{di_g}}{dt} = -\frac{R_g}{L_g} \vec{i}_g - \frac{1}{L_g} \vec{v}_g + \frac{1}{L_g} \vec{v}_{VSI} \quad (3.28)$$

FCS-MPC controller proposed for this system is formulated in the discrete time domain similar to the AFE rectifier controller. The discrete time model for the (k+1) sampling instant is (Parvez et al., 2015, Quevedo et al., 2012, Liu et al., 2016)

$$i_g(k+1) = \left(1 - \frac{R_g T_g}{L_g}\right) i_g(k) + \frac{T_s}{L_g}\left(v_{VSI}(k) - v_g(k)\right) \quad (3.29)$$

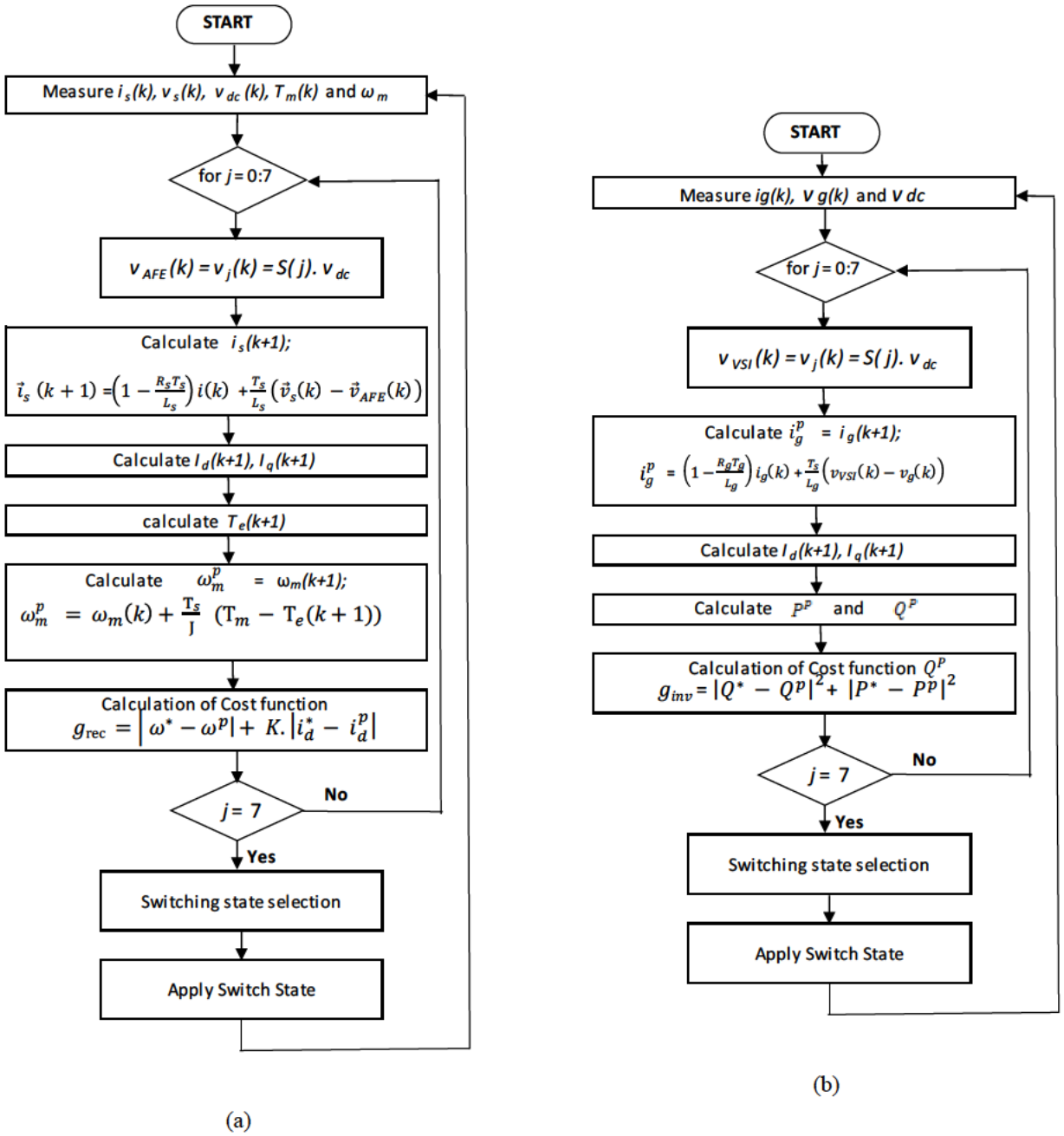

Figure 3. 5: a). MPC algorithm flow chart for the AFE rectifier, b). MPC algorithm flow chart for the grid-connecting inverter.

3.6.4 FCS - MPC for 2l_VSI

The proposed control structure is designed to minimize the errors between reference power and predictive power. The errors between active power denoted respectively by P^* and P^p and errors between reactive power denoted respectively by Q^* and Q^p. The reference power values are fixed for the 2L-VSI according to the transmission system operators (TSO) requirements. In

the control system, the future value of $P^p$and Q^p is calculated using future current i_g^p which is $i_g(k+1)$. This is calculated from (29) for each one of eight possible switching vectors ($\vec{S}$). Then the i_g^p and v_g^p is converted into dq rotating reference frame denoted as i_d^p, i_q^p , v_d^p, v_q^p to calculate predictive power values using (12) and (13) before they are compared to reference power value to select the switching state which minimise the cost function (g_{inv}) as (Rodriguez et al., 2013, Parvez et al., 2015)

$$g_{inv} = |Q^* - Q^p|^2 + |P^* - P^p|^2 \tag{3.30}$$

Figure 3. 5. b), illustrates the proposed FCS-MPC control algorithm for the 2L-VSI.

3.7 Simulation Results and Discussion

Simulations were carried out using MATLAB/Simulink software to evaluate and confirm the performance of the proposed FCS-MPC. The parameters given in Table 3. 2, are used to design PMSG, filters and dc link. The generator and battery parameters are taken from (2017b) and (2017a) respectively. The simulation results shown in Figure 3. 6, is used to evaluate the FCS –MPC performance of the AFE rectifier. The performance of the storage system and its ability to uphold the supply power to a set value is evaluated by simulation results shown in Figure 3. 7. The simulation results shown in Figure 3. 8, are used to evaluate the FCS-MPC performance of 2L-VSI.

Table 3. 2: System parameters used in the design.

PMSG	
Rated Power	2MW
Rated rotate speed	650 rpm
Rated Voltage	690VAC
Rated current	1673.5A
Number of pole pairs	6
Resistance (R_s)	0.0024Ω
Inductances ($L_d = L_q$)	0.355mH
Magnetic flux (Ψ_{pm}) (0.119Wb X 6)	0.666Wb
Li-Ion battery storage	
Nominal voltage/ Fully charged voltage	1000V/ 1050V
Rated capacity @ nominal voltage	150Ah (75Ah x 2)
Rated current @ nominal voltage	900A (450A x 2)
Initial state of charge in %	65%
Reference Values	
Active Power	265kW
Reactive Power	0

Generator side Filter	
Inductance	0.5mH
Resistance	0.01 Ω
dc-link	
Capacitance (C_{dc})	470mF
dc-link voltage (V_{dc})	1000V
Grid side Filter	
Inductance	1mH
Resistance	0.1Ω
Grid	
Voltage	690Vrms
Frequency	50Hz
Other	
Sample time	10^{-5} seconds
Simulator run-time	20 seconds
Total Inertia (J)	0.25kgm^2

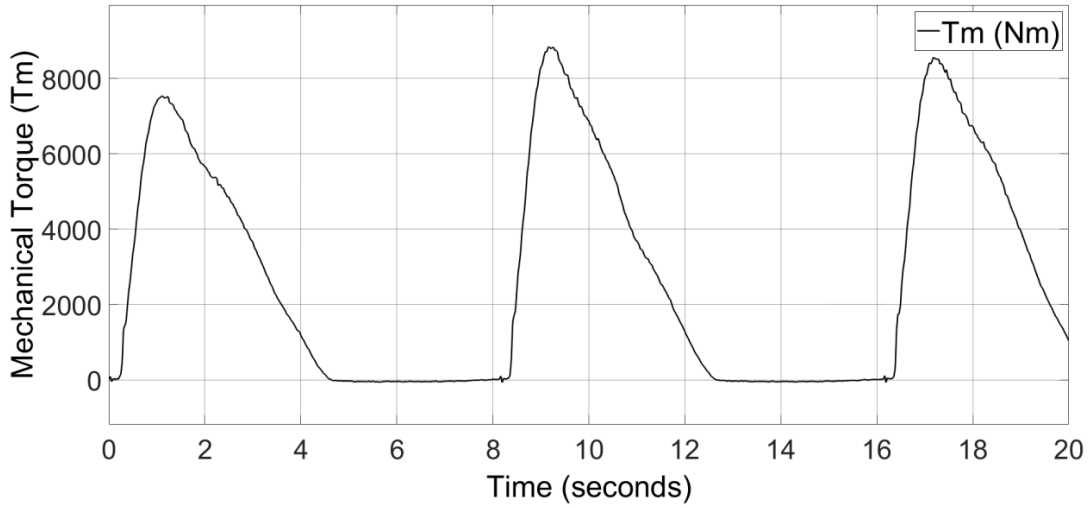
Tm (Nm)
Mechanical Torque (Tm)
8000
6000
4000
2000
0
0
2
4
6
8
10
12
14
16
18
20
Time (seconds)

(a)

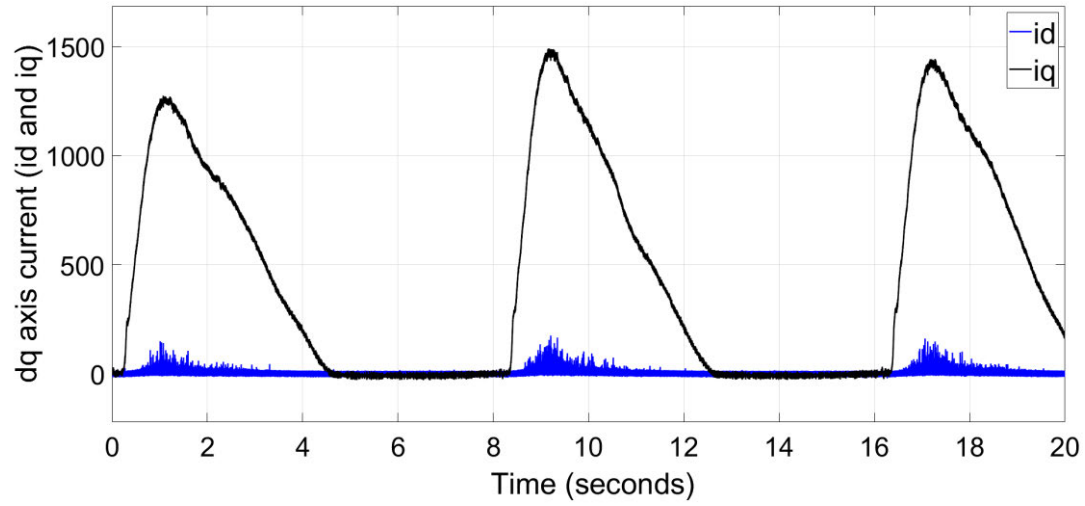
id
iq
dq axis current (id and iq)
1500
1000
500
0
0
2
4
6
8
10
12
14
16
18
20
Time (seconds)

(b)

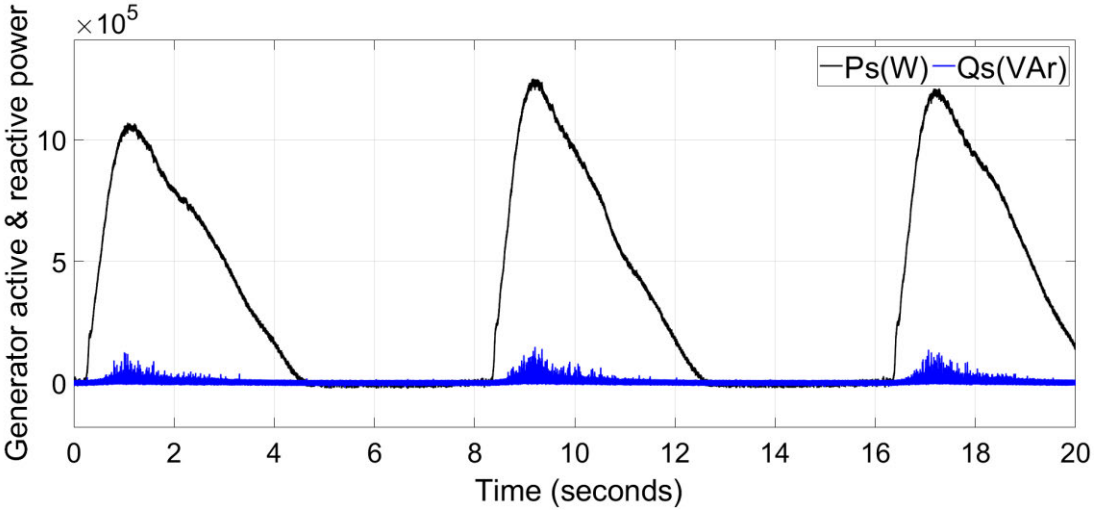
×10^5
Ps(W)
Qs(VAr)
Generator active & reactive power
10
5
0
0
2
4
6
8
10
12
14
16
18
20
Time (seconds)

(c)

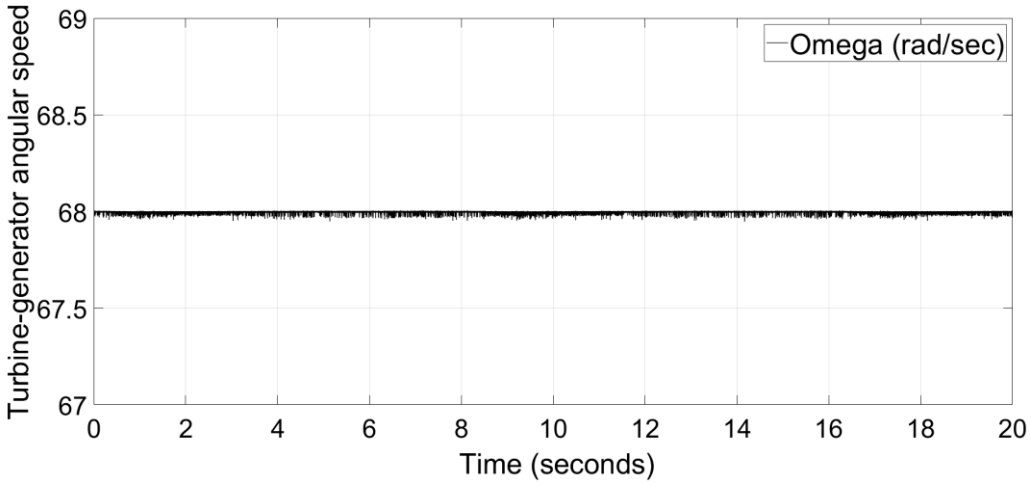
Omega (rad/sec)
Turbine-generator angular speed
69
68.5
68
67.5
67
0
2
4
6
8
10
12
14
16
18
20
Time (seconds)

(d)

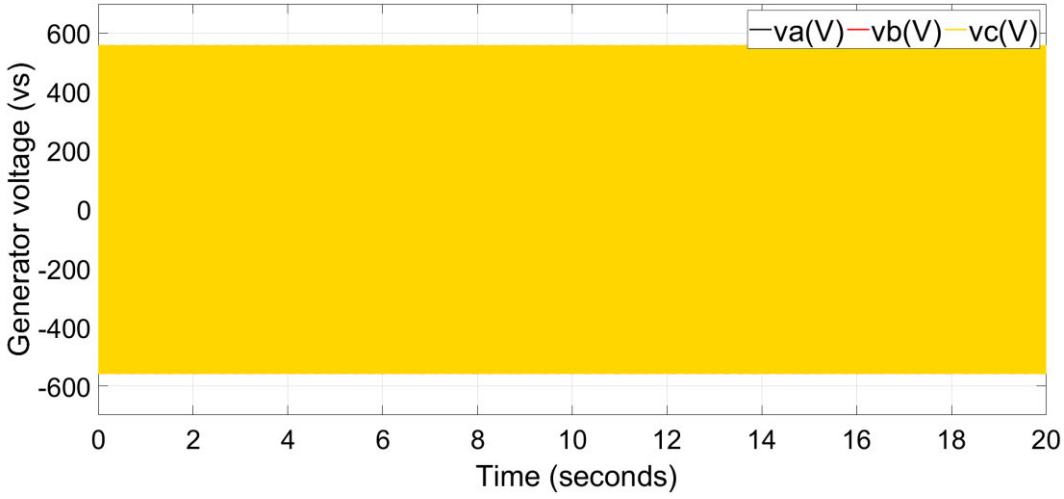
va(V)
vb(V)
vc(V)
Generator voltage (vs)
600
400
200
0
-200
-400
-600
0
2
4
6
8
10
12
14
16
18
20
Time (seconds)

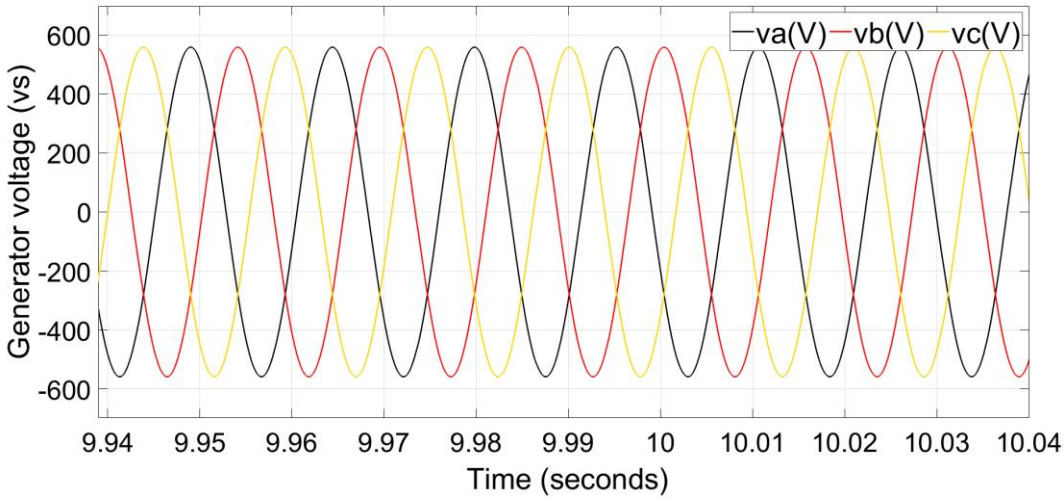
va(V)
vb(V)
vc(V)
Generator voltage (vs)
600
400
200
0
-200
-400
-600
9.94
9.95
9.96
9.97
9.98
9.99
10
10.01
10.02
10.03
10.04
Time (seconds)

(e)

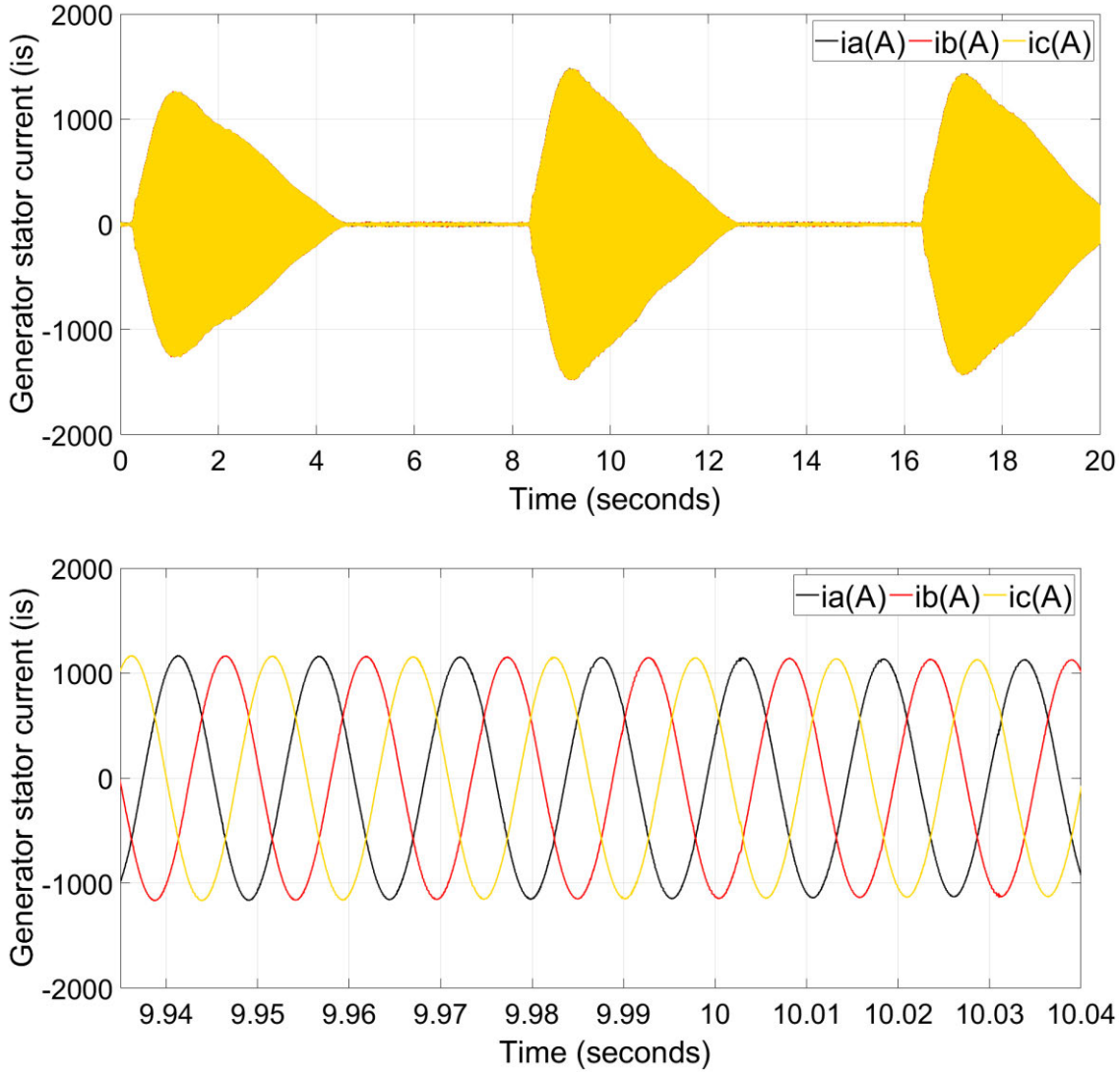

(f)

Figure 3. 6: The FCS –MPC performance of AFE rectifier: a). Mechanical torque profile T_m(Nm), b). PMSG stator current in dq(A) rotational reference frame, c). Generator active power P_s(W) and reactive power Q_s(VAr), d). Generator rotor angular speed Omegam(rad/sec), e). Generator voltage v_s(V), f). Generator current i_s(A).

The torque profile obtained from the research data from which is used as the mechanical input to the PMSG is shown in Figure 6. a). Figure 6. b), shows the stator current in dq rotational reference frame. The d-axis current remains closer to zero while the q-axis current varies in proportion to the torque input. This variation of the q-axis current directly affects the active power drawn from the generator which also varies in proportion to the torque as shown in Figure 6. c). This figure also illustrates the generator's reactive power which is maintained at zero. Figure 6. d), confirms that the rotor angular speed is following the reference value 68rad/s which is set as the target operating conditions of

the air turbine. Figure 6. e) and 6. f), illustrate the PMSG's output voltage and current respectively which are nearly sinusoidal. The MPC controller maintains the voltage input at a nearly constant level to the rectifier while current varies according to the power input. These results confirm the ability of the proposed controller to extract power from OWC air turbine under varying input torque.

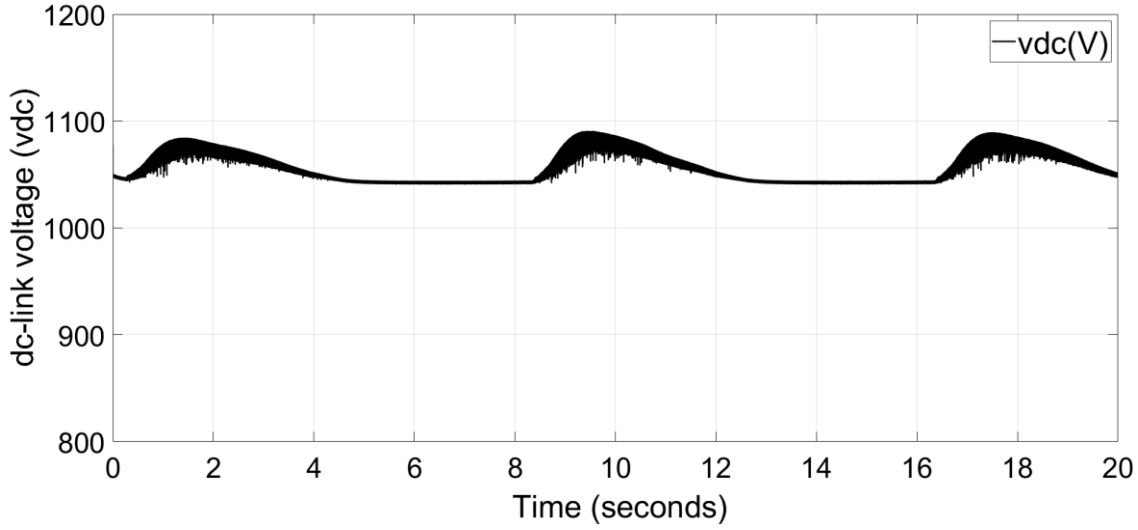

(a)

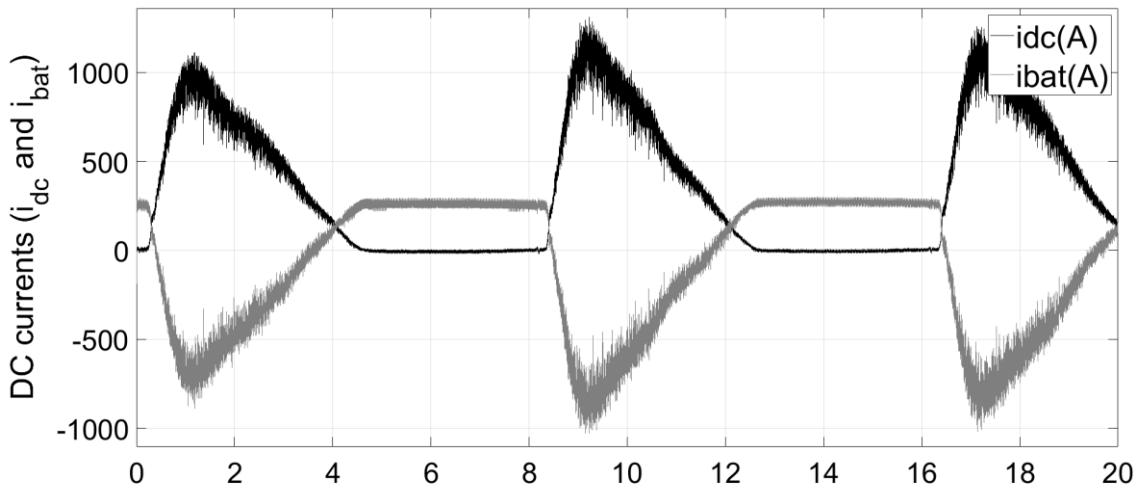

(b)

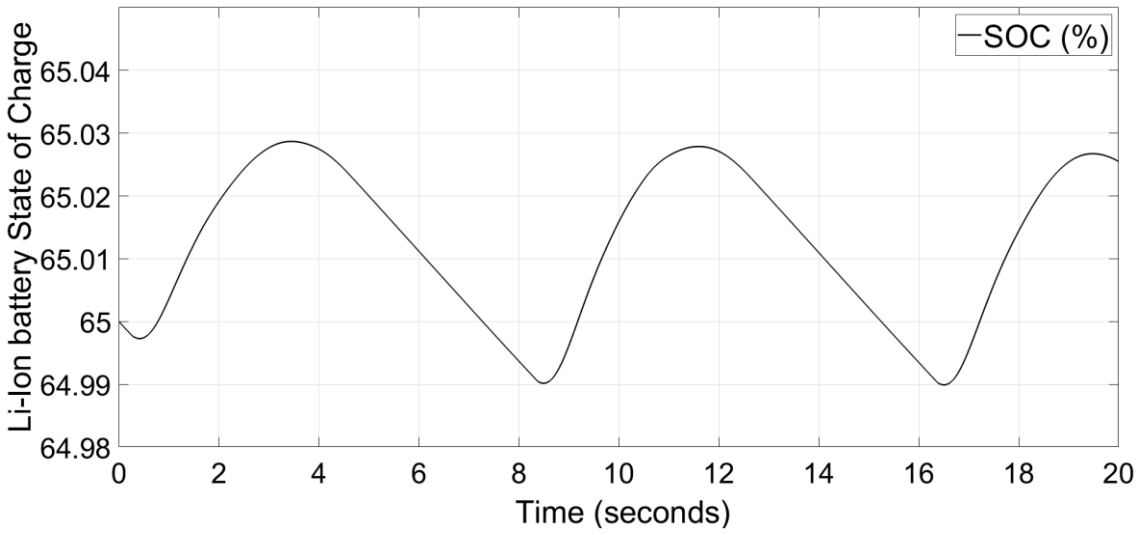

(c)

Figure 3. 7: The performance of Energy storage and the dc-link: a). dc link voltage V_{dc}(V), b). dc link current I_{dc}(A) and battery current I_{bat}(V), c). State of Charge of the battery SoC%.

Figure 3. 7. a), depicts the dc-link voltage which varies within a small range (5%) in proportion to the power captured by the turbine. Figure 3. 7. b), shows dc-link current and battery current, which vary with the input power. The battery current remains within its charge and discharge currents limits and thus these results confirm that the battery power is indirectly controlled by the rectifier controller and inverter controller. Figure 3. 7. c), illustrates the percentage of the battery's SoC which remains nearly at an initial value with about 0.03% variation for the given sea conditions. These results show that battery charges when the input power is higher than the set power output and discharges when the input power is lower. Therefore, the proposed battery direct- connection method and the control technology are able to deliver smooth power output to the grid without going into unstable conditions under varying input power conditions.

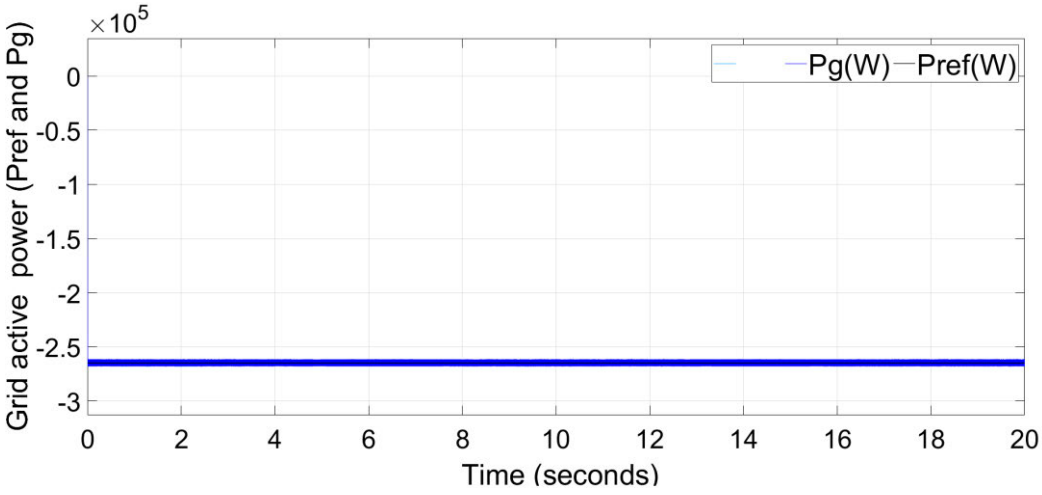
×10^5
Grid active power (Pref and Pg)
Pg(W)
Pref(W)
Time (seconds)

(a)

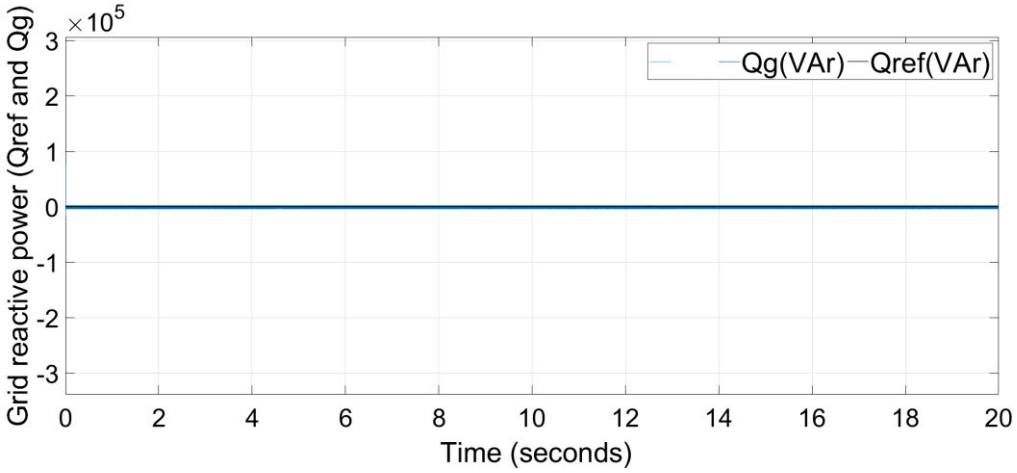
×10^5
Grid reactive power (Qref and Qg)
Qg(VAr)
Qref(VAr)
Time (seconds)

(b)

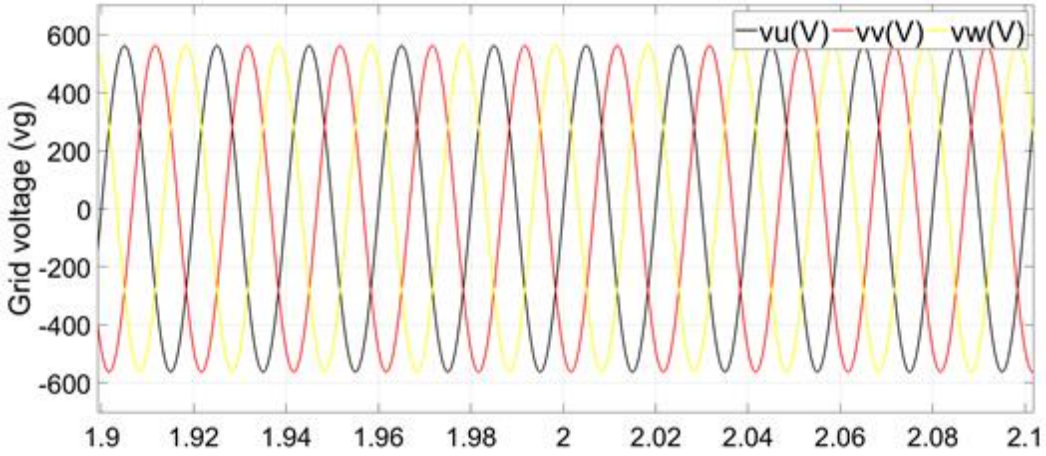
Grid voltage (vg)
vu(V)
vv(V)
vw(V)

(c)

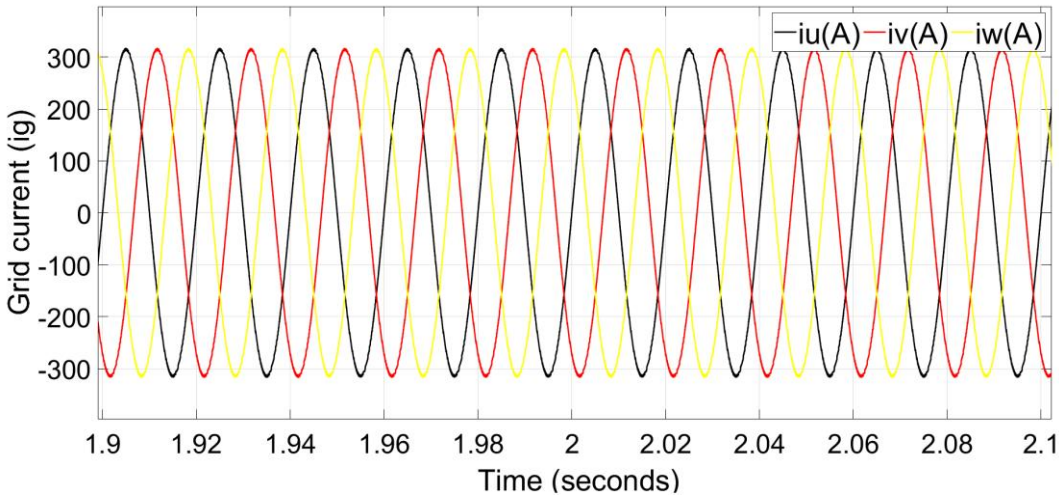

(d)

Figure 3. 8: The FCS –MPC performance of 2L-VSI: a). Active power output to the grid P_g(W), b). Reactive power output to the grid Q_g(VAr), c). Grid voltage v_g(V), d). Grid current i_g(A).

Figures 3. 8. a) and 3. 8. b), show the active and reactive power supplied to the grid respectively. The figures depict smooth power output with almost 0% deviation from the set power refernces. Figure 3. 8. c) and 3. 8. d), confirm that the 3 phase output voltage and current are in-phase and the total harmonic distortion (THD) of the three phase currents (I_{uvw}) is around 0.68% which is much lower than the IEEE standards (5%) (2014). These results depict the ability of the proposed MPC to deliver the constant and quality power to the ac grid under varying dc-link voltages.

3.8 Conclusion

This paper proposes a FCS-MPC strategy for electrical power control of OWC air turbine generators which uses a back-to-back power converter system and Li-ion BESS directly connected to the dc link. Simulation results confirmed that the proposed control strategy along with the direct-connected BESS enable smooth power delivery to the grid. The FCS-MPC applied to the AFE rectifier is able to control the speed of the turbine at the set point of 68 rad/sec to maintain the air turbine within its optimum efficiency range under varying wave conditions. The 2L-VSI's FCS-MPC is able to maintain the output power, minimising the error between the set point and the supply. The Li-ion BESS helps improve the smooth power delivery to the grid by absorbing fluctuations present in the input power. The THD of the output current is below the grid code requirement of 5%.

The battery charge and discharge currents are indirectly controlled by the controllers of the back to back power converter system to remain within safe operation limits. In overall, the proposed electrical power conversion system has confirmed its ability to improve the quality of power supply to match the grid codes irrespective of the intermittencies present in the extracted power from the waves under varying wave conditions.

Although the results obtained from this study are very promising further investigations and implementations are required for experimental validations and the development of an adaptive system against parameter variations.

4

GRID INTEGRATION AND POWER SMOOTHING OF AN OSCILLATING WATER COLUMN WAVE ENERGY CONVERTER

This chapter was published in the special issue on ‘Wave and Tidal Energy’ of the ‘Energies’ journal, the citation for the research article is:

G. Rajapakse, S. G. Jayasinghe, A. Fleming, and Michael Negnevitsky, "Grid Integration and Power Smoothing of an Oscillating Water Column Wave Energy Converter," *Energies 2018*, vol. 11, no. 07, 2018.

Abstract

This paper applies model predictive control for the power processing of an oscillating water column (OWC) wave energy converter (WEC) system to achieve smooth power delivery to the grid. The particular air turbine design adopted in this study produces large power pulses ranging from 0 to 1MW in magnitude and thus the direct connection to the grid is practically impossible, especially in weak grid conditions. Therefore, energy storage is an essential element that should be integrated into this particular WEC system in order to absorb power pulses and thereby ensure smooth delivery of power to the grid. Taking the repetitive nature, duration and magnitude of the power pulses this study has chosen 'supercapacitor' as the suitable energy storage technology. The supercapacitor energy storage is integrated into the dc-link of the back-to-back power converter of the WEC system through a bidirectional dc-dc converter. In order to achieve the desired operation of this complex power converter arrangement a finite control set model predictive control strategy is proposed in this paper. Performance of the proposed energy storage system and control strategy are evaluated through computer simulations. Simulation results show that the proposed supercapacitor energy storage system and the control strategy are able to achieve smooth power delivery to the grid amidst power pulses coming from the -generator.

Keywords: DC-DC bidirectional converter, finite control set - model predictive control, oscillating water column, supercapacitor energy storage.

4.1 Introduction

Oceans which cover 70% of the earth offer vast amount of renewable energy. Out of many forms, wave energy is an accessible and widely available type of ocean energy. Recent studies have shown that wave energy has the potential to make significant contributions to the renewable energy targets worldwide (Aderinto and Li, 2018, Hannon et al., 2016, Carson et al., 2014). Australia has been identified as a wave-energy rich country having the potential to extract more energy from waves than its total annual electricity demand (Hannon et al., 2016). Recognizing this potential many companies have invested in wave energy projects in Australia (Carson et al., 2010, Carson et al., 2014, Hughes and Heap, 2009). Out of many technologies used to harness energy from waves the oscillating water column (OWC) wave energy converter (WEC) technology has the advantage of having all of its moving parts above the water level allowing relatively straightforward installation and easy access for maintenance (Hannon et al., 2016, Wave Swell Energy, 2017). These are key factors for cost reduction in any renewable energy technology and thus, with the improved performance, OWC energy converters will be able to compete with other renewable and fossil-fuel energies in the energy market.

The OWC concept utilizes a water column inside a partially submerged hollow concrete structure. With the incident wave the oscillating water column inside the chamber oscillates the air column above it and result in exhale and inhale air streams through the open end of the chamber. The energy of these air streams is converted into electricity with the aid of the turbine coupled generator. The common turbine types used are bidirectional and absorb the energy during both inhale and exhale stages.

Australian maritime college, in collaboration with the Wave Swell Energy ltd., has developed a new OWC air turbine technology which has been recognized as efficient and simple design compared to many other OWC technologies (Wave Swell Energy, 2017, Australian Maritime Collage, 2017). This particular configuration has passive non-return air flow valves built into its chamber which activate during the exhale stage and equalize the pressure inside the chamber to the atmosphere which allows the rising water column to reach its maximum height. This results in higher differential pressure during the inhale stage resulting in high velocity air stream through the air-turbine. Since this particular air-turbine extracts power only during the inhale stage the output power inherently becomes

discrete pulses. These large and discrete power pulses create major operational issues such as frequency deviations, voltage sags/swells and instabilities if delivered to the grid without smoothing. Therefore, energy storage is an essential feature that should be incorporated into the power converter of the WEC system. Nevertheless, in contrast to wind energy or tidal energy turbines where the rotational speed should be changed according to the wind speed or tidal flow speed, the unidirectional air-turbine used in this study does not necessarily require variable speed operation. Therefore, according to (PerAero Turbine Design LLC., 2017), the turbine speed can be regulated to remain within the optimum speed range irrespective of the air flow. This eliminates the need for complex maximum power point tracking strategies and thus the machine side converter controller becomes relatively less complex. However, the abovementioned large and discrete power pulses are unique to this WEC system compared to other types OWC and thus special attention has to be paid when developing associated control strategies.

As mention above, the promising approach to overcome the issues related to power pulses is the use of an energy storage system (ESS). The ESS absorbs power pulses to provide smooth power delivery to the grid. A comprehensive review of ESS in renewable energy electric power systems is presented in (Hamidi et al., 2017). It has discussed different types of batteries, supercapacitors and hybrid energy storage system (HESS) along with their modeling techniques. It has also highlighted different utility-level power converter topologies and given six examples of ESS in field installations. Some of the desirable qualities of ESS are emphasized in (Rajapakse et al., 2017a), as high charge-discharge efficiency, high energy density, volume power density, high specific energy, high specific power with continuous power supply, long life, relatively cheaper value per usable kWh per cycle, etc. The evidence confirms that that supercapacitors lead the energy storage market with high power density whereas the Li-Ion batteries lead the industry with high energy density. In common, one or both of these ESS are used in many renewable energy applications to stabilize the dc-link voltage (Maercos et al., 2017, Murray et al., 2013). This study applies a commercially available supercapacitor to smooth the power of the unidirectional air-turbine OWC system. The supercapacitor energy storage (SCES) has very high energy storage efficiency and very high cycling stability with insignificant loss of energy storage capacity (Kim et al., 2017a). A full scale offshore OWC has been investigated in (Murray et al., 2011), and confirmed that supercapacitors are capable of

power smoothing satisfactorily over desirable long periods. Figure 4. 1, illustrates a grid integrated OWC system with SCES.

In (Rajapakse et al., 2017b), authors have proposed to use a Li-Ion battery energy storage (BES) system which is directly connected to the dc-link to absorb power pulses. It has used finite control set model predictive control (FCS-MPC) strategy for the rectifier and inverter of the back-to-back power converter. Due to the facts that the two controllers indirectly control the battery current and the dc-link voltage is governed by the battery, the direct connection is possible for batteries. If supercapacitors are used as the energy storage element the direct connection to the dc-link is not effective as the voltage should be allowed to vary in a wide range to store more energy in supercapacitors. Therefore, an interfacing dc-dc converter is essential for integrating supercapacitors into the power converter system. While the rectifier and inverter controllers proposed in (Rajapakse et al., 2017b) can still be used the dc-dc converter requires an additional converter.

The use of dc-dc bidirectional converters with energy storage such as battery and/or supercapacitor are common in utility level renewable energy systems which act fast to reduce the mismatch between supply and demand power (Hamidi et al., 2015). Several types of such converters have been presented in (Hamidi et al., 2017), that can be used as energy storage interface systems and found that half bridge (HB) type converters are more efficient than many other types since they use less number of passive electronics, smaller inductors and experience lower current stresses. In (hamidi et al., 2013, Wu et al., 2009, Maercos et al., 2017), ESS with HB dc-dc bidirectional converter for a grid connected renewable energy systems was proposed and has explained converter control algorithms using PI control strategy. Also, (Maercos et al., 2017), has provided battery supercacapacitor HESS and a literature review of eighteen similar approaches with respect to their application, system, topology, rated power, comparison, sizing, control and goals related to applications such as energy harvesting, microgrids, remote area power supply, load supply, etc.

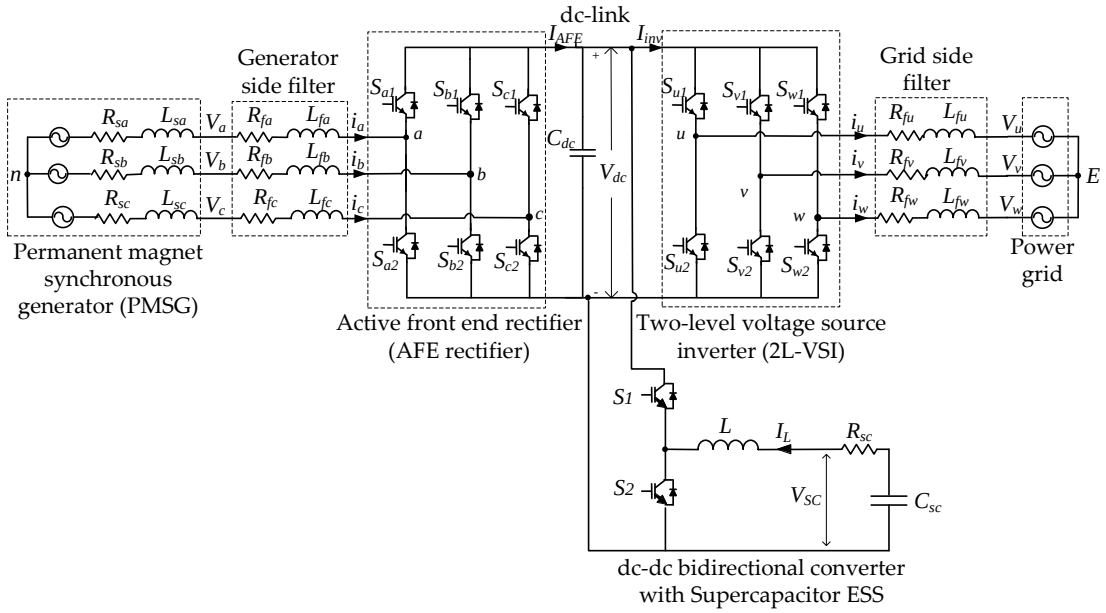

Figure 4. 1: Schematic diagram of electrical power conversion system of OWC - grid integration.

To gain the desirable results from any ESS, which is connected to dc-link using electrical power converter needs an effective control system. It has been achieved in this research applying FCS-MPC strategy for the dc-dc bidirectional converter controller. Figure 4. 2, depicts the schematic diagram of the controllers that are used for electrical power converters.

The MPC digital control approach is taken to control the converters due to its simple, fast, accurate and reliable nature (Rajapakse et al., 2017b, Rodriguez et al., 2013, Vazquez et al., 2014). In (Pirooz and Noroozian, 2016), same control strategy has been applied to dc-dc bidirectional converter with mode activation approach where charge, discharge, and idle modes were designed to operate independently. In (Ceballos et al., 2015), a SCES coupled to the dc-link with dc-dc bidirectional converter was proposed for wells turbine OWC system using field oriented control strategy (FOC). Also, a performance comparison was done between SCES, fixed and variable speed flywheel energy storage systems referring to (Ceballos et al., 2013), (Wu et al., 2009) and (Li et al., 2007). In (Zou and Cheng, 2017), HESS has been used for oscillating wave power generator applying sliding mode control strategy for the whole system. Nevertheless, the feasibility of using supercapacitors for the particular WEC system considered in this study, from the control perspective, is not reported so far. Therefore, the contributions of this paper are to propose supercapacitor energy storage for this particular WEC system, develop a FCS-MPC

strategy for the entire power converter system and verify its performance through computer simulations.

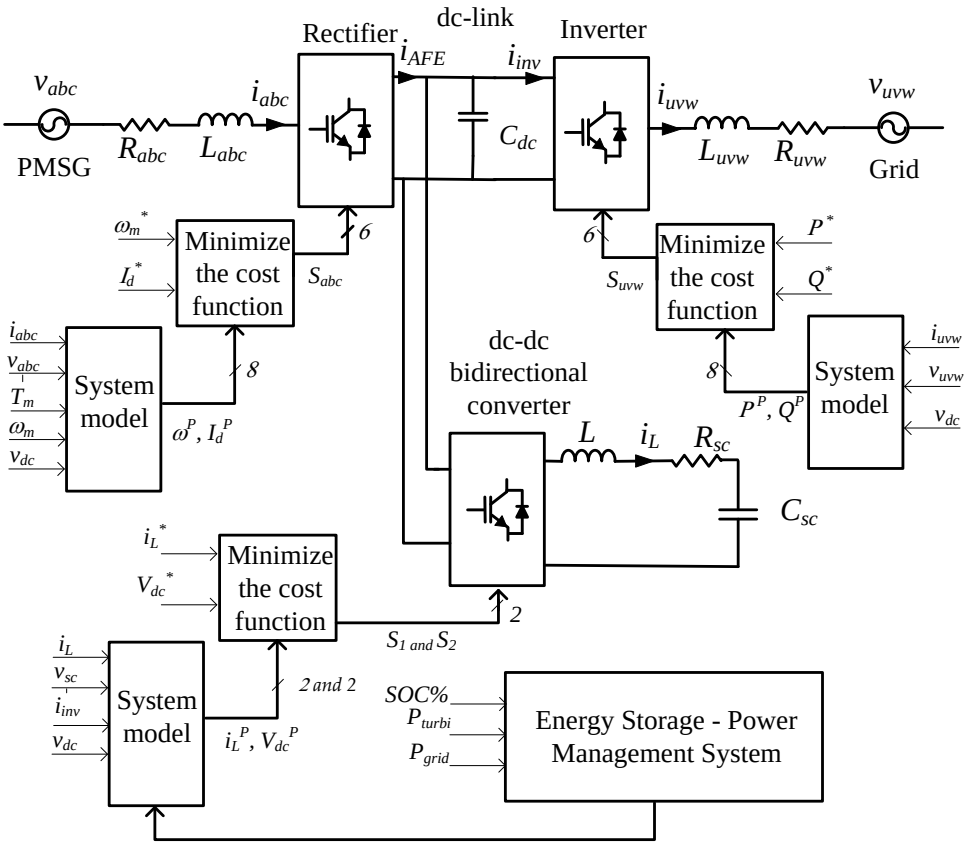

Figure 4. 2: Schematic diagram of the proposed controllers for grid interface of OWC unidirectional air turbine generator with HESS.

The paper is organized as follows. Section 4.2 presents the modeling of SCES. Section 4.3 presents the model predictive control for electrical power converter, followed by the power management system presented in section 4.4. Section 4.5 presents simulation results and discusses the implications of the results. Conclusions derived from the discussion are presented in Section 4.6.

4.2 Supercapacitor Energy Storage

This study uses a supercapacitor bank as the energy storage element which is connected to the dc-link through a bidirectional dc-dc converter. Supercapacitors have the advantage of long life, high power density, attractive temperature range and high charge-discharge efficiency (Rajapakse et al., 2017a). The SCES is cascaded into the OWC electrical power converter system to compensate the power fluctuations and improve the

system dynamics to deliver quality and constant amount of power to the grid despite of the sea condition. With the recent advancements of energy storage technologies supercapacitors have become popular and commercially available for large power applications such as WEC systems. The supercapacitor specification sheet in (Maxwell Technologies, 2017), confirms that the industrial 83F or 165F supercapacitor single modules with 48 VDC can be connected in series and parallel configurations to gain required voltage and capacity. Moreover, these modules provide up to 1,000,000 duty cycles or 10 years of DC life. In this particular system to attain the required voltage of the SCES (1000V) minimum 21 of 48V modules are needed to connect in series which result in decrease of the total capacitance and increase of the total inner resistance (R_{sc}) in each pole. Then, these high voltage modules can be connected in parallel to obtain required total capacitance to gain the energy storage capacity that decreases R_{sc}. Considering R_{sc} which represents only static losses, the stored energy and instantaneous voltage of the supercapacitor are given by (Thounthong et al., 2014)

$$E_{sc} = \frac{1}{2} C_{sc} v_{sc}^2 \tag{4.1}$$

$$v_{SC}(t) = v_0 * e^{-\frac{t}{R_{sc}C_t}} = \frac{Q_0}{C_{SC0}} * e^{-\frac{t}{R_{sc}C_t}} \tag{4.2}$$

where E_{sc} is the supercapacitor energy, C_{SC} is the capacitance of the supercapacitor, v_{SC} is the voltage across supercapacitor, v_0 , $C_{SC0}$and Q_0 are the initial voltage, capacitance and charge of the supercapacitor. C_t is the total equivalent capacitance.

The state of charge (SOC) of the supercapacitor is

$$\begin{aligned} SOC_{sc} &= \left(\frac{Q_0 - \int_0^t i_{sc}(t)\, dt}{Q_t} \right) x\ 100 \\ &= \left(\frac{(C_{SC(0)} * v_{SC(0)}) - \int_0^t i_{sc}(t)\, dt}{C_{SC(t)} * v_{SC(t)}} \right) x\ 100 \end{aligned} \tag{4.3}$$

where i_{sc} and Q_t are the supercapacitor's current and its charge at time t respectively. It is to be noted that the method shown in (3) is one of the conventional methods of estimation of SOC and the nominal capacity decreases gradually over time due to variations in load and the internal chemical reactions. More advanced methods of estimation of SOC have been discussed in (Hannan et al., 2017, Zhi et al., 2017).

The supercapacitor charge (Q_{Sc}) is equal to the product of its capacitance and voltage ($Q_{Sc} = C_{SC} * v_{SC}$). Therefore, SOC_{sc} changes with respect to v_{SC} and vice versa. Figure 4. 3. a), shows a typical supercapacitor charge/current behavior with respect to the time and Figure 4. 3. b), shows the charge/discharge curves of supercapacitor and Li-Ion battery.

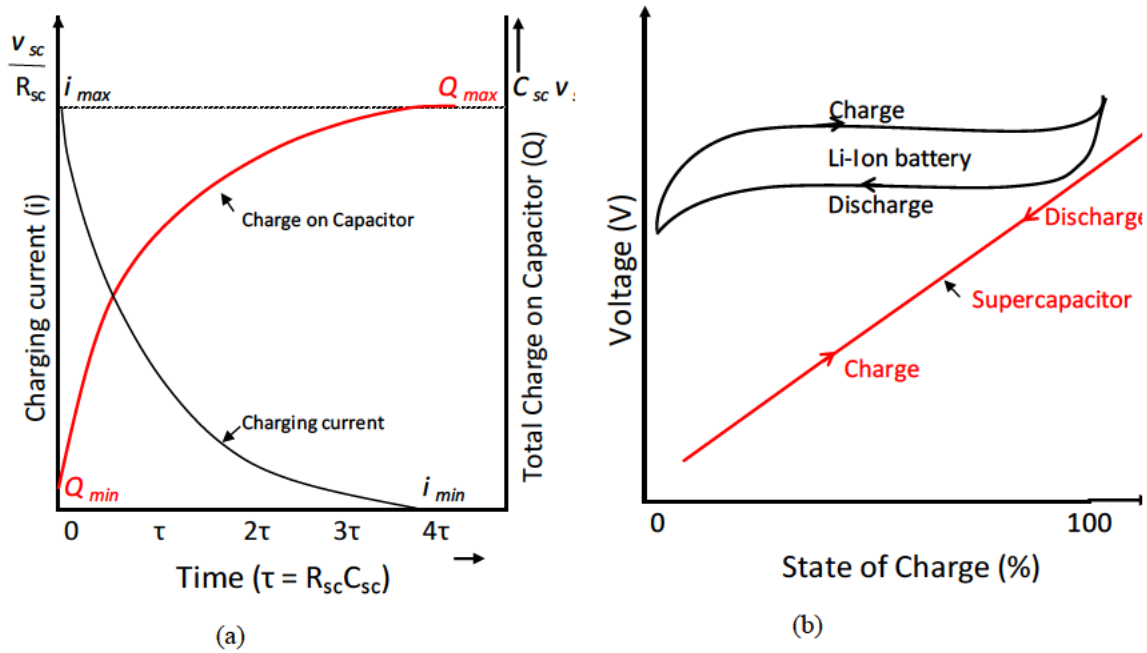

Figure 4. 3: a). Behavior of supercapacitor charge Q(C) and its current i(A) with time, b). charge/discharge curves of supercapacitor and Li-Ion battery.

The simple electrical model of a supercapacitor available in the MATLAB/Simulink was utilized in this study which satisfactorily model the dynamics. More detailed models of supercapacitors can be found in (Bernal, 1997, Zubieta and Bonert, 2000, Islam et al., 2010).

4.3 MPC based converter control strategies

4.3.1 Rectifier controller

As in (Rajapakse et al., 2017b), the input current dynamics of the rectifier were found using Kirchhoff's voltage law and the resultant equation for the predicted current in the next sampling interval was written in the discrete time domain as

$$i_s(k+1) = \left(1 - \frac{R_s T_s}{L_s}\right) i_s(k) + \frac{T_s}{L_s}\left(v_s(k) - v_{AFE}(k)\right) \quad (4.4)$$

where i_s is the rectifier input current vector, R_s is the combination of source and line filter resistance, L_s is the combination of source and line filter inductance, k is the sampling instant and T_s is the sampling time, v_s is the generator voltage vector and v_{AFE} is the rectifier voltage vector. The generator current in the next sampling interval,$i_s(k+1)$, was predicted for each of the eight switching states using (4.4). Each of the current values were then converted into the dq frame currents, $i_d(k+1)$, $i_q(k+1)$, and used to predict the future angular speed of the generator, $\omega_m(k+1)$ as (Rajapakse et al., 2017b)

$$\omega_m(k+1) = \omega_m(k) + \frac{T_s}{J}\left(T_m - 1.5 n_p \Psi_{pm} i_q(k+1)\right) \quad (4.5)$$

where T_m is the mechanical torque applied on the motor, n_p is the number of pole pairs and Ψ_{pm} is the permanent magnet synchronous generator (PMSG) flux. Then the values $\omega_m(k+1)$ and $i_d(k+1)$ were used in the cost function, g_{rec}, given in (6) to select the switching state that gives the minimum value for the cost function (Rajapakse et al., 2017b).

$$g_{rec} = |\omega^* - \omega_m(k+1)| + K.|i_d^* - i_d(k+1)| \quad (4.6)$$

where ω^* is the reference speed, i_d^* is the reference for the d-axis current component of the generator which was set to zero. The constant, K, has been added to reduce the d axis current in the generator and thus prevent flux weakening and overheating effects on the generator (Rajapakse et al., 2017b).

4.3.2 Inverter controller

As in (Rajapakse et al., 2017b), in the inverter controller three phase grid current, i_g and grid voltage, v_g were converted into the αb stationary reference frame by taking the projections of the three-phase quantities on an orthogonal axis using Clark's Transformation when α axis is aligned with phase A axis (Bimbhra, 1992)

$$\begin{bmatrix} f_\alpha \\ f_\beta \\ f_0 \end{bmatrix} = \begin{bmatrix} \frac{2}{3} & -\frac{1}{3} & -\frac{1}{3} \\ 0 & \frac{1}{\sqrt{3}} & -\frac{1}{\sqrt{3}} \\ \frac{1}{3} & \frac{1}{3} & \frac{1}{3} \end{bmatrix} \begin{bmatrix} f_a \\ f_b \\ f_c \end{bmatrix} \tag{4.7}$$

where f represents current or voltage. Then the input current dynamics of the inverter was found using the Kirchhoff's voltage law. The resultant equation for the predicted current in the next sampling interval was written in the discrete time domain as (Rajapakse et al., 2017b)

$$i_g\,(k+1) = \left(1 - \frac{R_g T_s}{L_g}\right) i_g(k) + \frac{T_s}{L_g}\left(v_{VSI}(k) - v_g(k)\right) \tag{4.8}$$

where v_{VSI} is the inverter voltage vector, R_g is the combination of grid and line filter resistance, L_g is the combination of grid and line filter inductance. The grid current in the next sampling interval, $i_g(k+1)$, was predicted for each of the eight switching states using (8). Then, each of the current values were converted into the dq frame currents and used to predict the power values, $P_g(k+1)$ and $Q_g(k+1)$ considering the $v_g(k+1) = v_g(k)$ as (Rajapakse et al., 2017b)

$$P_g(k+1) = (v_d i_d(k+1) + v_q i_q(k+1)) \tag{4.9}$$

$$Q_g(k+1) = (v_q i_d(k+1) - v_d i_q(k+1)) \tag{4.10}$$

where i_d, i_q, v_d and v_q are grid currents and grid voltages in dq rotating reference frame. The values $P_g(k+1)$ and $Q_g(k+1)$ were used in the cost function, g_{inv}, given in (4.11) to select the switching state that gives the minimum value for the cost function (Rajapakse et al., 2017b)

$$g_{inv} = \left|Q_g{}^* - Q_g\,(k+1)\right|^2 + \left|P_g{}^* - P_g\,(k+1)\right|^2 \tag{4.11}$$

where $P_g{}^*$ is the active power reference which was set to 265kW and $Q_g{}^*$ is the reactive power reference for the grid which was set to zero.

4.3.3 DC-DC Converter Controller

Generally, the voltage of the energy storage system (battery and/or supercapacitor) is lower than the dc-link voltage and the polarity of the energy storage and its output is set to the same with respect to the common ground. The dc-dc bidirectional converter suites well for this type of applications since proper control of the switches regulate the dc-link power fluctuations by directing them to the energy storage (Vilathgamuwa et al., 2015, Abdullah et al., 2013, Samosir and Yatim, 2010). This is a simple converter which can be used in high power applications where the switch rating of the converter becomes the key concern (Leuchter, 2011, Li et al., 2017). This converter consists with two IGBT switches, two anti-parallel diodes and an inductor connected as shown in Figure 4. 4. a). This dc-dc bidirectional converter is a combination of buck and boost topologies as shown in Figure 4. 4. b) and Figure 4. 4. c) respectively.

In this type of converters, the inductor is the main energy transfer element which is also responsible for the output current ripple. The ESS can be either a battery or supercapacitor and is connected to the low voltage side. The high voltage side of the converter is connected to the dc-link. The converter is designed to operate in both buck and boost modes. This two-quadrant dc-dc converter allows inductor current flow in either direction while keeping polarity of the dc voltage fixed during boost and buck modes. The mode it should operate at any given time is decided by the dc-link voltage and the voltage of the energy storage. If the dc-link voltage drops below the set voltage, the ESS would supply the power. And when the power generated is more than the power needed for the grid, the dc-link voltage rises above the set voltage, the converter charges the ESS absorbing the power. During the buck mode when the S1 IGBT is on and S2 IGBT is off; the excess current from the generator charges the ESS. During the boost mode S1 IGBT is off and S2 IGBT is on; the ESS supplies the power to the dc-link. The opening and closing of each switch generates a pulse output and this can be controlled to regulate the desired output voltage.

Since this converter operates in a discontinuous conduction mode to gain a smooth current/voltage output, high converter switching frequency and adequate filtering capacitance on the dc-link are required. Both the dc-link voltage and the ESS voltage

could be fixed by duty cycle of IGBTs neglecting the voltage drop across IGBTs and diodes (Leuchter, 2011, Hart, 2011)

$$D = \frac{t_{on}}{T} = t_{on}\, f_{sw} \tag{4.12}$$

$$(1 - D) = \frac{t_{off}}{T} \tag{4.13}$$

where D is the duty cycle, f_{sw} is the switching frequency and T is the switching period of the dc-dc bidirectional converter controller ($T = t_{on} + t_{off}$).

The steady state operation of buck and boost modes of dc-dc bidirectional converter with ESS considering average value modelling; the average inductor voltage and the net change in inductor current are zero for periodic operation (Hart, 2011). In buck mode of operation, the derivative of inductor current is a positive constant when the S1 IGBT is on as

$$\frac{\Delta i_L}{\Delta t} = \frac{\Delta i_L}{DT} = \frac{v_{dc} - v_{ESS}}{L} \tag{4.14}$$

where v_{dc} is the dc-link voltage, v_{ESS} is the voltage across ESS, and i_L is the inductor current ($i_L = i_{ESS}$).

The derivative of i_L is negative constant when the S1 IGBT is off as

$$\frac{\Delta i_L}{\Delta t} = \frac{\Delta i_L}{(1 - D)\, T} = \frac{-v_{ESS}}{L} \tag{4.15}$$

Since the net change in inductor current over one period is zero the relationship between v_{dc} and v_{ESS} is

$$\left(\frac{v_{dc} - v_{ESS}}{L}\right) DT + \left(\frac{-v_{ESS}}{L}\right)(1 - D)\, T = 0 \tag{4.16}$$

$$v_{dc} = \frac{v_{ESS}}{D} \tag{4.17}$$

The voltage ratio D should be kept smaller than unity to have efficient power conversion (Hart, 2011). This is to enable the buck converter to produce an output voltage that is equal or less than the input while the boost converter to produce equal or greater output voltage than the input. In boost mode of operation, the derivative of i_L is a positive constant when the S2 IGBT is on as

$$\frac{\Delta i_L}{\Delta t} = \frac{\Delta i_L}{DT} = \frac{v_{ESS}}{L} \tag{4.18}$$

and a negative constant when the S2 IGBT is off as

$$\frac{\Delta i_L}{\Delta t} = \frac{\Delta i_L}{(1-D)\,T} = \frac{v_{ESS} - v_{dc}}{L} \tag{4.19}$$

Since the net change in inductor current over one period is zero the relationship between v_{dc} and v_{ESS}

$$\left(\frac{v_{ESS}}{L}\right) DT + \left(\frac{v_{ESS} - v_{dc}}{L}\right)(1-D)\,T = 0 \tag{4.20}$$

$$v_{dc} = \frac{v_{ESS}}{(1-D)} \tag{4.21}$$

4.3.3.1 Space State Model of Bidirectional dc-dc Converter

The states of the S1 and S2 switches directly affects the charging and discharging of the inductor. As shown in Figure 4. 4, the HB dc-dc bidirectional converter operates in buck mode only when the ESS is charging and operates in boost mode only when it discharging (Vilathgamuwa et al., 2015). The space state equations for the buck converter as in Figure 4. 4. b), and for the boost converter as in Figure 4. 4. c), in continuous current mode operation are discussed below, assuming that all the circuit elements are ideal.

In buck Mode, when the S1 IGBT is on and the S2 IGBT is off, the S2 diode is reverse biased. Therefore, the inductor (L) charges. The voltage equation is

$$L\frac{di_L}{dt} = v_{ESS} - v_{dc} \tag{4.22}$$

When the S1 IGBT is off and S2 IGBT is off, the S2 diode becomes forward biased since L tries to maintain the current continues in the same direction and L start discharging. The voltage across inductor is

$$L\frac{di_L}{dt} = v_{ESS} \tag{4.23}$$

Considering, the state of the S1 IGBT, equation (4.22) and (4.23) gives

$$\frac{di_L}{dt} = \frac{1}{L} v_{ESS} - \frac{1}{L} s v_{dc} \tag{4.24}$$

where s is 1 when the S1 is on and s is 0 when the S1 is off.

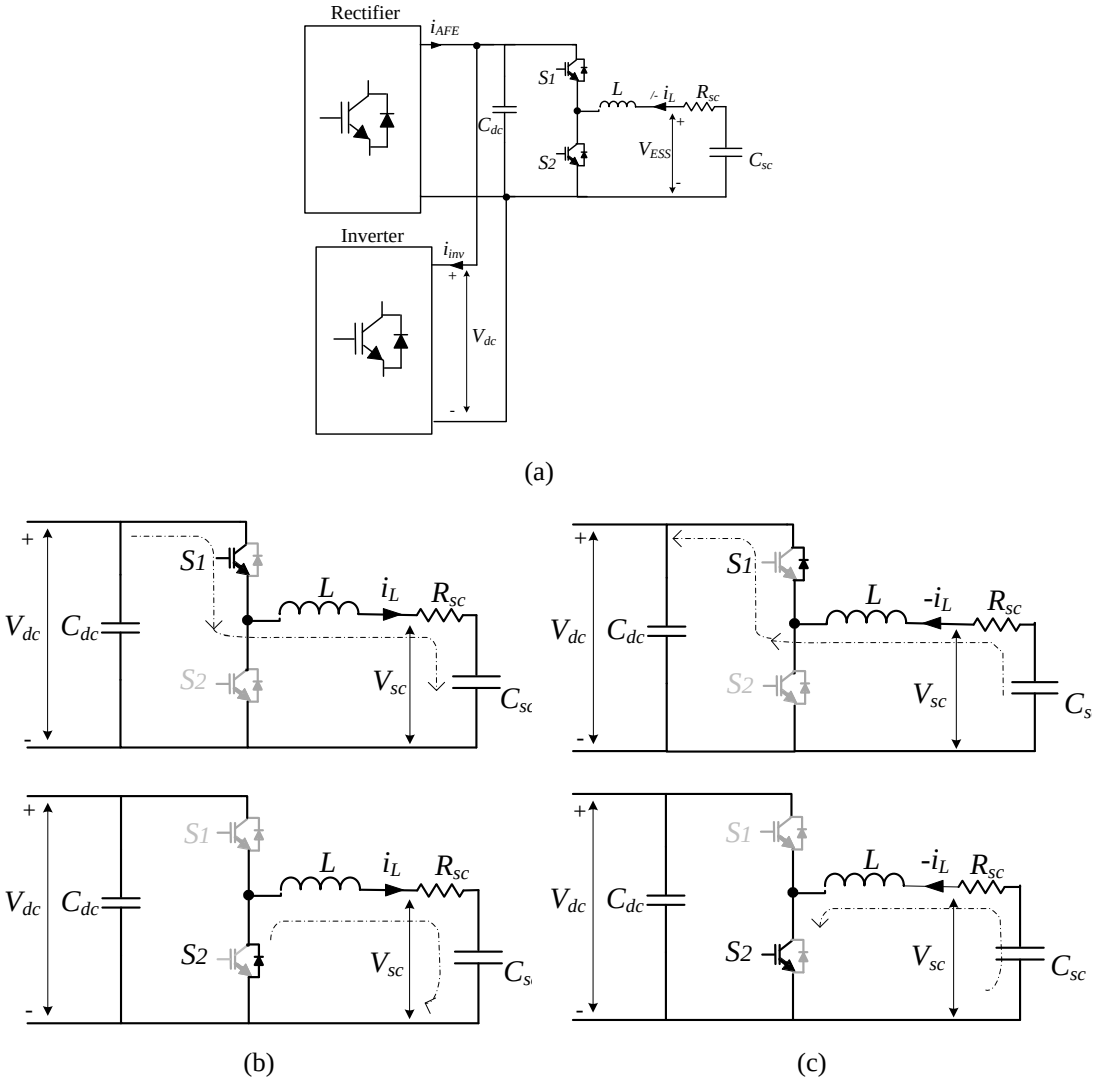

Figure 4. 4: Half Bridge dc-dc bidirectional converter of supercapacitor energy storage: a). dc-link with electrical power converters, b). Buck mode operation of bidirectional dc-dc converter, c). Boost mode operation of bidirectional dc-dc converter.

In boost Mode, when the S1 IGBT is off and the S2 IGBT is on the L charges. The voltage equation is

$$L\frac{di_L}{dt} = v_{ESs} \tag{4.25}$$

When the S1 IGBT is off and the S2 IGBT is off the diode S1 becomes forward-biased and L tries to maintain the current in the same direction and starts discharging as

$$L\frac{di_L}{dt} = v_{ESS} - v_{dc} \tag{4.26}$$

Considering, the state of the S2 IGBT, equation 25 and 26 gives

$$\frac{di_L}{dt} = \frac{1}{L} v_{ESS} + (s-1)\frac{1}{L} v_{dc} \tag{4.27}$$

where s is 1 when the S2 is on and s is 0 when the S2 is off.

4.3.3.2 Bidirectional dc-dc converter in discrete time domain

Since the sampling time is sufficiently small and sampling frequency is much higher than the fundamental frequency no extrapolation is considered for this study (Yaramasu, 2014). Instead, the simple one step method was used which selects the switching state that minimize the error at the (k+1) instant and apply it at the k^{th} instant. Fast microcontrollers such as Tiva TM4C123G, TMS320F28377S, etc. with high speed calculations allow the online implementation of these power converters.

In Buck Mode (S1 on = L charging; S1 off = L discharging), Using Euler's approximation method with one switching period, predicted inductor current is

$$i_L(k+1) = \frac{T_s}{L} v_{ESS} - \frac{T_s}{L} s v_{dc} + i_L(k) \tag{4.28}$$

The buck mode control objective is to maintain dc-link voltage and maintain the ESS at its upper limit by charging the SCES. During this process the ESS SOC is designed to maintain below 80%. This constraint is included in the FCS-MPC algorithm. And the main objective of FCS-MPC is taken as to minimize the error between inductor current reference (i_L^*) and predicted inductor current ($i_L^p = i_L(k+1)$). The maximum allowable charging current of ESS, ($i_{L_{max}}$), is included as one of the constraints. The cost function, g_{buck} is

$$g_{buck} = |i_L^* - i_L^p| \tag{4.29}$$

The inductor current reference is

$$i_L^* = \frac{((P_g - P_{PMSG}) + (v_{dc} - v_{dc}^{ref}) * 100)}{v_{ESS}} \tag{4.30}$$

where P_g and P_{PMSG} are grid supply power and PMSG generated power respectively.

In the boost mode when S2 is on the inductor will charge. When S2 is off the inductor will discharge. The switch S1 is turned off. Using Euler's approximation method with one switching period, predicted inductor current is

$$i_L\,(k+1) = \frac{T_s}{L}\,v_{ESS} + (s-1)\,\frac{T_s}{L}\,v_{dc} + i_L(k) \tag{4.31}$$

The boost mode control objective is to maintain dc-link voltage at its set value by discharging the ESS. During this process the ESS SOC should be maintained above 30%. This is also included in the FCS-MPC algorithm as a constraint, and the main objective of FCS-MPC is taken as to minimize the error between i_L^{*} and i_L^{p}. The maximum allowable discharging current of ESS ($i_{L_{max.}}$) is included as one of the constraints. The cost function, g_{boost} is

$$g_{boost} = |\,i_L^{*} - i_L^{p}\,| \tag{4.32}$$

The equations from (4.12) to (4.32) are common for any type of ESS with bidirectional dc-dc converter. Therefore, the proposed FCS-MPC can be used as a mutual algorithm for both supercapacitor and Li-Ion battery ESS. Figure 4. 5, depicts the flow chart of FCS-MPC algorithm of dc-dc bidirectional converter that controls the charging/ discharging of the EES.

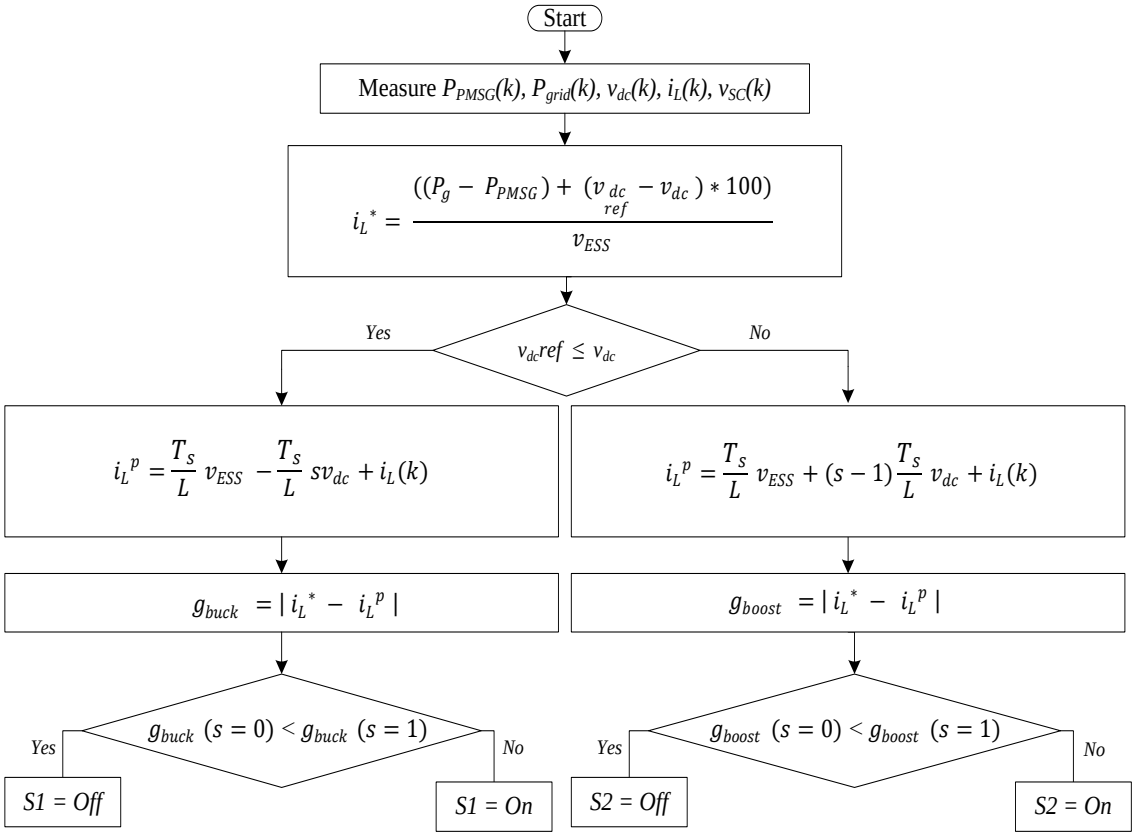

Figure 4. 5: The flow chart of MPC algorithm of dc-dc bidirectional converter.

4.4 Power Management System

The OWC power conversion system as in many other renewable energy systems depends on future availability of wave resources and the condition of ESS. Thus, model predictive control strategy based predictive power management system (PPMS) can be used to predict the future level of power supply to the grid based on future availability of renewable resources. This can be applied when determining the time period and level of power commitment to the grid. Moreover, the future SOC% of energy storage can be used to control switching of the dc-dc bidirectional converter and protective circuit which can be effectively utilized to co-ordinate control of the OWC system as in (Brka et al., 2015). In situations such SOC% closing up the maximum limit, maintaining the dc-link voltage can be achieved using a protective circuit such as resistors which dissipates extra energy (Brka et al., 2015). The PPMS has been used in (Brka et al., 2015), to manage the switching of components in stand-alone hydrogen systems with Lead-acid BES and has validated PPMS over other power management system (PMS) such as rule-based. A similar strategy can be used to build efficient and reliable OWC system with ESS to

minimize the energy lost and system cost with improve system dynamics. Nevertheless, wave energy forecast unit commitment estimation is beyond the scope of this paper. Instead a simple power management strategy is used in this study by taking the average power over a 20s period. This study aims to maintain an optimal and safe operation of OWC power convention to protect SCES from over-discharging and overcharging while maintaining the dc-link voltage in desirable range. The PMS is used to control the dc-dc bidirectional converter to maintain the SCES SOC% between its minimum and maximum limits (30% – 80%) to improve its lifespan.

4.5 Simulation Results and Discussion

The parameters in Table 1, given in Appendix 1(a), were used for modeling and simulation of the OWC wave energy conversion system and ESS in MATLAB/Simulink. Modeling of air-turbine, PMSG, back to back converter, grid and filters can be found in (Rajapakse et al., 2017b). The simulation results shown in Figure 4. 6. a) – 4. 6. k) were used to evaluate the FCS-MPC performance of dc-dc bidirectional power converter along with back to back converter.

The main control goal in this study was to supply a set quality grid power output by regulating dc-bus voltage at safe and effective voltage range while controlling the charging and discharging of the ESS within its technical limits. The other major control objective in this study as in (Rajapakse et al., 2017b) was to maintain OWC air-turbine speed within the optimum range while extracting large discrete power pulses.

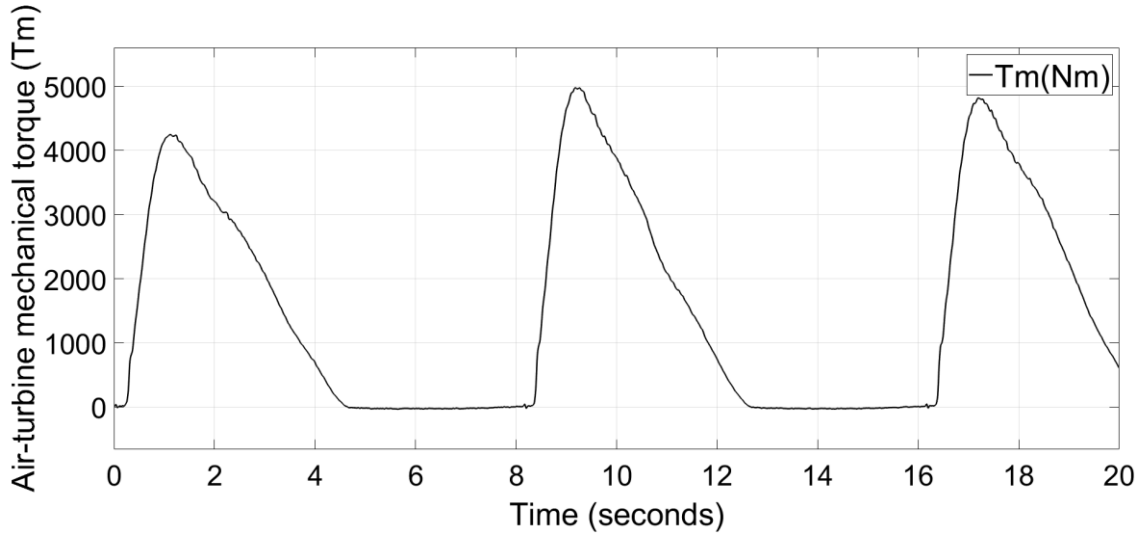

(a)

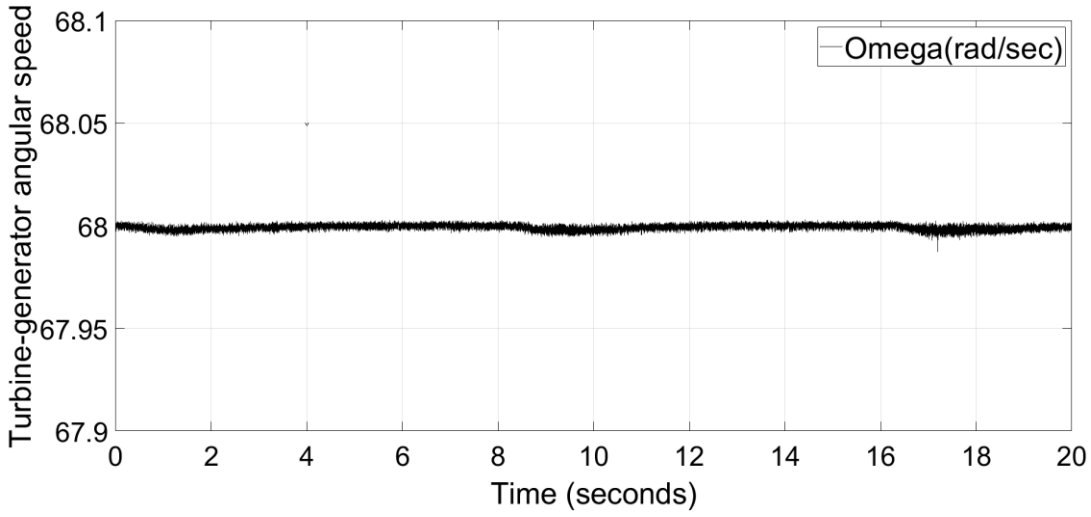
Turbine-generator angular speed
Omega(rad/sec)
68.1
68.05
68
67.95
67.9
0
2
4
6
8
10
12
14
16
18
20
Time (seconds)

(b)

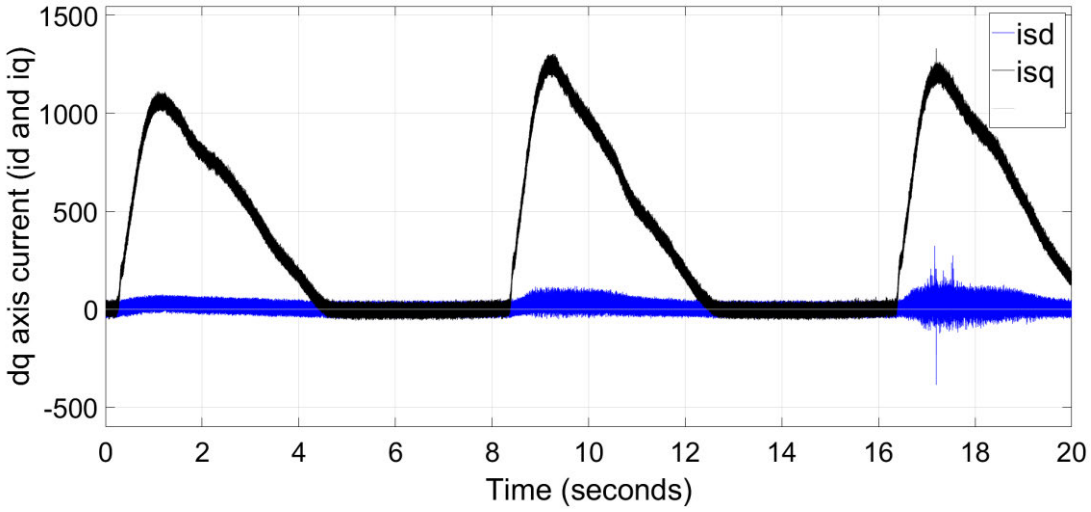
dq axis current (id and iq)
isd
isq
1500
1000
500
0
-500
0
2
4
6
8
10
12
14
16
18
20
Time (seconds)

(c)

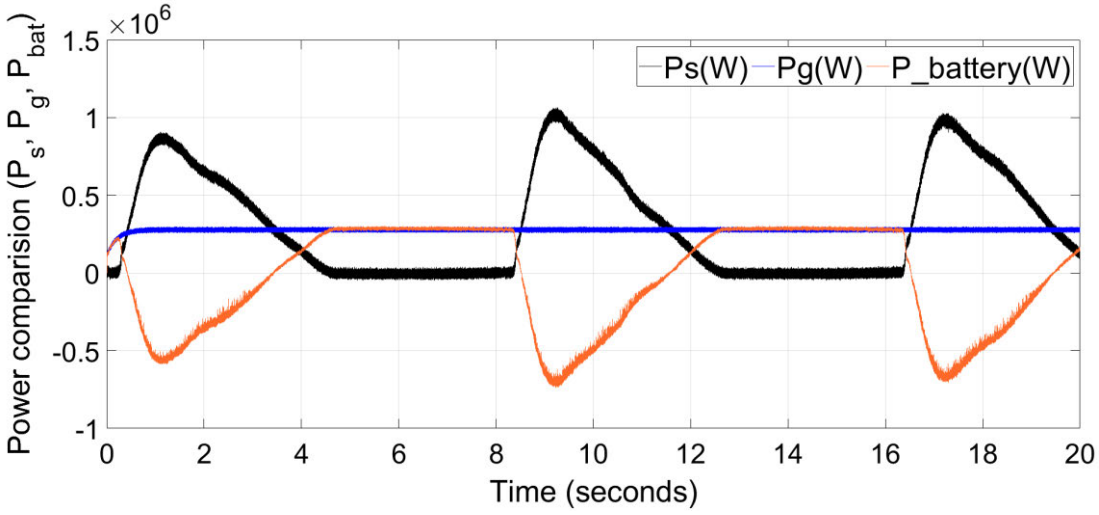
Power comparision (P_s, P_g, P_bat)
×10^6
Ps(W)
Pg(W)
P_battery(W)
1.5
1
0.5
0
-0.5
-1
0
2
4
6
8
10
12
14
16
18
20
Time (seconds)

(d)

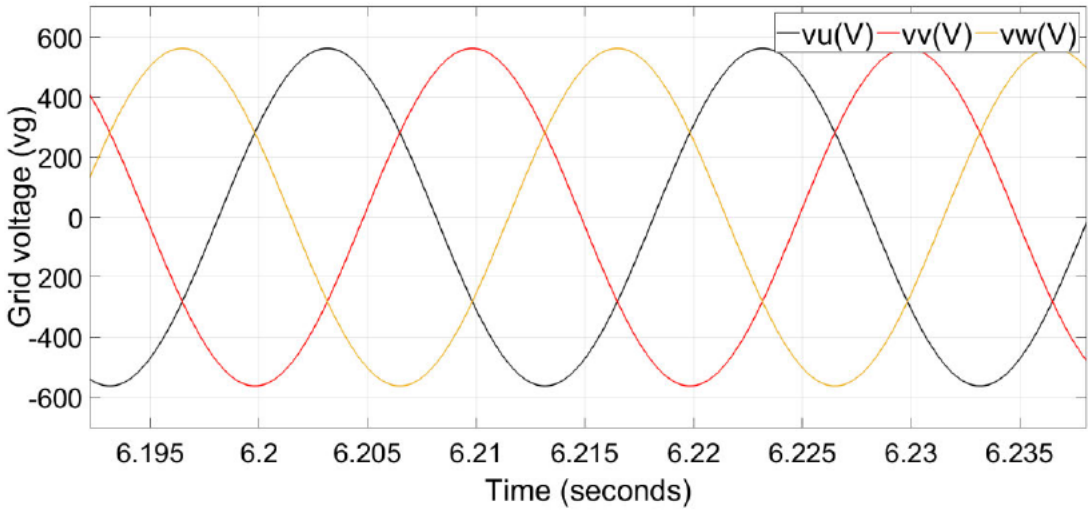
vu(V)
vv(V)
vw(V)
Grid voltage (vg)
600
400
200
0
200
-400
-600
6.195
6.2
6.205
6.21
6.215
6.22
6.225
6.23
6.235
Time (seconds)

(e)

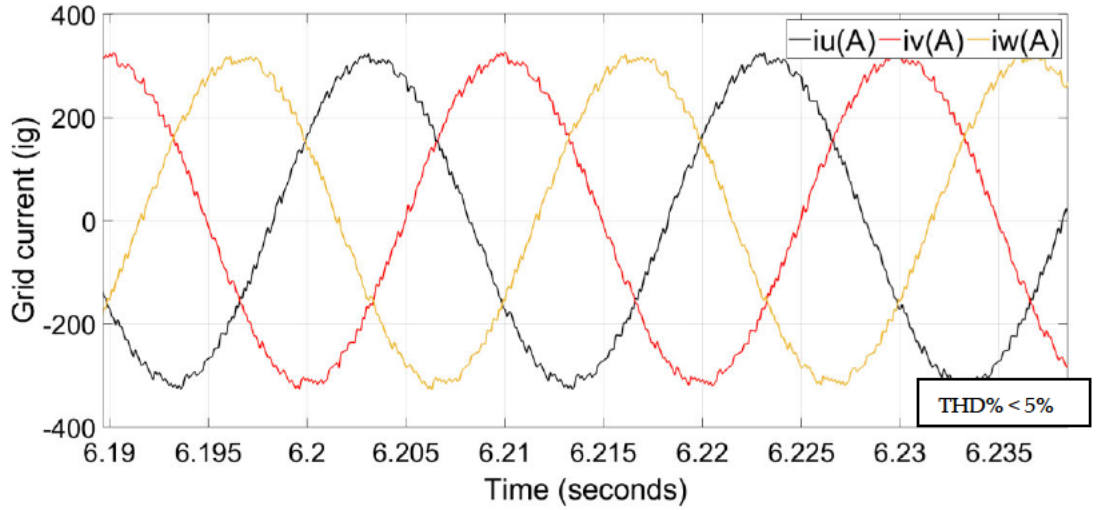
iu(A)
iv(A)
iw(A)
Grid current (ig)
400
200
0
-200
-400
THD% < 5%
6.19
6.195
6.2
6.205
6.21
6.215
6.22
6.225
6.23
6.235
Time (seconds)

(f)

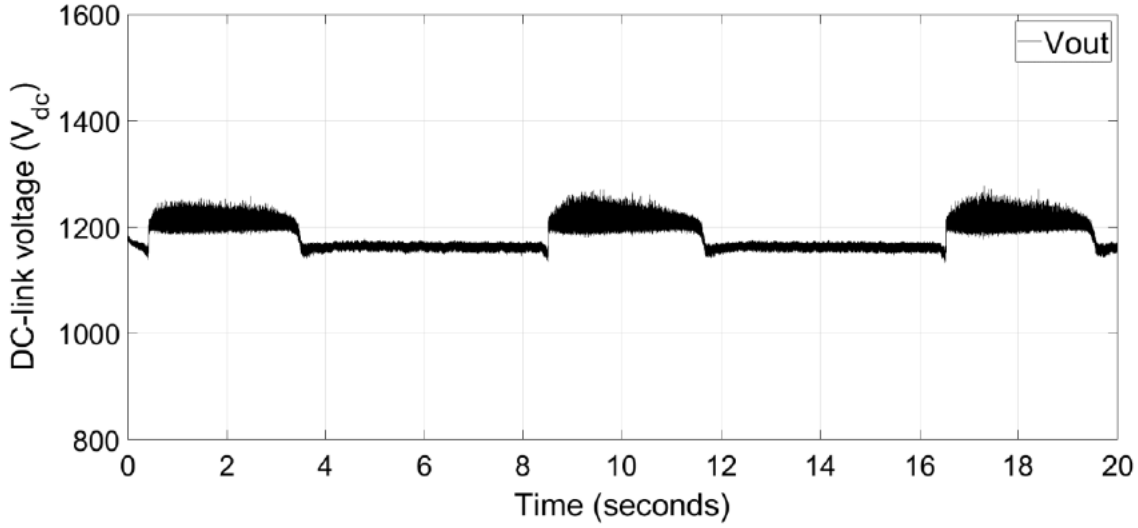
Vout
DC-link voltage (Vdc)
1600
1400
1200
1000
800
0
2
4
6
8
10
12
14
16
18
20
Time (seconds)

(g)

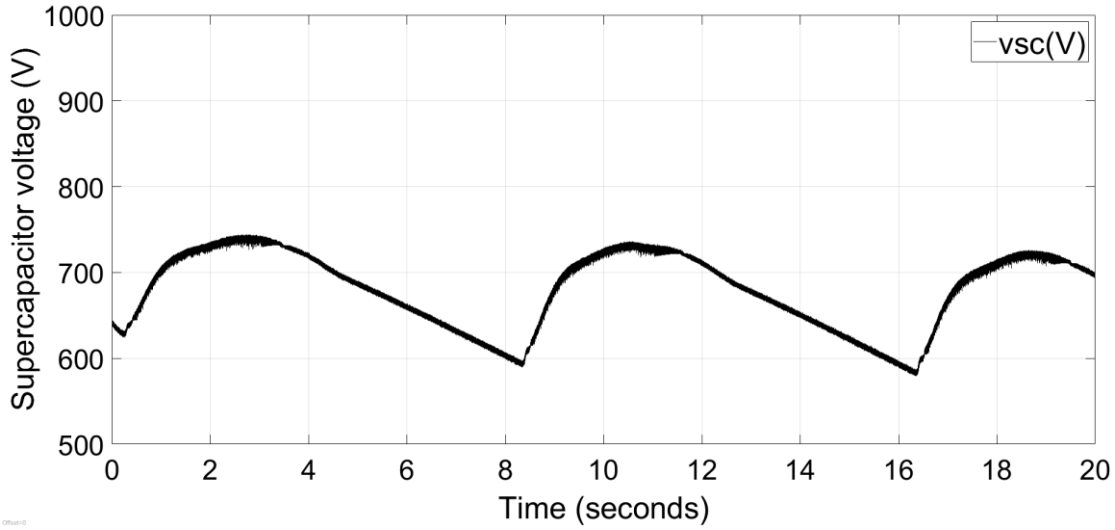
vsc(V)
Supercapacitor voltage (V)
1000
900
800
700
600
500
0
2
4
6
8
10
12
14
16
18
20
Time (seconds)

(h)

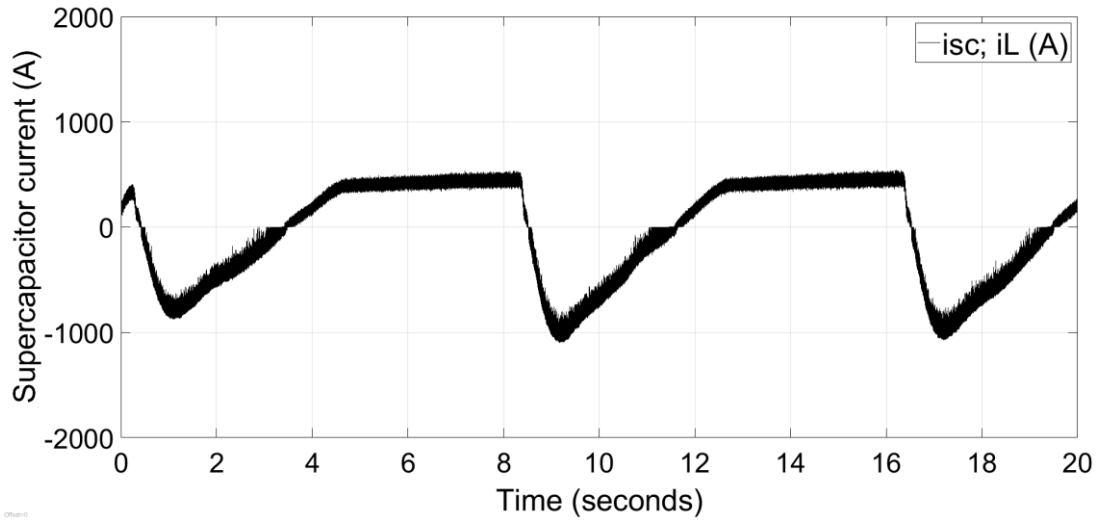
isc; iL (A)
Supercapacitor current (A)
2000
1000
0
-1000
-2000
0
2
4
6
8
10
12
14
16
18
20
Time (seconds)

(i)

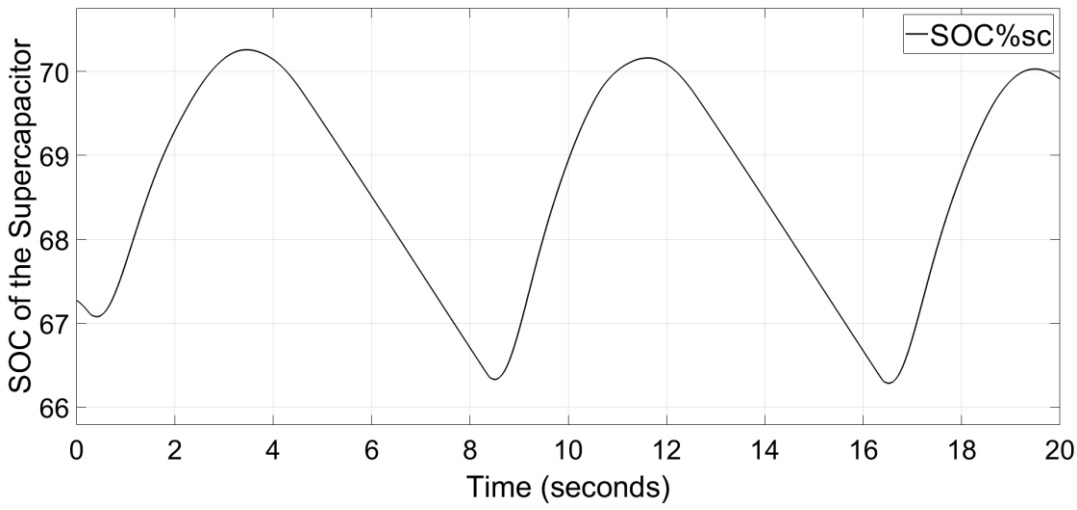
SOC%sc
SOC of the Supercapacitor
70
69
68
67
66
0
2
4
6
8
10
12
14
16
18
20
Time (seconds)

(j)

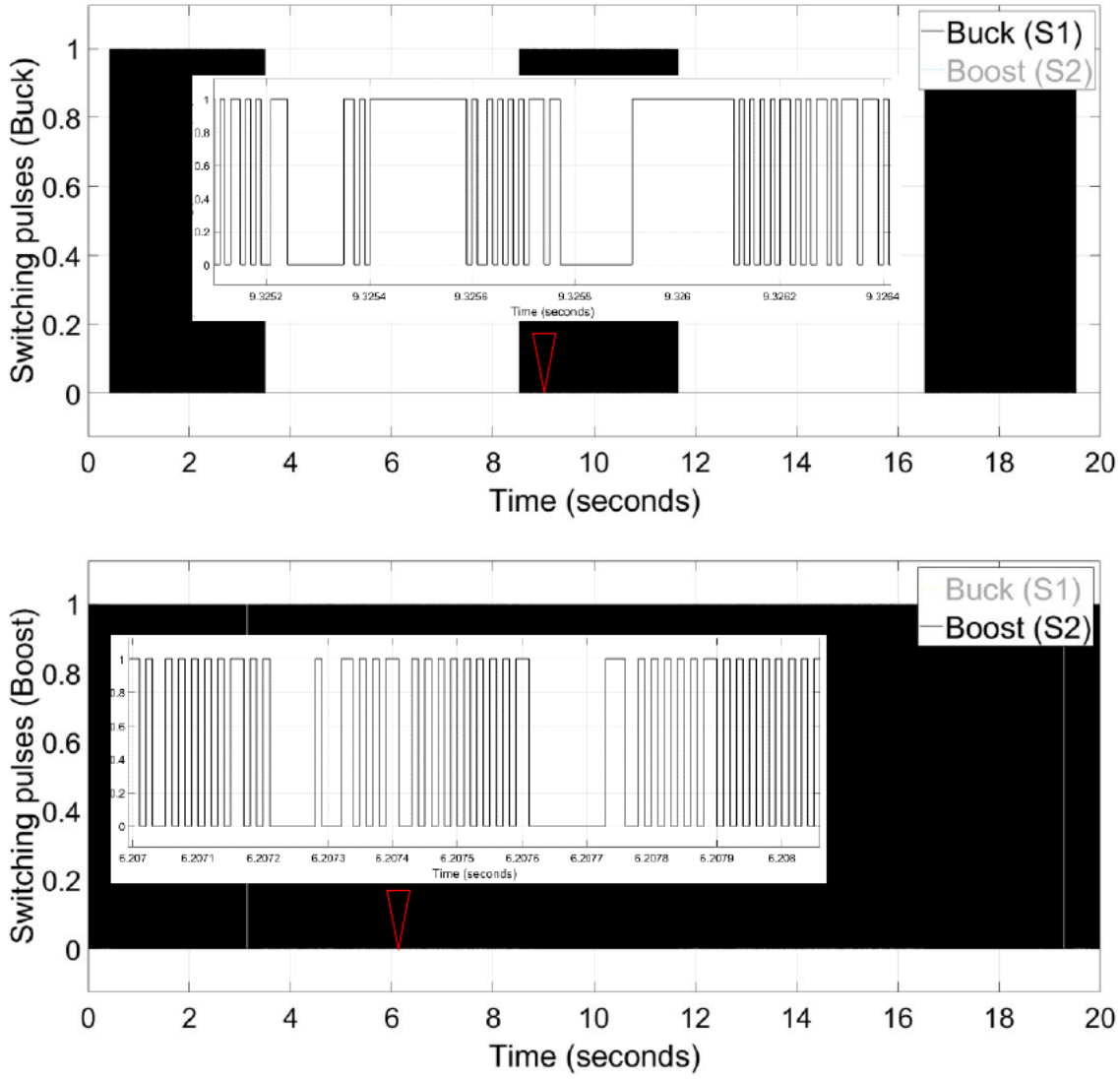

(k)

Figure 4. 6: The simulation results of OWC- grid integrated system with SCES: a). Mechanical torque profile T_m(Nm), b). generator rotor angular speed ω_m(rad/sec), c). PMSG stator current in dq frame (i_{sd} (A) and i_{sq}(A)), d). power of PMSG, Grid, and SCES (W), e). grid voltage v_g(V), f). grid current i_g(A), g). dc-link voltage v_{dc}(V), h). Supercapacitor voltage v_{sc}(V), i). inductor current i_L(A), j). state of charge of the SCES (SOC%), k). dc-dc bidirectional converter switching pulses.

Figure 4. 6. a), depicts the mechanical torque produced by the unidirectional air-turbine at its design speed (650rpm ≈ 68rad/sec) (Wave Swell Energy, 2017) while the turbine-generator rotor angular speed is shown in Figure 4. 6. b). As evident in this figure, the rotational speed of the air-turbine is regulated to be within the optimum region throughout the simulation. This confirms that the turbine speed is kept at its control objective throughout the simulation regardless the significant variation in extracted power (0 – 1MW). Figure 4. 6. c), depicts the PMSG stator current in dq reference frame. The d-axis

current is maintained closer to zero while the q-axis current varies in proportion to the torque input. This q-axis current is directly proportional to the active power drawn from the PMSG which also varies with the extracted power as shown in Figure 4. 6. d).

Figure 4. 6. d), also illustrates the grid power and SCES power. The PMSG power and SCES power waveforms confirm that the FCS-MPC of dc-dc bidirectional converter successfully controls the power exchange between SCES and dc-link. The grid power is maintained at its reference throughout the simulation. This is achieved by charging and discharging the supercapacitor, compensating the generated and demand power differences. The grid voltage and grid current are shown in 4. 6. e) and 4. 6. f) respectively. The total harmonic distortion (THD%) of the grid three phase current is less than 5% for this simulation, which allows the OWC to be integrated to the grid (2014). Figure 4. 6. g), depicts the dc link voltage which is kept almost constant at 1200V with more than 90% accuracy. This waveform confirms that the dc-link voltage is controlled successfully by the proposed MPC of dc-dc bidirectional converter adhering to constrains. Also, according to the results, when the generated power is less than the grid power the dc-link voltage is maintained below its set voltage by discharging the SCES, and when the generated power is more than the grid power the dc-link voltage is maintained almost at its set level while charging the SCES. Figure 4. 6. h), 4. 6. i) and 4. 6. j) illustrate SCES's voltage, current, and SOC respectively. These figures confirm that the FCS-MPC and simple PMS are capable of directing buck and boost operation of the bidirectional converter adhering to ESS's technical limits such as maximum discharge current, maximum charging current, SCES maximum voltage, cut-off voltage, minimum SOC, maximum SOC, etc. The dc-dc bidirectional converter buck boost operation and switching pulses are shown in Figure 4. 6. k) and confirms the proposed control strategy of bidirectional dc-dc converter controls the switching between buck and boost modes depending on the supply-demand power difference. The expanded figures show how the duty cycles change in buck and boost modes.

4.6 Conclusion

This paper can be considered as the preliminary study that looks into a grid connected OWC unidirectional air turbine-generator with SCES system. The air turbine-generator is integrated to the grid using a back-to-back power converter as in authors' previous

work. This study applies and connects a commercially available, affordable type supercapacitor to the dc-link with a dc-dc bidirectional converter. This approach confirms the smooth and quality power delivery to the grid by absorbing the large discrete power pulses generated by the PMSG. FCS-MPC is applied to the controller of the bidirectional dc-dc converter to direct charging and discharging of SCES to maintain the dc link voltage at the set voltage range directly controlling the inductor current. The control algorithm used for this power converter does not consider the SCES parameters other than SCES's voltage. Therefore, it can be used for any type of ESS with minor adjustments. This also, allows the authors to carry out further research using either Li-Ion battery or supercapacitor ESS using the same converter control algorithm. Moreover, power management strategy is addressed to maintain the SOC of the SCES at predefined technical limitations to increase ESS's lifespan. The simulation results are analyzed to confirm the feasibility of the applied MPC strategy. The rotational speed of the turbine generator is almost constant at 68rad/sec while the THD of the output current is below the grid code requirement of 5% during the entire simulation. These results confirm that the proposed MPC strategy for the controllers are capable of maintaining a quality power supply adhering to grid code irrespective of the significant intermittencies present in the extracted power from the waves under varying sea conditions.

Although these results obtained from software simulation are very promising further investigations and implementations are in progress for lab-scale hardware experimental validations and the development of an adaptive system against parameter variations.

5

POWER MANAGEMENT OF AN OSCILLATING WATER COLUMN WAVE ENERGY CONVERTER WITH BATTERY/SUPERCAPACITOR HYBRID ENERGY STORAGE

This chapter was originally presented as a paper at International Conference on Power and Energy System (ICPES2018) in Colombo, Sri Lanka on 21-22/12/2018. This chapter has been published by '*IEEE Conference Proceedings'*. The citation for the research article is:

G. Rajapakse, S. G. Jayasinghe, and A. Fleming, "Power Management of an Oscillating Water Column Wave Energy Converter with Battery/Supercapacitor Hybrid Energy Storage," In conference proceedings of the 2018 International Conference on Power and Energy System (ICPES2018), Colombo, Sri Lanka, 21–22 December 2018, *IEEE Xplore*, 2019.

Abstract

This paper focuses on developing a power management system (PMS) for a grid connected oscillating water column (OWC) wave energy converter with a battery/supercapacitor hybrid energy storage system. The main objective of the PMS is to transfer large power pulses present in the input to the energy storage elements and thereby maintain smooth power delivery to the grid. In addition, maintaining state of charge (SOC) of the battery and supercapacitor within safe limits and ensuring sufficient reserves are other objectives of the PMS. In the proposed PMS, power sharing between energy storage elements is determined based on the deviation of the supercapacitor SOC from the mid-point and its rate of change. Moreover, the power commitment to the grid is adjusted based on the deviation of battery SOC from the mid-point and its rate of change. Successful operation of the proposed PMS is verified using MATLAB/Simulink simulations. Apart from that, the variable speed operation of the turbine is also simulated to observe its effect on the supercapacitor sizing. Simulation results show that the variable speed operation help reduce required capacity of the supercapacitor.

Keywords: Hybrid energy storage system, Li-Ion battery energy storage, oscillating water column wave energy converter, power management system, supercapacitor energy storage.

5.1 Introduction

As in many other countries, Australia's greenhouse gas emission levels are rising, mostly due to the increasing use of fossil fuels in the energy sector (Environment and Communications References Committee Australia, 2017, Hannon et al., 2016) On the other hand, regardless of the climate factor, the country needs to replace 72% of its coal generator plants due to aging (Climate Council of Australia, 2014). This paves an opportunity to replace these with zero or low emission power plants. Moreover, by 2020, Australia is required to produce an additional 18000 TWh of renewable energy annually to meet its renewable energy target commitments in accordance with the 2015 Paris agreement (Clean Energy Council, 2016). This can be achieved only by investing in large-scale renewable energy projects. According to (Carson et al., 2014), this amount could be attained by harvesting just 2% of the wave energy available along the Southern and Western coastlines. Therefore, it is worth looking into technical challenges in ocean wave energy conversion systems. This leads to further research and development in overall technical aspects in order to maximize the renewable energy production while reducing the levelized cost of electricity (Hemer et al., 2018, Hughes and Heap, 2009).

Recent research have identified vented type oscillating water column (OWC) as a step change in improving the competitiveness of wave energy conversion compared to alternative technologies such as wind and solar (Wave Swell Energy, 2017, Australian Maritime Collage, 2017). Nevertheless, for OWC wave energy converter's (WEC's) to compete with other technologies, it must meet power quality requirements specified in grid codes.

One of the biggest challenges with OWC's is the presence of large power pulses ranging from zero to Megawatts of power levels at a timescale corresponding to the wave period. This issue has been discussed by the authors' in their previous publications and energy storage-based solutions have been proposed (Rajapakse et al., 2017b, Rajapakse et al., 2018b). In (Rajapakse et al., 2017b), a battery energy storage system (BESS), directly connected to the dc-link of the back-to-back power converter, is used to absorb power pulses to improve the quality of power delivered to the grid. In (Rajapakse et al., 2018b), a bidirectional dc-dc converter is used to integrate a supercapacitor energy storage (SCES) to the dc-link with a simple power management system (PMS) aiming to absorb

power pulses. A PMS is used to maintain the energy storage system (ESS) within operational limits. Even though the results were promising in both circumstances, the researches had not considered some important extrinsic factors such as energy storage reliability, availability and power supply duration anxiety. To overcome these challenges a battery-supercapacitor hybrid energy storage system (HESS) is considered in this paper for the OWC WEC system as shown in Figure 5. 1. Complimentary characteristics of the two energy storage elements help overcome limitations in individual elements (Zhang et al., 2017, Hamidi et al., 2017).

Power management plays a critical role in renewable energy systems with energy storage. This has a direct impact on the energy conversion efficiency, smooth power delivery to the grid and lifetime of energy storage element. The bespoke PMS reported in (Tang et al., 2017) forecasts wind energy and determines the level of power that can be committed to the grid for a certain period. Similarly, (Lekube et al., 2017) forecasts wave energy. There are many PMSs proposed in literature for renewable energy systems with HESS (Kim et al., 2017b, Roy et al., 2018). Nevertheless, feasibility of a PMS applied to the particular OWC WEC used in this study has not previously been reported.

The proposed PMS uses a rule-based approach to coordinate and control of individual electrical power conversion systems. It takes into account the power generated in the WEC, available capacity of energy storage elements and power commitment to the grid to decide the power sharing among different elements of the system. Moreover, based on the deviation of the Li-Ion battery state of charge (SOC) from 65% and rate of change of SOC, the grid power reference is modified to keep the battery SOC in desirable limits.

The paper is organized as follows. Section 5.2 presents the modeling of the OWC wave energy system. Section 5.3 presents the proposed power management system. Simulation results and discussion are presented in section 5.4. Conclusions derived from the discussion are presented in Section 5.5.

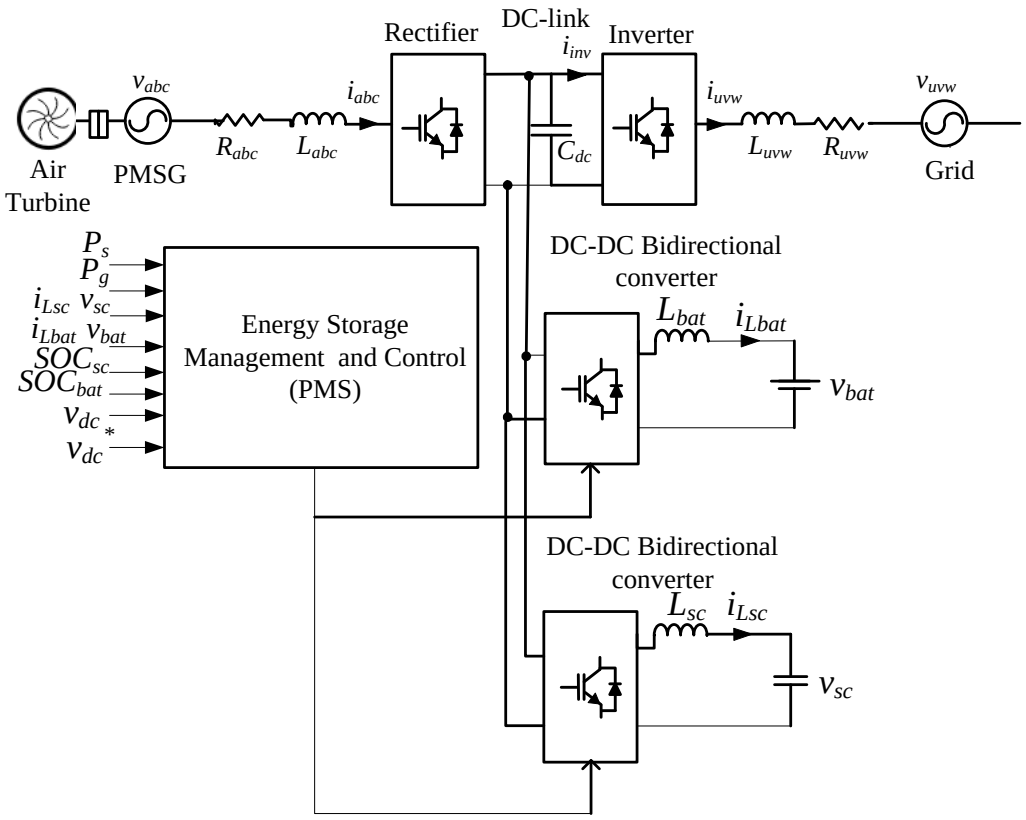

Figure 5. 1: Schematic diagram of the grid connected OWC wave energy conversion system.

5.2 System Modelling

5.2.1 Wave Climate and Sea States

To estimate the performance of a wave energy converter and average power generation it is essential to investigate the temporal, directional and spectral characteristics of the ocean waves. The web based Australian Wave Energy Atlas (AWavEA) is an open access portal that provides seven parameters to characterise the available wave energy resource. The seven parameters provided by AWavEA are omnidirectional wave energy flux, significant wave height, wave energy period, spectral width, maximum directionally resolved wave power, the direction of maximum directionally resolved wave power, and directionality coefficient (Hemer et al., 2017). Table 5.1, shows the joint occurrence results of full-scale equivalent irregular waves depending on wave height and wave period considering the yearly mean climatology referring to the period from 1997/01 to 2010/12 (Cardno Pty Ltd, 2017). The numerical figures are based on the detailed wave energy climate at the west coast of King Island.

Table 5. 1, has been constructed showing most of the sea states and their frequency of occurrence. It also depicts the average significant wave height, average wave period and average wave power related to the respective sea state. As per this Table, the average power of the sea states, 258kW, is taken as the baseline for reference power output to the grid during the commitment period, T_{commit}. This value will be adjusted slowly to maintain battery SOC within safe limits.

5.2.2 Incident Wave Power

Equations (5.1) and (5.2) are used to calculate the power in regular (P_R) and irregular (P_I) incident waves respectively, neglecting the influence of water depth (Fleming et al., 2017)

$$P_R = \frac{\rho_w g^2 h^2 T_p}{32\pi} \text{ (per wave crest length)} \quad (5.1)$$

$$P_I = \frac{\rho_w g^2 h_{m0}^2 T_E}{64\pi} \text{ (per wave crest length)} \quad (5.2)$$

where ρ_w is the sea water density, g is gravitational acceleration, h is wave height measured crest to though, T_p is the wave period. $h_{mo} = 4\sqrt{m_0}$, with m_0 is the first spectral moment. T_E is the energy period derived from spectral analysis.

5.2.3 Pneumatic Power

Pneumatic power (P) applied to the unidirectional air-turbine is calculated as (Fleming et al., 2017)

$$P = \Delta p Q \quad (5.3)$$

where Δp is the pressure head in the OWC chamber and Q is the air volumetric flow rate which is equal to $\frac{C_d A_0}{\sqrt{|\Delta p|/\rho_a}}$. C_d is the orifice discharge coefficient, A_0 is the restricted orifice cross sectional area and $\boldsymbol{\rho}_a$ is air density.

Table 5. 1: Joint Occurrence (%) of Wave Height, Wave Period and Wave Power (Cardno Pty Ltd, 2017, Fleming et al., 2017)

Sea State n	Period T_m (sec)	Height H_m (m)	Power available (kW)	Freq. of occurrence f_n %	Power content (%)
1	9	0.75	7	0.1	0.1%
2	9	1.25	11	0.4	0.1%
3	9	1.75	16	0.8	0.2%
4	9	2.25	20	0.9	0.3%
5	9	2.75	25	0.5	0.3%
6	9	3.25	29	0.2	0.4%
7	11	0.75	8	0.1	0.1%
8	11	1.25	14	1.1	0.2%
9	11	1.75	19	3.9	0.2%
10	11	2.25	25	5.6	0.3%
11	11	2.75	30	3.8	0.4%
12	11	3.25	36	2.1	0.5%
13	11	3.75	41	1.2	0.5%
14	13	1.25	16	0.7	0.2%
15	13	1.75	23	4.1	0.3%
16	13	2.25	29	9	0.4%
17	13	2.75	36	10.5	0.5%
18	13	3.25	42	8.5	0.5%
19	13	3.75	49	5.7	0.6%
20	15	1.25	19	0.3	0.2%
21	15	1.75	26	1.5	0.3%
22	15	2.25	34	3.3	0.4%
23	15	2.75	41	4.6	0.5%
24	15	3.25	49	5.4	0.6%
25	15	3.75	56	4.6	0.7%
26	17	1.25	21	0.1	0.3%
27	17	1.75	30	0.6	0.4%
28	17	2.25	38	1	0.5%
29	17	2.75	47	1.2	0.6%
30	17	3.25	55	1.2	0.7%
31	19	1.25	24	0.1	0.3%
32	19	1.75	33	0.3	0.4%
33	19	2.25	43	0.4	0.6%
34	19	2.75	52	0.4	0.7%

5.2.4 Air-Turbine Power

As mentioned in (Rajapakse et al., 2017b), OWC air-turbine torque (T_m) considered in this paper is a function of a Δp. For a constant rotational speed T_m is

$$T_m = 30.815\Delta p^2 - 653\Delta p \tag{5.4}$$

Air-turbine output power (P_T) is a function of T_m and instantaneous rotor speed (ω_T)

$$P_T = T_m \omega_T \tag{5.5}$$

Likewise, the generator power (P_s) can be given by generator rotor electromagnetic torque (T_e) and generator rotor speed (ω_m) which is same as ω_T

$$P_s = T_e \omega_m \tag{5.6}$$

where $T_e = 1.5 n_p \Psi_{pm} i_q$. n_p and Ψ_{pm} are the number of pole pairs and permanent magnet flux of the permanent magnet synchronous generator (PMSG), respectively. i_q is the q axis current in dq reference frame. If the total system inertia (J) is known, then T_m is

$$T_m = T_e + J\frac{d\omega_m}{dt} \tag{5.7}$$

In the first case study, the air-turbine speed reference is set to fixed speed aiming to transfer all the power fluctuations to the energy storage elements. In the second case study, the air-turbine speed is allowed to vary in a predefined range and thereby absorb part of the power fluctuations through turbine inertia, achieving the short-term smoothing effect. This helps reduce the capacity of energy storage elements. All these possibilities can be considered to reduce the overall cost and increase the efficiency of the OWC system. The rotational speed references used for the simulation studies are selected from the efficiency curve given in (Rajapakse et al., 2017b), with respect to rotational speeds when Δp is 6.44kPa. The fixed speed, 68rad/sec, which gives the air-turbine 85% efficiency is taken as the reference angular speed for case study 1. For the second case study the variable speed rage, 52rad/sec - 90rad/sec, is selected.

5.2.5 Energy Storage

Since the reference power output to the grid during the committed period is taken as the average power of the sea states, the energy system should be able to absorb the surplus of power or supply the deficit and thereby maintain power commitment.

For a committed period, the maximum energy (E_{bat_max}), and minimum energy (E_{bat_min}), stored in the battery are (Khiareddine et al., 2018).

$$E_{bat\_max} = SOC_{max} * C_{bat} * v_{bat} \tag{5.8}$$

$$E_{bat\_min} = SOC_{min} * C_{bat} * v_{bat} \tag{5.9}$$

where SOC_{max} and SOC_{min} are maximum and minimum SOC of the Li-Ion battery. C_{bat} and v_{bat} are the capacity (charge stored) and the voltage across the Li-Ion battery respectively. The remaining energy in a supercapacitor and battery can be given as a fraction of the nominal by SOC. This is to be calculated based on parameters such as energy storage current capacity, temperature, number of cycles, etc. Moreover, the maximum capacity of the battery degrades non-linearly over time. Therefore, estimation of exact value is out of the scope of this paper. Instead, the electrical model available in MATLAB/Simulink is used to calculate the SOC of the supercapacitor at the current time step (SOC_{sc}) as

$$\begin{aligned} SOC_{sc} &= \left(\frac{Q_0 - \int_0^t i_{sc}\,(t)\,dt}{Q_T} \right) x\ 100 \\ &= \left(\frac{(C_{sc(0)} * v_{sc(0)}) - \int_0^t i_{sc}\,(t)\,dt}{C_{sc} * v_{sc}} \right) x\ 100 \end{aligned} \tag{5.10}$$

where C_{sc} is the capacitance of the supercapacitor, v_{sc} is the voltage across supercapacitor, $v_{sc(0)}$, $C_{sc(0)}$ and Q_0 are the initial voltage, capacitance, and charge of the supercapacitor. $i_{sc}(t)$ is the supercapacitor's current at time t. Q_T is its total charge. The SOC of the Li-Ion battery at the current time step (SOC_{bat}) as

$$SOC_{bat} = SOC_0 - \frac{1}{C_{bat}} \int_0^t i_{bat}(t).\,dt \tag{5.11}$$

where $i_{bat}(t)$ is the battery current, and SOC_0 is the initial SOC of the battery.

5.3 Power Management System

The proposed PMS plays an important role in the OWC-WEC system in maintaining power quality and availability. The power equilibrium can be written as:

$$P_g = P_s + P_{sc} + P_{bat} \tag{5.12}$$

where P_g, P_s, P_{sc} and P_{bat} are power supplied to the grid, OWC generated power, supercapacitor power, and battery power respectively. $P_s + P_{sc}$ is used as the primary source of power. P_{bat} is used only if the primary source of power is unable to maintain the committed power output to the grid. This approach is used to minimize the usage of Li-Ion battery storage. Moreover, the proposed PMS forces the supercapacitor and battery SOCs to remain within their upper and lower thresholds (30%-80%). The limits given in equations 5.13 – 5.15 are chosen to avoid over-charging/over-discharging aiming to improve the energy storages' lifetime. This gives 55% depth of discharge for the energy storage element. Even though it is possible to extend the depth of discharge even up to 30% by pushing the energy storage element to the extremes, it drastically decreases the lifetime. Therefore, 55% depth of discharge is chosen as a good value for this study. The PMS can be expressed as

$$P_{SC\_\%} = \begin{cases} 100 - X & \text{if } (P_s > P_g \text{ and } SOC_{SC} > 75) \text{ or } (P_s < P_g \text{ and } SOC_{SC} < 55) \\ 100 & \text{otherwise} \end{cases} \tag{5.13}$$

$$X = k_1(SOC_{SC} - 65) + k_2 \frac{d}{dx} SOC_{SC} \tag{5.14}$$

$$P_g = P_{base} + k_3(SOC_{bat} - 65) + k_4 \frac{d}{dx} SOC_{bat} \tag{5.15}$$

where $P_{sc\_\%}$ is the percentage of power difference (P_s-P_g) transferred to the supercapacitor, P_{base} is the initial grid power reference. k_1, k_2, k_3, and k_4 are scaling factors.

According to (5.13) – (5.15), when there is a surplus of power (P_s>P_g) and supercapacitor has room for storing energy the total amount of excess power is transferred to the supercapacitor. When it is reaching the upper threshold part of the charging power is diverted to the battery. This helps prevent supercapacitor overcharging. On the other hand, when there is a deficit of power (P_s<P_g) and supercapacitor has sufficient amount

of energy stored (SOC>55) the entire power deficit is taken from the supercapacitor. If the supercapacitor continues to discharge and reaching the lower threshold part of the power deficit is taken from the battery to prevent over-discharging of the supercapacitor.

The grid power reference is adjusted based on the deviation of the Li-Ion battery SOC from 65% and rate of change of SOC to maintain battery SOC within the normal working range.

5.4 Simulation Results and Discussion

The grid integrated OWC system with the proposed PMS is modelled in MATLAB/Simulink. System parameters are given in Table 5. 2. More details on modelling of the OWC air-turbine, generator, grid, and ESSs can be found in (Rajapakse et al., 2017b) and (Rajapakse et al., 2018b). Simulations are carried out for 1000 seconds. Simulation results shown in Figures 5. 2 – 5. 5 are used to evaluate performance of the proposed PMS in two different scenarios namely, turbine-generator (TG) controlled at set rotational speed and variable rotational speed.

5.4.1 Turbine-generator operated at set speed

This first case study is designed to maintain the rotational speed of turbine-generator at 68rad/sec. The pressure head of the OWC chamber is shown in the Figure 5. 2. a). Figure 5. 2. b), depicts the OWC air-turbine torque. As mentioned in Section 5.2, the air-turbine torque varies with the differential air pressure as it controls the airflow through the turbine. Figure 5. 2. c), shows the turbine-generator rotor angular speed. The controller has maintained the angular speed close to the set point throughout the simulation.

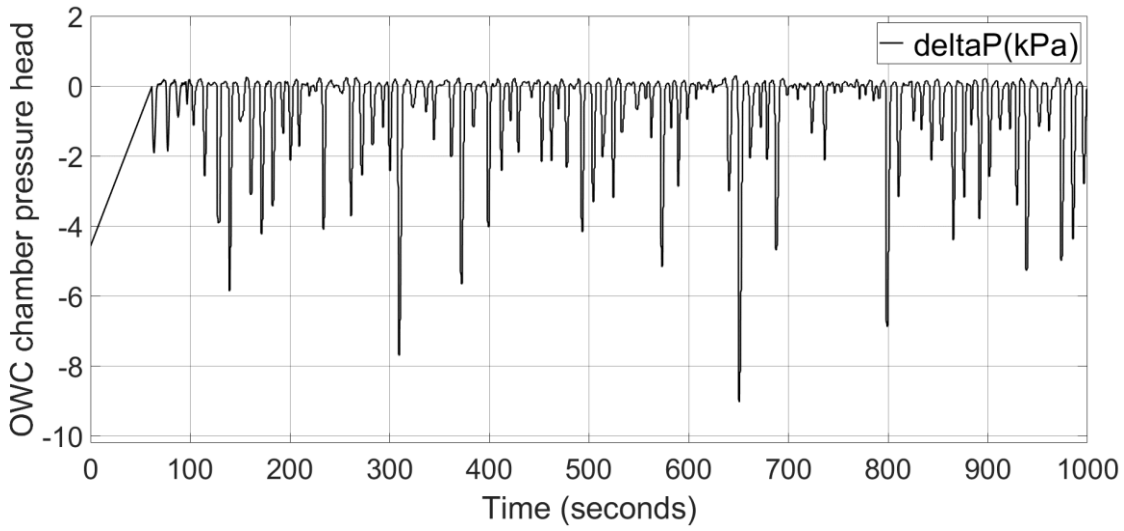
deltaP(kPa)
OWC chamber pressure head
Time (seconds)
2
0
-2
-4
-6
-8
-10
0
100
200
300
400
500
600
700
800
900
1000

(a)

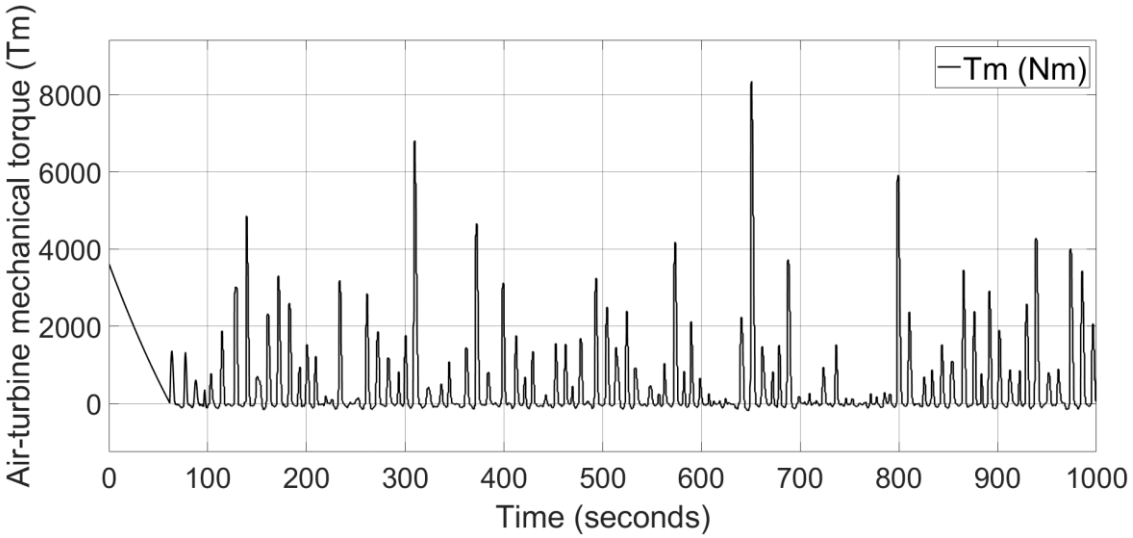
Tm (Nm)
Air-turbine mechanical torque (Tm)
Time (seconds)
8000
6000
4000
2000
0
0
100
200
300
400
500
600
700
800
900
1000

(b)

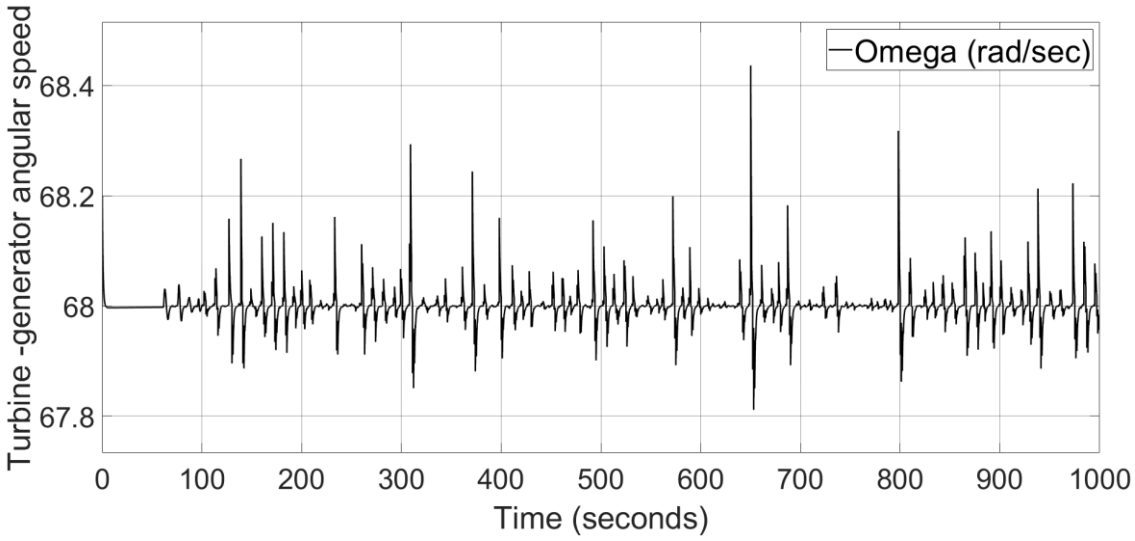

(c)

Figure 5. 2: First case study: a). OWC chamber pressure head ΔP(kPa), b). air-turbine mechanical torque T_m(Nm), c). turbine-generator rotor angular speed ω_m(rad/sec).

Simulation results of the output power of the turbine-generator, supply power to the grid, and supercapacitor power under the proposed power management strategy are shown in Figure 5. 3. a). The Li-Ion battery power is shown in Figure 5. 3. b). These results confirm that, irrespective of the large power pulses coming from the generator, supply power to the grid is maintained at a steady level. The grid power, P_g, is adjusted based on the deviation of battery SOC from 65% and its rate of change to maintain battery SOC within the safe range. The SOCs of the supercapacitor and Li-Ion battery are shown in Figure 5. 3. c). The results confirm that the proposed PMS is capable of maintaining the ESS's SOC within their set limits. The dc-link voltage is shown in Figure 5. 3. d). This is regulated close to its reference, 1200V, within 7% deviation throughout the simulation. Successful regulation of dc-link voltage confirms the quality power output to the grid and assists to regulate the generator rotor speed. These results confirm the efficacy of the proposed PMS in maintaing smooth power flow to the grid while ensuring that enegry storage elements are operatined withing their safe limits.

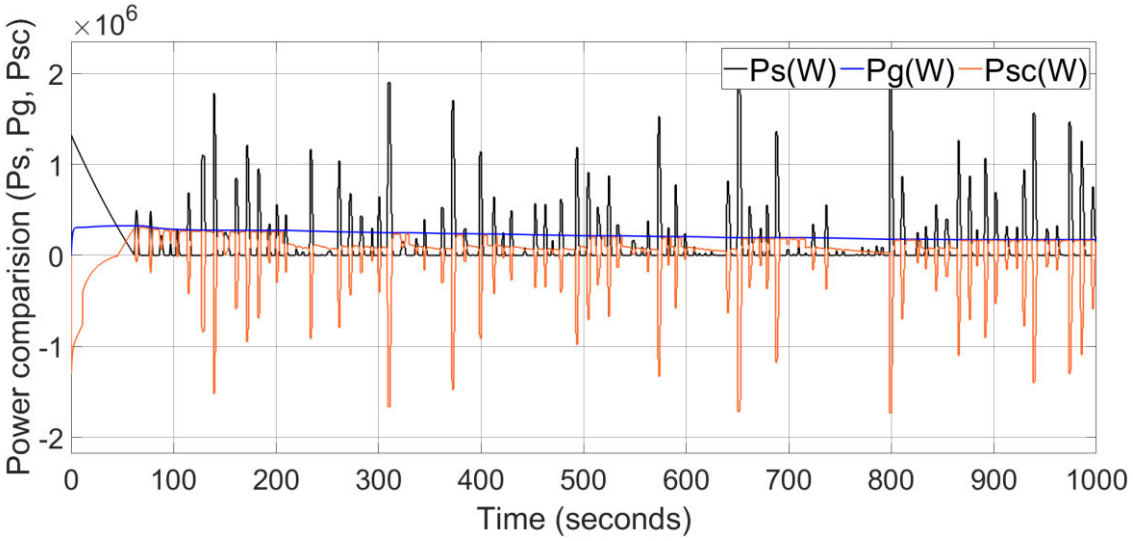
×10^6
Power comparision (Ps, Pg, Psc)
Ps(W)
Pg(W)
Psc(W)
Time (seconds)

(a)

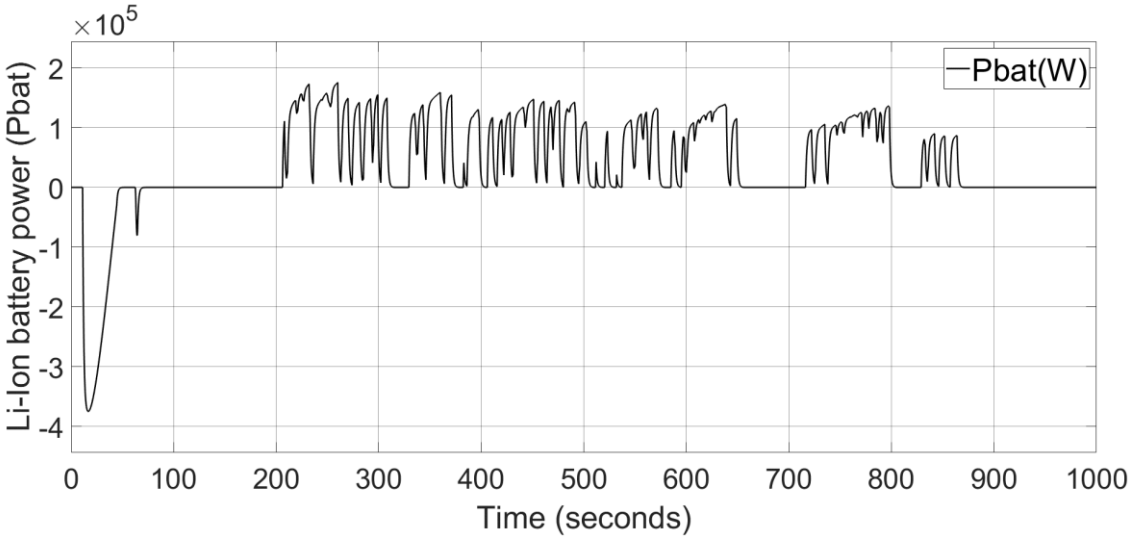
×10^5
Li-Ion battery power (Pbat)
Pbat(W)
Time (seconds)

(b)

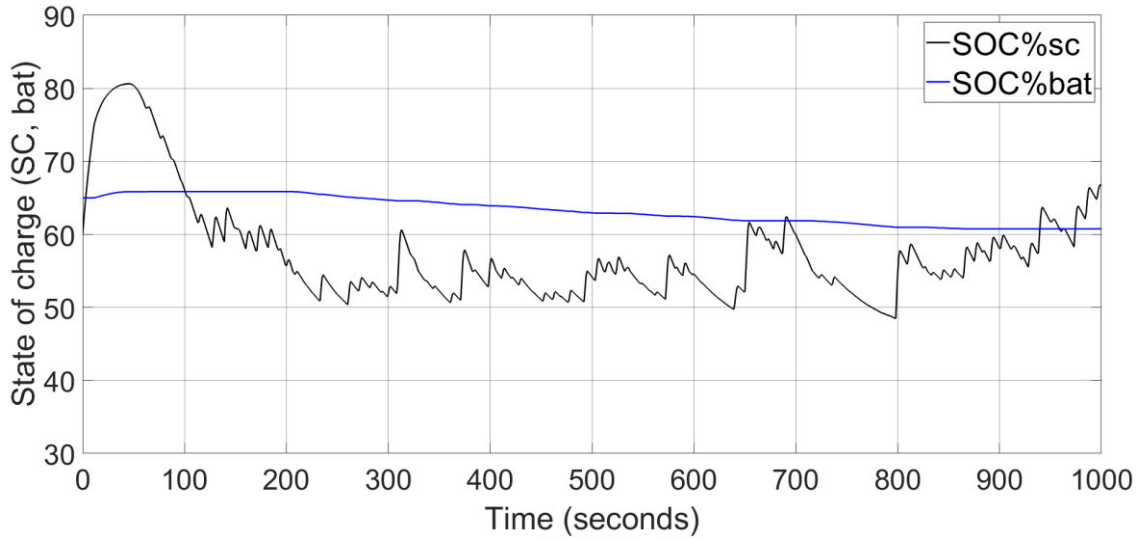

(c)

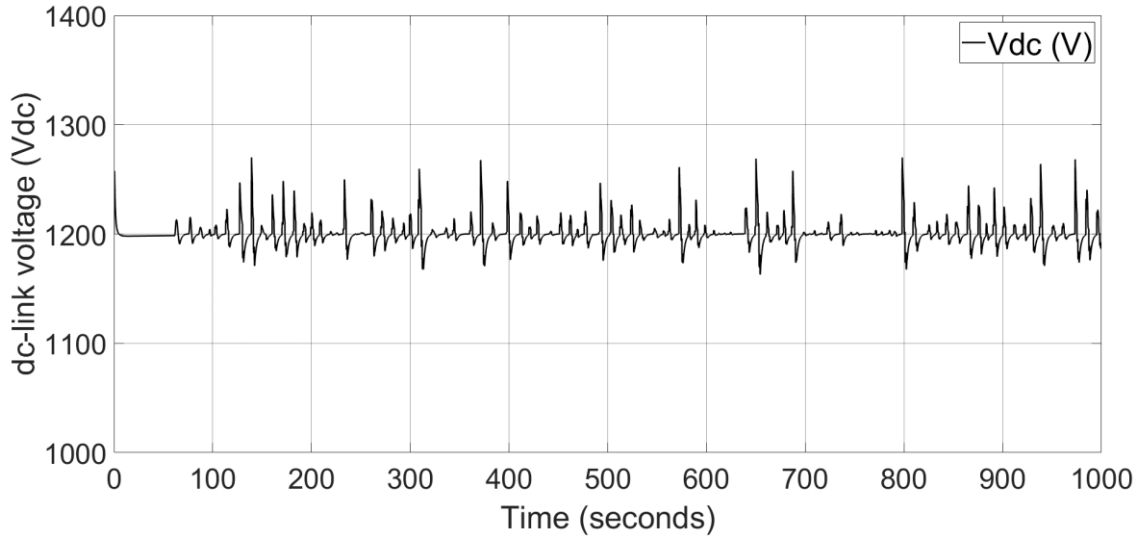

(d)

Figure 5. 3: Fist case study: a). Power comparison of OWC generator power P_s(W), Grid power P_g(W), and Supercapacitor power P_{sc}(W), b). Li-Ion battery power P_{bat}(W), c). state of charge of the supercapacitor ($SOC\%_{sc}$) and battery ($SOC\%_{bat}$), d). dc-link Voltage v_{dc}(V).

5.4.2 Turbine-generator operated at variable speed

In the second case study, the turbine speed is controlled with 30% variation (52rad/s and 90rad/s) compared the to fix speed setting to observe the effect on the supercapacitor sizing. All other parameters are same as in the first case study.

The air-turbine mechanical torque is shown in Figure 5. 4. a). Figure 5. 4. b), illustrates the turbine-generator rotor angular speed. The angular speed is maintained in between the

predesigned speed range for most of the simulation. This variable rotational speed control approach can be effectively applied to the future experiments to widen the response of the turbine to varying power level of the waves, enabling the turbine to respond efficiently to a wider range of sea states. Figure 5. 4. c), depicts the simulation results of the output power of the turbine-generator, supply power to the grid, and supercapacitor power under the proposed power management strategy. The supercapacitor size used in this study is half of the previous study to gain the similar or better power output. This confirms that the variable speed operation of the turbine helps reduce the supercapacitor size. The Li-Ion battery power is shown in Figure 5. 4. d). Figure 5. 4. e) and 5. 4. f) illustrate the enlarged output power to the grid and rate of change of the Li-Ion battery SOC% respectively. These results confirm that more output power is supplied to the grid and more power is transferred to the Li-Ion battery compared to the case study 1. Also, the supply power to the grid is maintained closer to the reference, 258kW, compared to the previous study.

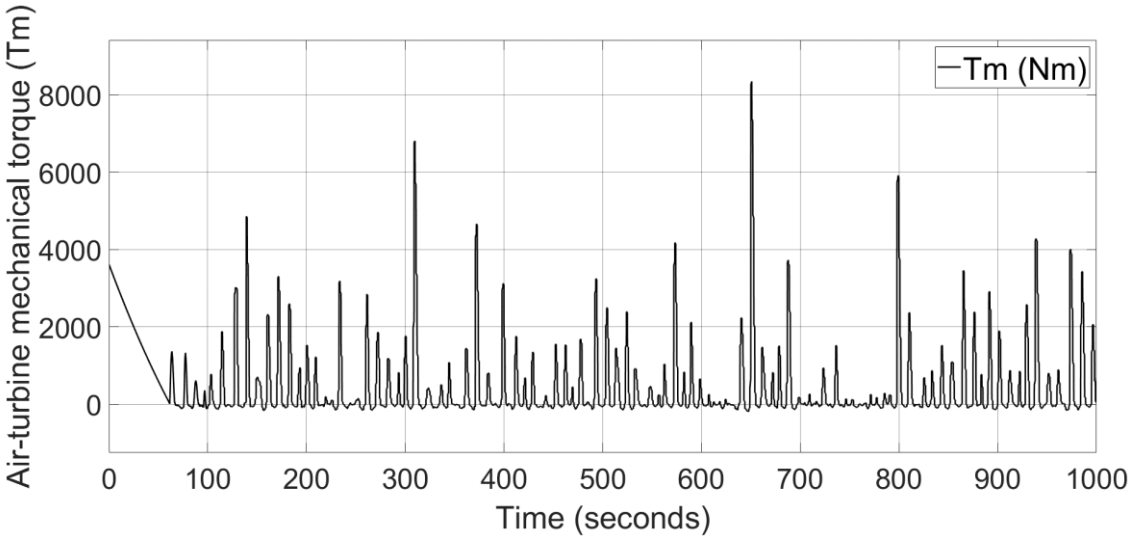

(a)

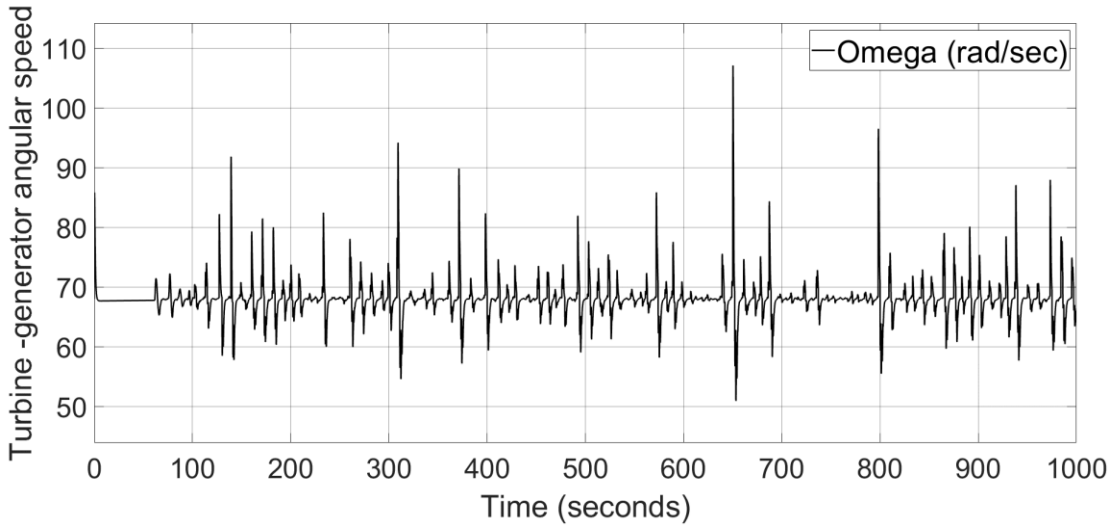
Omega (rad/sec)
Turbine -generator angular speed
110
100
90
80
70
60
50
0
100
200
300
400
500
600
700
800
900
1000
Time (seconds)

(b)

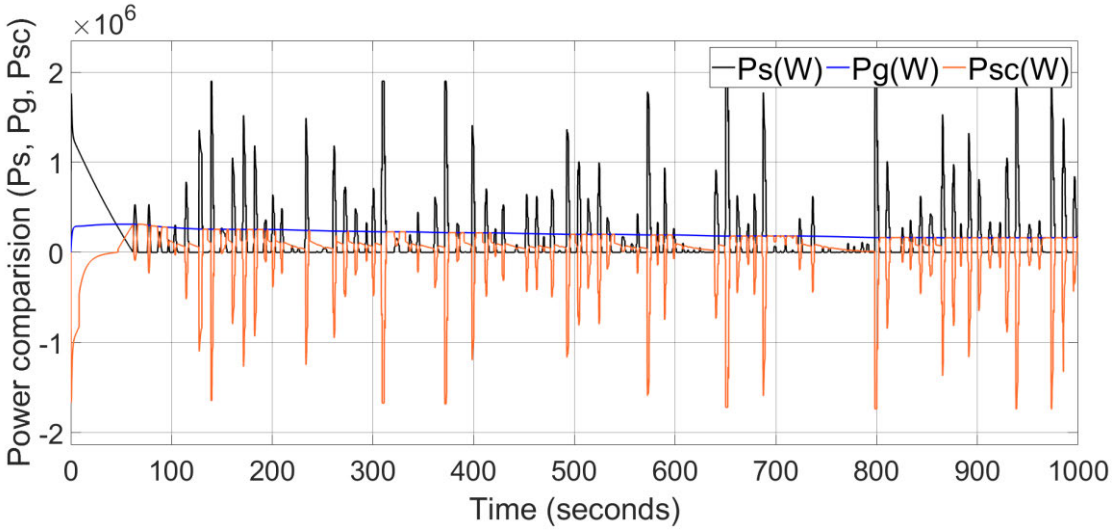
×10^6
Ps(W)
Pg(W)
Psc(W)
Power comparision (Ps, Pg, Psc)
2
1
0
-1
-2
0
100
200
300
400
500
600
700
800
900
1000
Time (seconds)

(c)

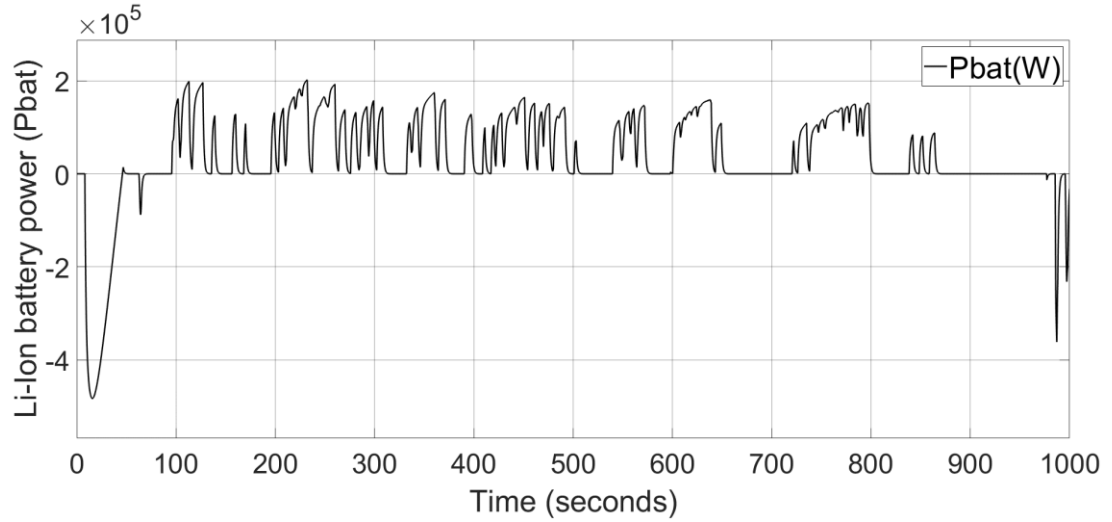
×10^5
Pbat(W)
Li-Ion battery power (Pbat)
2
0
-2
-4
0
100
200
300
400
500
600
700
800
900
1000
Time (seconds)

(d)

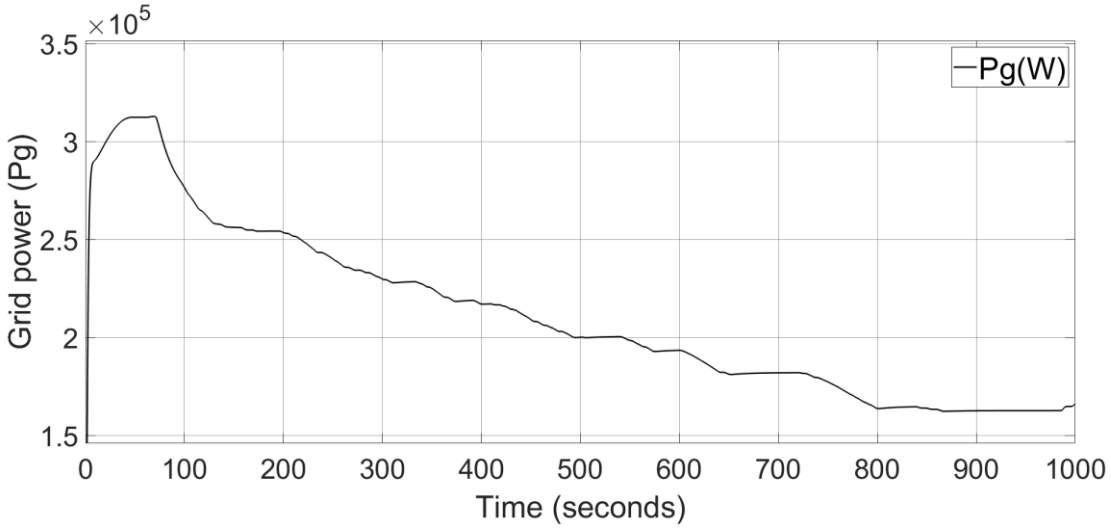
×10^5
3.5
3
2.5
2
1.5
Grid power (Pg)
Pg(W)
0
100
200
300
400
500
600
700
800
900
1000
Time (seconds)

(e)

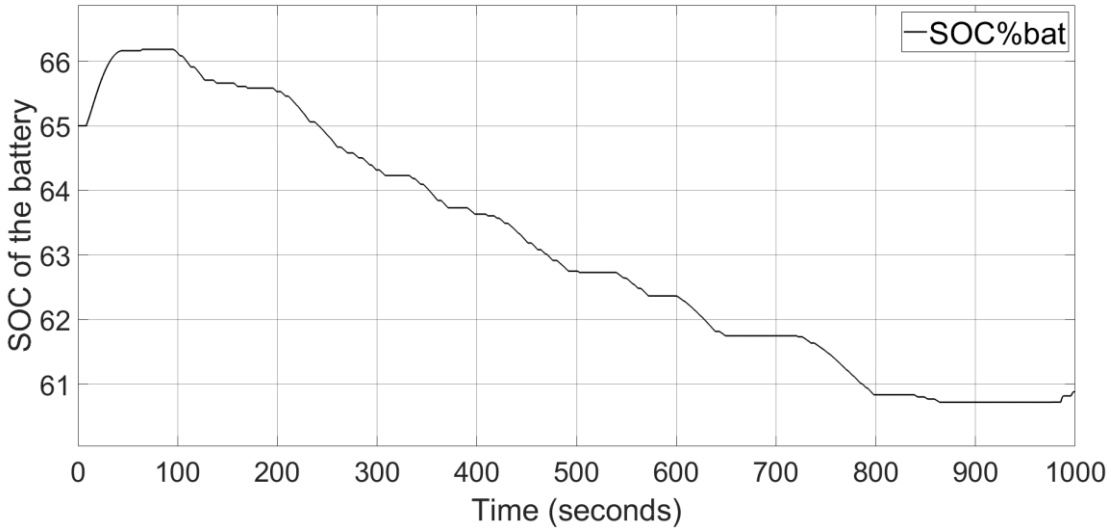
SOC%bat
66
65
64
63
62
61
SOC of the battery
0
100
200
300
400
500
600
700
800
900
1000
Time (seconds)

(f)

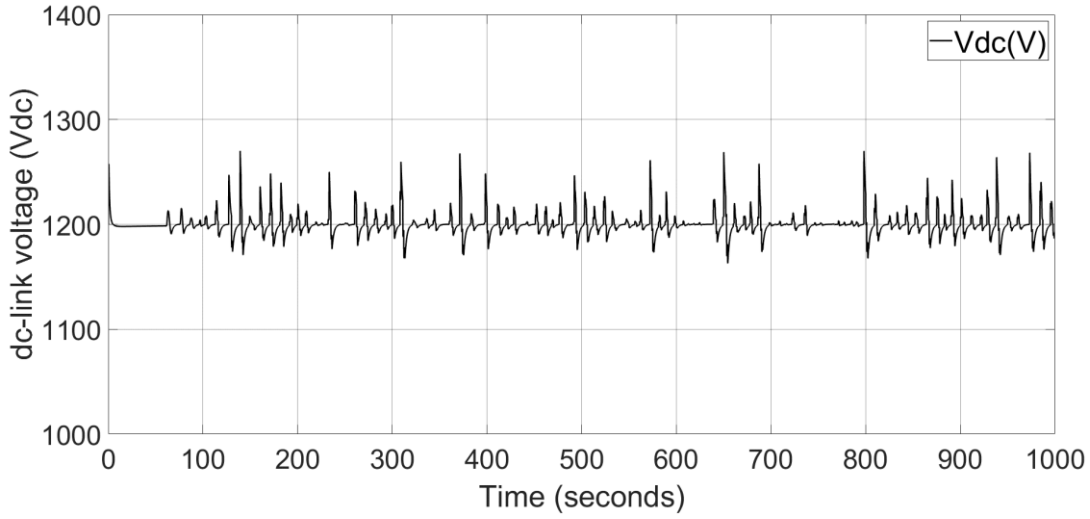
Vdc(V)
1400
1300
1200
1100
1000
dc-link voltage (Vdc)
0
100
200
300
400
500
600
700
800
900
1000
Time (seconds)

(g)

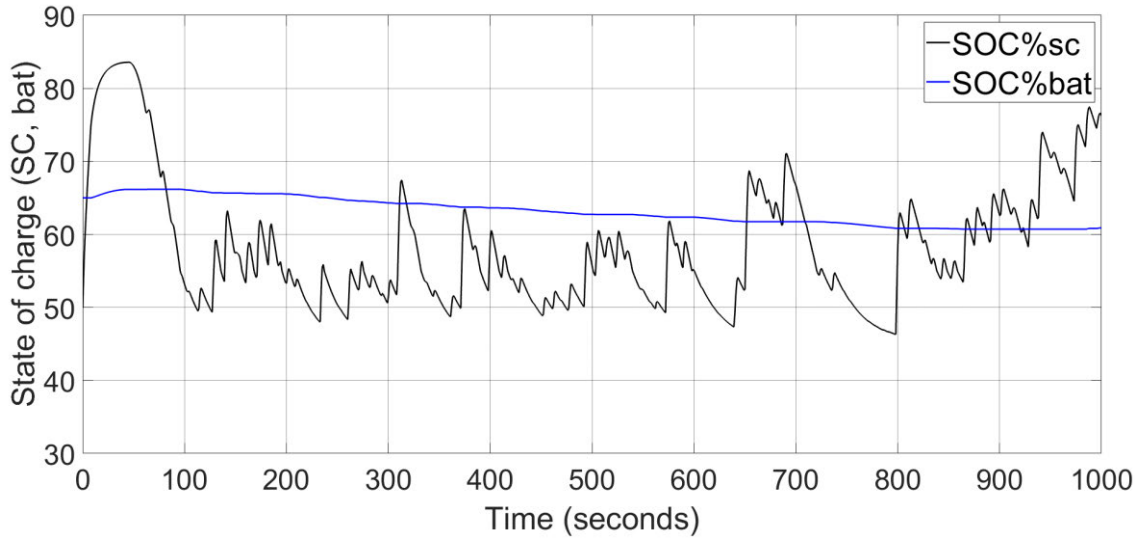

(h)

Figure 5. 4: Second case study: a). Air-turbine mechanical torque T_m(Nm), b). Turbine-generator rotor angular speed ω_m(rad/sec), c). Power comparison of OWC generator power P_s(W), Grid power P_g(W), and Supercapacitor power P_{sc}(W), d). Li-Ion battery power P_{bat}(W), e). grid power P_g(W), f). SOC% of the Li-Ion battery (SOC%bat), g). dc-link Voltage v_{dc}(V), h). state of charge of the supercapacitor (SOC%$_{sc}$) and battery (SOC%$_{bat}$).

The dc-link voltage is shown in Figure 5. 4. g), which is regulated close to its reference with ±7% deviation. As in case study 1, the PMS efficiently coordinates and controls the OWC system to maintain the dc-link voltage. The SOCs of the supercapacitor and Li-Ion battery are shown in Figure 5. 4. h). These results indicate that, compared to case study 1, controlling of the turbine-generator angular speed at variable speed range along with proposed PMS help increase the overall performance of the OWC system.

Table 5. 2: Parameters used in the OWC system design (Rajapakse et al., 2018b).

PMSG		**Supercapacitor**	
Rated Power	2MW	Capacitance (C_{sc}) Case1 Case2	 99.6F 49.8F
Rotational speed Case study 1 Case study 2	 68rad/s 52-90rad/s	Resistance	31.25mΩ
Rated Voltage	690Vrms	Maximum voltage	1200V
Rated current	1673.5A	Maximum current	3000A
Resistance (Phase) (R_s)	0.0024Ω	**Li-Ion battery**	
Inductances (Phase) (L_d=L_q)	0.355mH	Voltage	800V

Number of pole pairs	4	Rated Capacity	300AH
Magnetic flux (Ψ_{PM})	0.666Wb	Min and maximum voltage	693-900V
Inertia (J) Case study 1	$20kgm^2$	maximum current	1008A
Grid		Resistance	200mΩ
Voltage	690Vrms	Energy	100kWh per cell
Frequency	50Hz	C rate RMS	1.4C
Power reference	258kW	**Other**	
DC-link		Sample time	$2x10^{-4}$ s
DC-link voltage (v_{dc})	1200V	Simulator run time (T_{commit})	1000 s
DC-link current (i_{inv_max})	1000A		
DC-link capacitor (C_{dc})	4.4mF		

5.5 Conclusion

This paper presents a power management strategy to improve the power quality and availability of a grid connected unidirectional air turbine-generator OWC wave energy converter with HESS. The study can be considered as a preliminary study as well that compares fixed and variable speed operation of the particular WEC used in this work. The proposed PMS is used to coordinate and control the bidirectional dc-dc converters which connect the ESSs to the dc-link. Performance of the proposed PMS is assessed in two case studies namely, fixed speed operation and variable speed operation of the turbine. In both cases, proposed PMS is able to reduce the mismatch between supply and demand and maintain smooth delivery of power to the grid. Simulation results reveal that the variable speed operation helps reduce the capacity of the SCES to almost a half compared to the fixed speed operation. Therefore, variable speed operation can be used to reduce the overall cost.

6

POWER SMOOTHING AND ENERGY STORAGE SIZING OF VENTED OSCILLATING WATER COLUMN WAVE ENERGY CONVERTER ARRAYS

This chapter was published in the special issue on ‘Grid Connected Converters’ of the ‘Energies’ journal. The citation for the research article is:

G. Rajapakse, S. G. Jayasinghe, and A. Fleming, " Power Smoothing and Energy Storage Sizing of Vented Oscillating Water Column Wave Energy Converter Arrays ," *Energies 2020*, vol. 13, 1278, 2020.

Abstract

Oscillating water column wave energy converter arrays can be arranged to enhance the energy production and quality of power delivered to the grid. This study investigates four different array configurations of vented oscillating water columns and their effect on power quality and capacity of the energy storage systems required to absorb power fluctuation. Configuring the array of vented oscillating water columns as a nearshore detached breakwater allows combining the benefits of their complementary features. This increases the economic optimization of wave energy converters, paving the path to the energy market. The operations of the integration schemes are evaluated using the results obtained from simulations carried out using MATLAB/Simulink software. Simulation results show that the array of vented oscillating water columns and array of vented oscillating water columns as nearshore detached breakwater configurations increase the quality of power delivered to the grid and reduce the capacity of the energy storage systems required.

Keywords: Hybrid energy storage system, Li-Ion battery energy storage, vented oscillating water column wave energy converter, detached breakwater, power quality, supercapacitor energy storage, wave energy converter arrays.

6.1 Introduction

Wave energy is a promising source of renewable energy available worldwide. At present, research and development of efficient, reliable, and sustainable wave energy converters (WECs) are in progress (Falcao, 2010, Vicinanza et al., 2019, Falcao and Henriques, 2016). The oscillating water column (OWC) technology equipped with an air turbine is one of the most promising and possibly the most reliable and fastest thriving technologies in the wave energy harvesting sector (Falcao and Henriques, 2016, De Fonseca et al., 2019). Nevertheless, to gain economic optimization to enter the energy market and make a significant contribution, these converters must be large enough with many converters deployed as an array (O' Sullivan et al., 2013). To further improve economic feasibility, these arrays can be integrated with power management systems (PMSs) with the aim of enhancing energy harvesting and the quality of electrical power delivered to the grid. The WEC array configurations and PMSs are not new to the renewable energy sector (Hamidi et al., 2015, Kim et al., 2017b, Tang et al., 2017). Nevertheless, the feasibility of a PMS applied to an array of OWC wave energy converter systems is yet to be reported. This paper expands the research in (Rajapakse et al., 2018a), which is based on a grid integrated single/isolated fixed vented oscillating water column (VOWC) with supercapacitor and Li-ion battery hybrid energy storage system (HESS). This paper reports on array configurations for VOWCs.

The OWC principle is based on passing oscillating air through an air turbine fixed in a partially submerged chamber due to oscillating motion of the water column inside it (Falcao, 2010). A generator coupled to the air turbine converts the mechanical energy of the air turbine to electrical energy. The VOWC is a variation on the standard OWC format to vent the OWC chamber on positive pressure to make the air flow through the turbine unidirectionally. The pneumatic conversion efficiency has been shown at model scale to be equivalent to or better than the standard bi-directional configuration (Ansarifard et al., 2019). This study is vital, since the array of VOWC technology is adaptable for existing ocean structures or future developments such as breakwaters.

Placing multiple VOWCs in a breakwater may affect the pressure profiles of each VOWC and thus significantly change the energy capture. Therefore, the array layout should be designed in a way to gain the benefit of these interactions. Moreover, spacing between

the VOWC devices should be tuned to the local peak wavelength as explained in (De. Chowdhury et al., 2015, Nader et al., 2014). Since the research in OWC array configuration is still at an early stage, information regarding optimal OWC array configurations or the efficiency reductions/fluctuations of OWC array devices is limited. Therefore, this model does not include hydrodynamic interactions of VOWCs. Instead, it concentrates on (1) a single PMS for grid integration of an isolated VOWC, (2) a nearshore detached breakwater (VOWCDBW), and (3) two different array configurations of VOWCs with a shared hybrid energy storage system as shown in Figure 6. 1.

This paper investigates one of the worst-case scenarios in terms of energy management by assuming that both the VOWCs in the VOWCDBW experience the same pressure profile. Four case studies were carried out to identify and compare the output of VOWC array configurations with regard to electrical power generation and smoothing as shown in Figure 6. 1.

The four cases studied in this paper are: (1) single VOWC, (2) two VOWCs in a detached breakwater structure, (3) an array of three isolated VOWCs, and (4) an array of three VOWCDBWs. For this study, two of the VOWCs in the VOWCDBW system are used with thrice the width of the model spacing to minimise the effects of interaction (Ashlin et al., 2018). In respect to energy harvesting and electrical power generation, all these approaches have pros and cons. A VOWCDBW that can be built into a coastal protection structure can considerably increase the average power compared to an isolated VOWC but has minimal effect on power smoothing compared to an array.

An array of VOWCs can be designed effectively to smooth the electrical power output taking advantage of the temporal–spatial distribution of the wave energy. For an array layout, researchers have proposed different patterns such as rectangular, semicircular, triangular, etc. Nonetheless, the pattern is given less importance compared to the distribution of surge separation distance (De. Chowdhury et al., 2015, Nader et al., 2014, Ashlin et al., 2018, Jansson, 2016, Manasseh et al., 2018). Therefore, three isolated VOWCs and three VOWCDBCs placed in a hypotenuse of a right triangle as shown in Figure 6. 1. c), 6. 1. d) were selected to improve the power smoothing. The configuration of five times the width of the VOWC for the spacing between two VOWCs was also considered as recommended in (Nader et al., 2014).

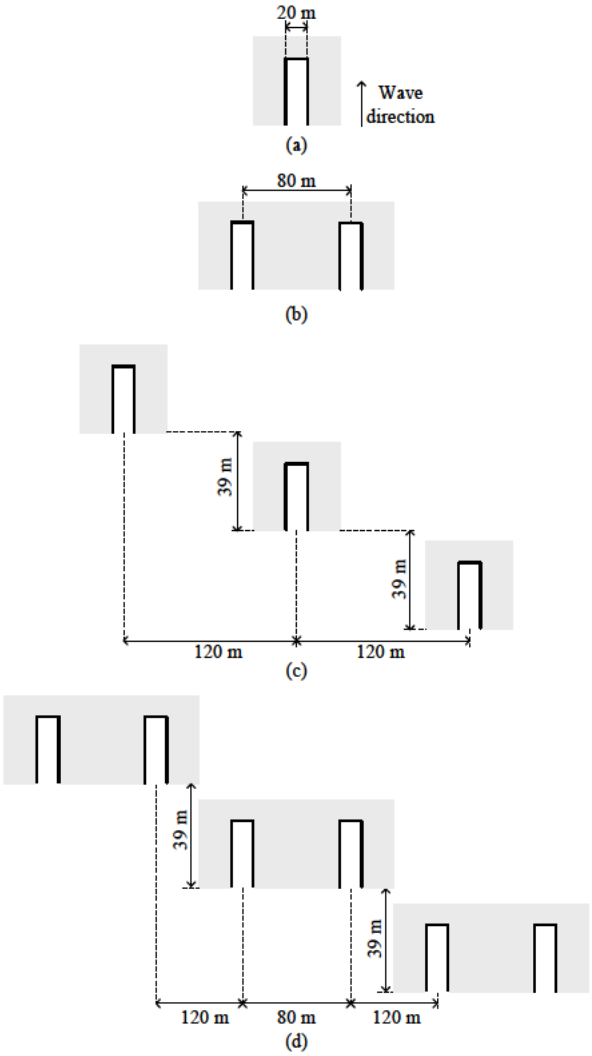

Figure 6. 1: Vented oscillating water column (VOWC) wave energy converter layouts: a). single VOWC, b). two VOWC devices with three times spacing, c). array of three individual VOWCs in the nearshore detached breakwater (VOWCDBW), d). hybrid array of VOWCs in the VOWCDBW.

This study proposes to combine VOWCDBW with an array configuration to get the advantage of complimentary dynamic features of both types of arrays that make provisions for enhancing energy capture and the smoothing effect simultaneously. The schematic layouts of the isolated VOWC, VOWCDBW, VOWC array, and VOWCDBW array are shown in Figure 6. 1. The schematic diagram of the electrical power conversion system is illustrated in Figure 6. 2. The schematic diagram of the single VOWC WEC, which corresponds to the configuration in Figure 6. 1. a), is shown in Figure 6. 2. a). The electrical connection of two WECs in the VOWCDBW configuration in Figure 6. 1. b) is shown in Figure 6. 2. b). Electrical connections of the other two array configurations also follow the same trend where all the rectifier outputs are connected to the same DC-link.

The electrical connection of the hybrid array of VOWCs in the VOWCDBW configuration in Figure 6. 1. d) is shown in Figure 6. 2. c).

The paper is organised as follows. Section 6. 2 outlines the power management strategy, which is derived from (Rajapakse et al., 2018a). Section 6. 3 explains the system design of VOWC arrays. Simulation results and discussion of the implications of the results are given in Section 6. 4. Conclusions derived from the discussion are presented in Section 6. 5.

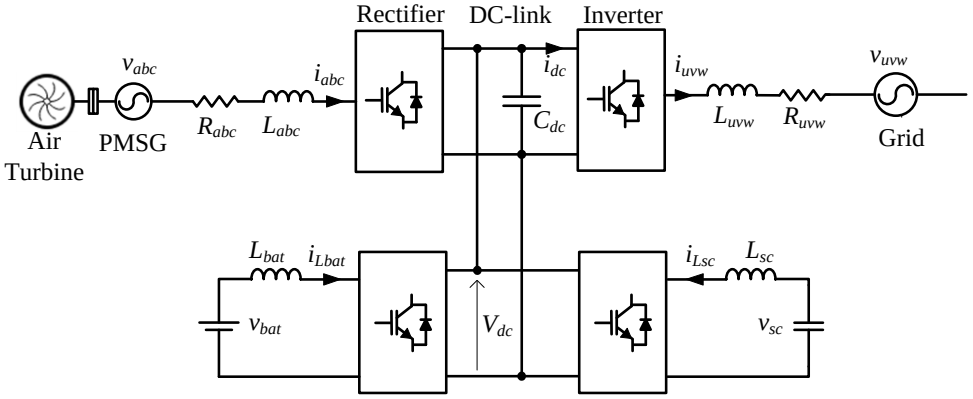
Rectifier
DC-link
Inverter
v_{abc}
i_{abc}
i_{dc}
i_{uvw}
v_{uvw}
Air
Turbine
PMSG
R_{abc}
L_{abc}
C_{dc}
L_{uvw}
R_{uvw}
Grid
L_{bat}
i_{Lbat}
i_{Lsc}
L_{sc}
v_{bat}
V_{dc}
v_{sc}

(a)

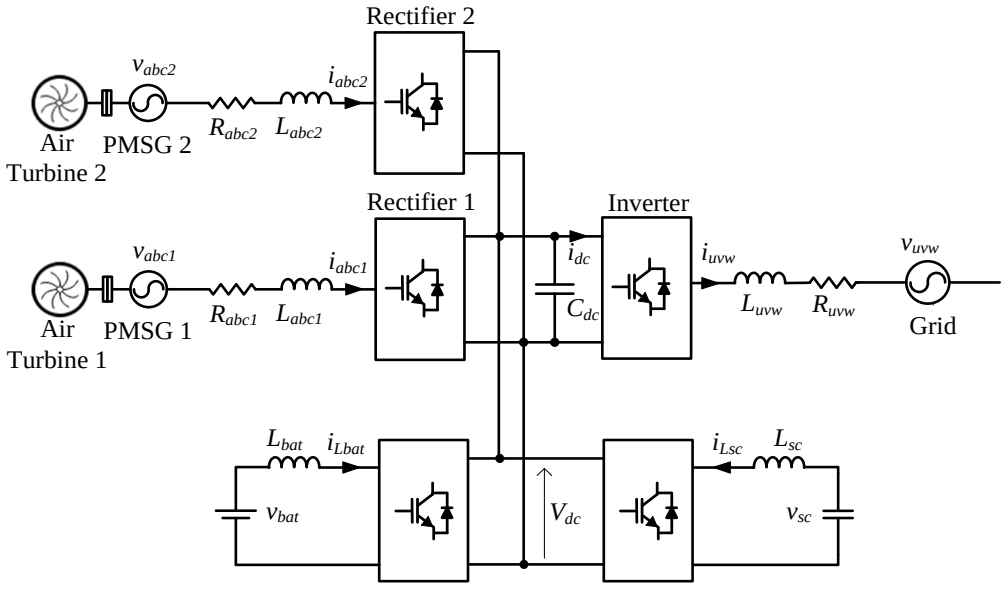
Rectifier 2
v_{abc2}
i_{abc2}
Air
Turbine 2
PMSG 2
R_{abc2}
L_{abc2}
Rectifier 1
Inverter
v_{abc1}
i_{abc1}
i_{dc}
i_{uvw}
v_{uvw}
Air
Turbine 1
PMSG 1
R_{abc1}
L_{abc1}
C_{dc}
L_{uvw}
R_{uvw}
Grid
L_{bat}
i_{Lbat}
i_{Lsc}
L_{sc}
v_{bat}
V_{dc}
v_{sc}

(b)

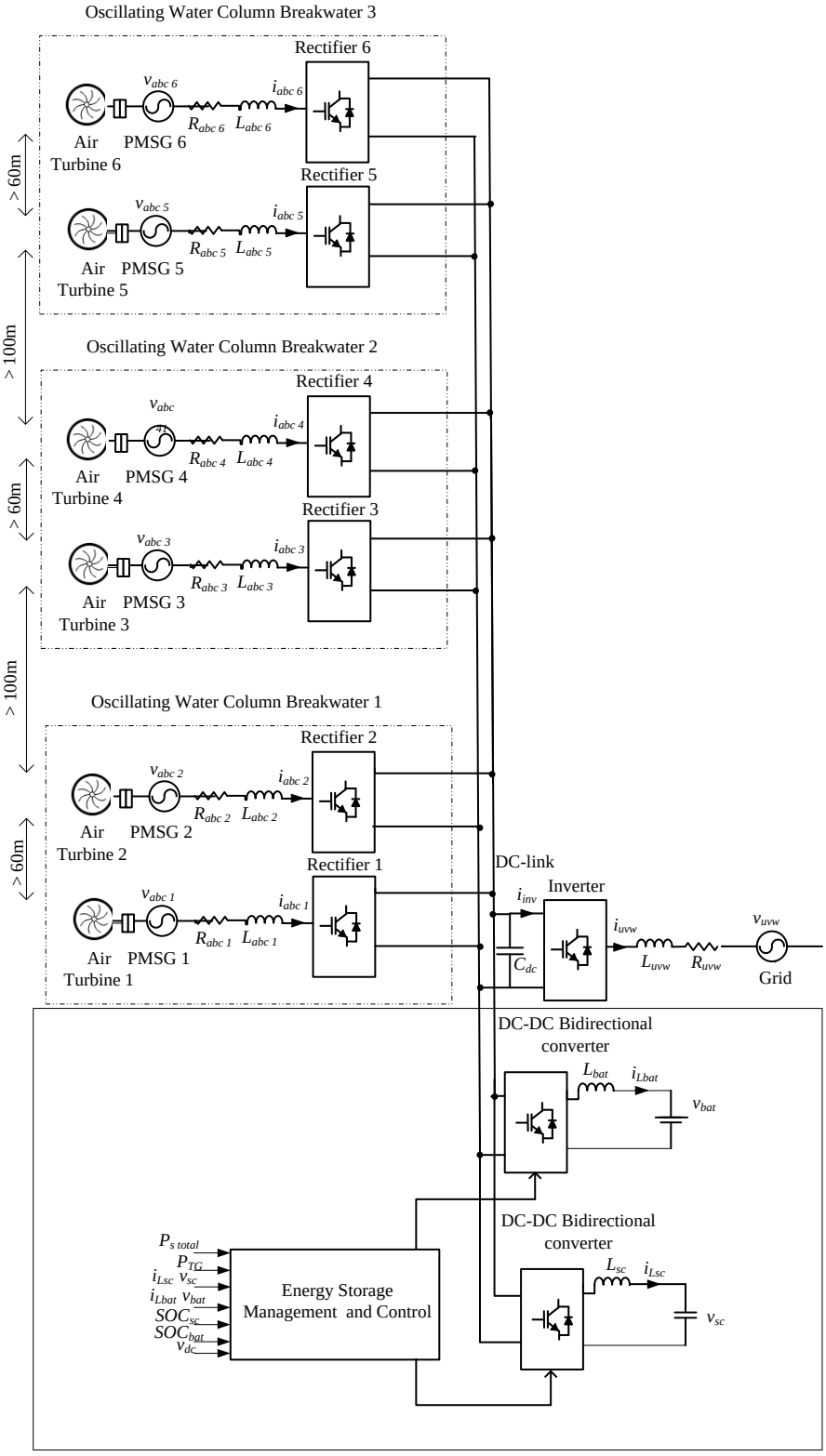

(c)

Figure 6. 2: Schematic diagram of the electrical power conversion system: a). single VOWC wage energy converter (WEC), b). single VOWCDBW with two VOWC WECs, c). hybrid array of VOWCs in the VOWCDBW.

6.2 Power Management System

The same PMS proposed by the authors in (Rajapakse et al., 2018a) was used in all four of the case studies without any changes. This approach was taken to confirm the validity of this PMS in any configuration of VOWC–grid integration. The PMS is expressed as (Rajapakse et al., 2018a)

$$P_{SC\_\%} = \begin{cases} 100 - X & \text{if } (P_s > P_g \text{ and } SOC_{SC} > 75) \text{ or } (P_s < P_g \text{ and } SOC_{SC} < 55) \\ 100 & \text{otherwise} \end{cases} \quad (6.1)$$

$$X = k_1(SOC_{SC} - 65) + k_2 \frac{d}{dx} SOC_{SC} \quad (6.2)$$

$$P_g = P_{base} + k_3(SOC_{bat} - 65) + k_4 \frac{d}{dx} SOC_{bat} \quad (6.3)$$

where P_g is the grid power, P_s is the VOWC generated power, and P_{sc} and P_{bat} are supercapacitor and battery power, respectively. $P_{sc\_\%}$ is the percentage difference of generated and grid power (P_s-P_g), which is transferred to the supercapacitor. The initial grid power reference is represented by P_{base}. SOC_{sc} is the state of charge of the supercapacitor. The state of charge of the battery is signified by SOC_{bat}. k_1, k_2, k_3, and k_4 are scaling factors, which are 1, 1, 2×10^4 and 10^5, respectively.

$P_s + P_{sc}$ is the primary source of power used by the PMS. P_{bat} is used only if $P_s + P_{sc}$ is unable to maintain the committed power output to the grid. When there is surplus power, the total amount of excess power is transferred to the supercapacitor if the supercapacitor's state of charge (SOC) is lower than its upper threshold (75%). Once it reaches its upper threshold, part of the charging power is diverted to the battery to prevent overcharging of the supercapacitor. Conversely, when there is a deficit of power, the entire power deficit is taken from the supercapacitor until the supercapacitor reaches its lower threshold (55%). Once it reaches its lower threshold, part of the power deficit is taken from the battery to prevent over-discharging of the supercapacitor. This minimises the usage of Li-ion battery storage. The proposed PMS aims to control the supercapacitor and battery SOCs to remain within their upper and lower thresholds (30–85%) to avoid overcharging/over-discharging to improve their lifetime. Rate of change of SOC of the Li-ion battery and its SOC deviation from 65% are used to adjust the grid power reference to maintain the battery SOC within the normal working range.

6.3 System Design and Modelling

As mentioned in the introduction, this study investigates isolated arrays of VOWCs and a VOWCDBW. In the VOWC, the pneumatic energy is only converted during a half wave cycle (inhalation). Therefore, the power pulse experienced is approximately twice as intense as the pulse experienced in a bi-directional air turbine configuration. These array systems are designed in such a way that both types of arrays enhance energy capture and power smoothing simultaneously. The pressure head of the VOWC chambers for the simulation is taken from the lab scale experiments done in (Bennet et al., 2017). Assumptions made in this study are listed below.

- Each of the VOWC device lengths is tuned to the local peak wavelength/wave period (in this case 13 s). A phase shift of 120° is introduced to each device in the array of VOWCs/VOWCDBWs as shown in Figure 6. 1 c), 6. 1. d) and 6. 5;
- In array configurations, the VOWCs/VOWCDBWs are placed in a hypotenuse of a right triangle as shown in Figure 6. 1, where the base is the coastline. This type of geometry is used to improve the quality of the power extracted by the combined air turbines, which will allow reducing the energy storage capacity;
- VOWC/VOWCDBWs are placed in a manner such that multiple device arrangements do not affect the efficiency of each device.
- The standard method of finding the energy deficit for the given period and choosing an energy storage capacity to match the deficit is used (Nimma et al., 2018).

The parameters given in Table 6. 1 were used to model each case study in MATLAB/Simulink to gain the simulation results discussed in the next section. The details of modelling the VOWC air turbine, turbine-generator, grid, energy storage systems (ESSs), and DC-to-DC bidirectional converters can be found in (Rajapakse et al., 2017b) and (Rajapakse et al., 2018b). The PMS is modelled using the rules presented in (Rajapakse et al., 2018a). The simulation was carried out for 1200 s. To observe the effect of the VOWC configuration on the power output and the supercapacitor sizing, the supercapacitor energy storage (SCES) SOC limits were set to vary between 45% to 85%.

Table 6. 1: Parameters used in the oscillating water column (OWC) system design.

Permanent Magnet Synchronous Generator (PMSG)		**Supercapacitor**	
Rated power	2 MW	Capacitance (C_{sc}) Case 1 Case 2 Case 3 Case 4	 19.8 F 39.6 F 39.6 F 39.6 F
Rated rotate speed	200–1500 rpm	Resistance	31.25 mΩ
Rated voltage	690–1140 Vac	Maximum voltage	1200 V
Rated frequency	10–60 Hz	Maximum current	3000 A
Resistance (phase) (R_s)	0.0024Ω	**Li-ion battery**	
Inductances (phase) ($L_d = L_q$)	0.355 mH	Voltage	800 V
Number of pole pairs (p)	4	Rated Capacity for all four cases	300 AH
Magnetic flux (Ψ_{PM})	0.667 Wb	Min and maximum voltage	693–900 V
Inertia (J)	23 kg m^2	maximum current	1008 A
Grid		Resistance	200 mΩ
Voltage	690 Vrms	Energy	100 kW h per cell
Frequency Power reference Case 1 Case 2 Case 3 Case 4	50 Hz 425 kW 0.9 MW 1.275 MW 2.7 MW	C rate RMS **Other**	1.4 C
DC-link		Sample time	2×10^{-4} s
DC-link voltage (v_{dc})	1200 V	Simulator run time (T_{commit})	1200 s
DC-link current (i_{inv_max})	1000 A		
DC-link capacitor (C_{DC})	4.4 mF		

6.4 Simulation Results and Discussion

The grid integrated VOWC, VOWCDBW, and array configurations with their respective air turbines and PMSs were modelled in MATLAB/Simulink, using the parameters that are given in Table 6. 1. The simulation results are shown in Figures 6. 3 – 6. 7, which are used to evaluate the proposed configurations and efficiency of those layouts in four different scenarios: case 1: isolated VOWC, case 2: two VOWC devices in the VOWCDBW with three times spacing, case 3: an array of three individual VOWCs, case 4: an array of three VOWCDBWs.

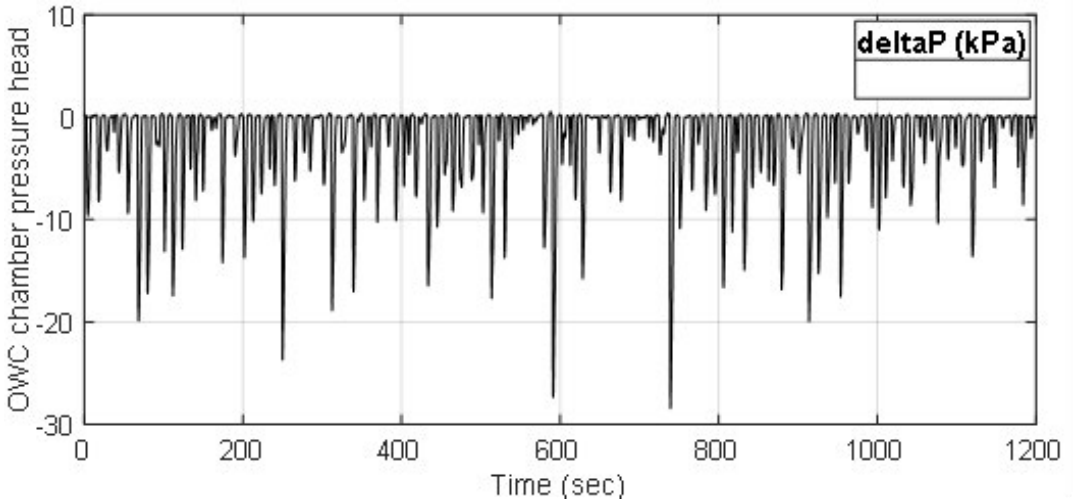
deltaP (kPa)
OWC chamber pressure head
Time (sec)
10
0
-10
-20
-30
0
200
400
600
800
1000
1200

(a)

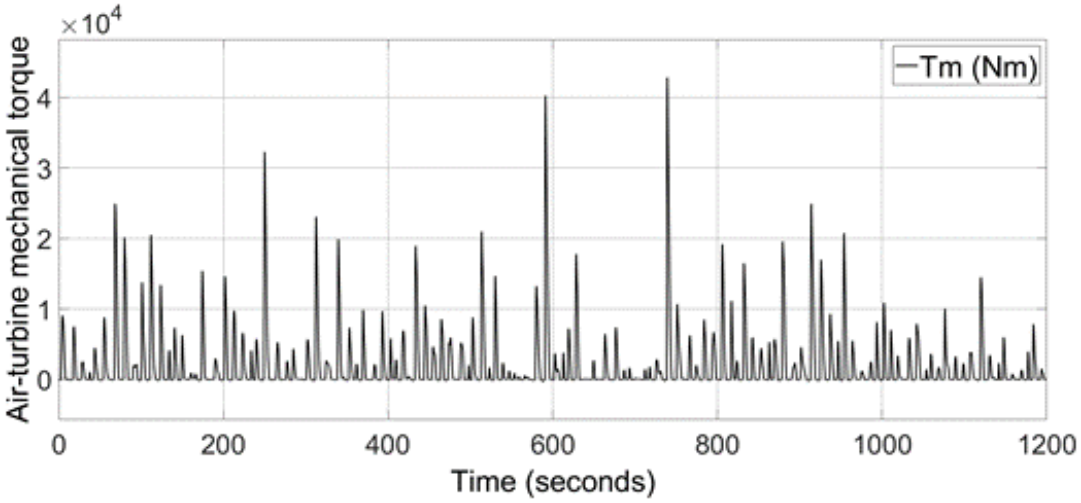
×10^4
Tm (Nm)
Air-turbine mechanical torque
Time (seconds)
4
3
2
1
0
0
200
400
600
800
1000
1200

(b)

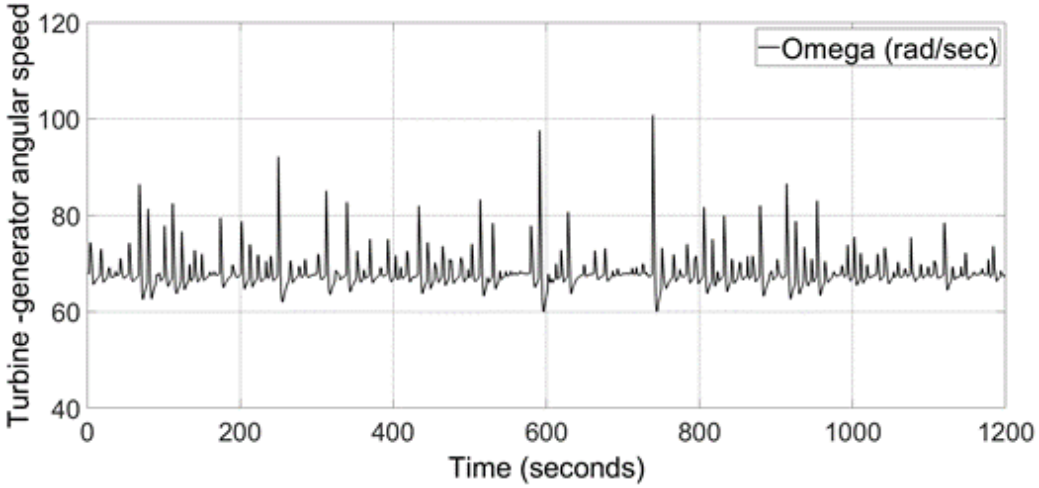
Omega (rad/sec)
Turbine -generator angular speed
Time (seconds)
120
100
80
60
40
0
200
400
600
800
1000
1200

(c)

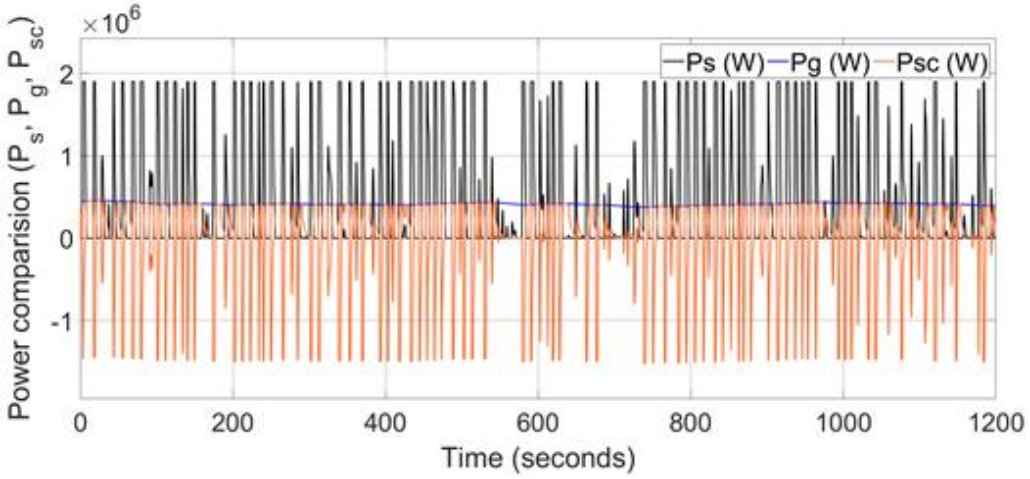
×10^6
Ps (W) Pg (W) Psc (W)
Power comparision (P_s, P_g, P_sc)
2
1
0
-1
0
200
400
600
800
1000
1200
Time (seconds)

(d)

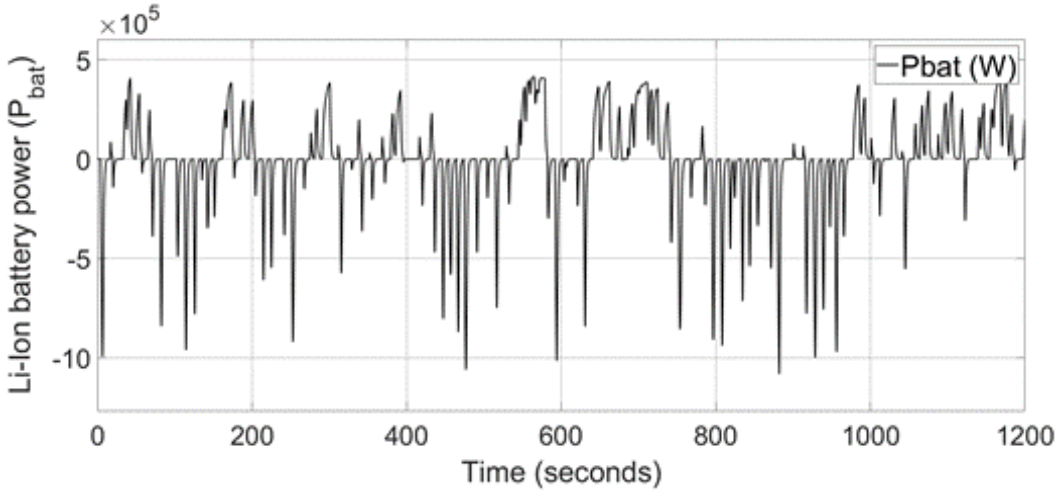
×10^5
Pbat (W)
Li-Ion battery power (P_bat)
5
0
-5
-10
0
200
400
600
800
1000
1200
Time (seconds)

(e)

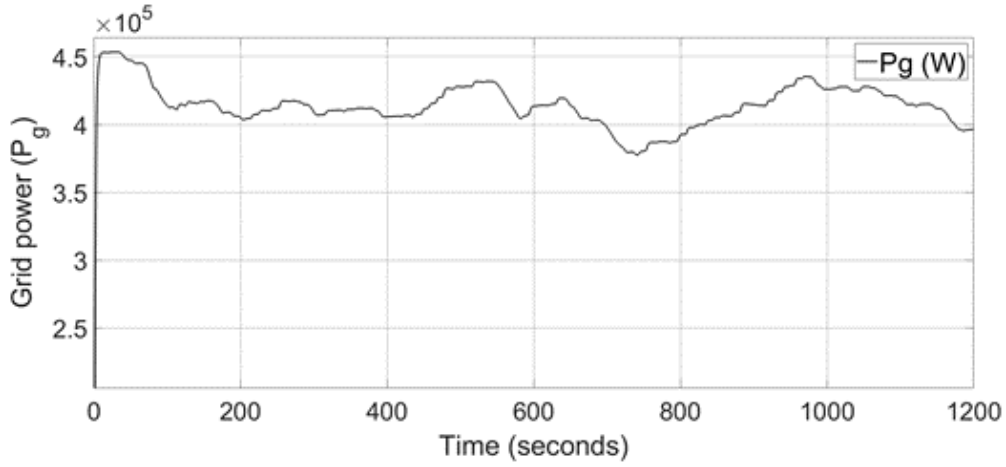
×10^5
Pg (W)
Grid power (P_g)
4.5
4
3.5
3
2.5
0
200
400
600
800
1000
1200
Time (seconds)

(f)

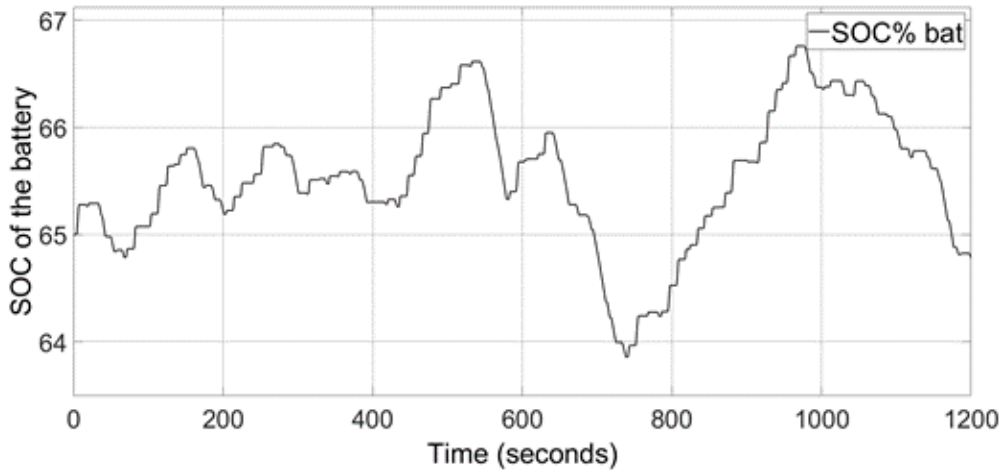

(g)

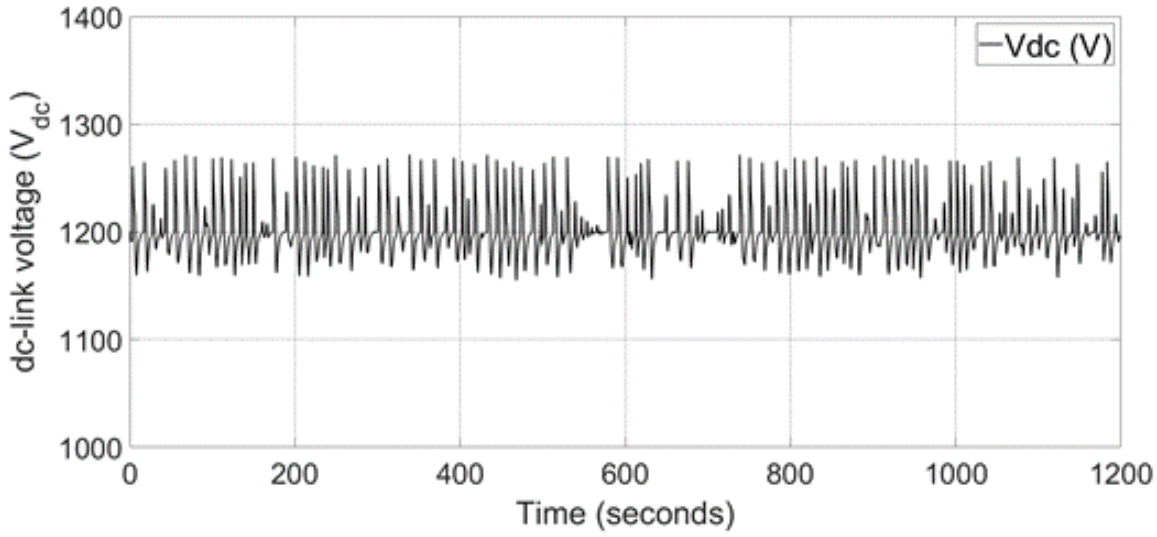

(h)

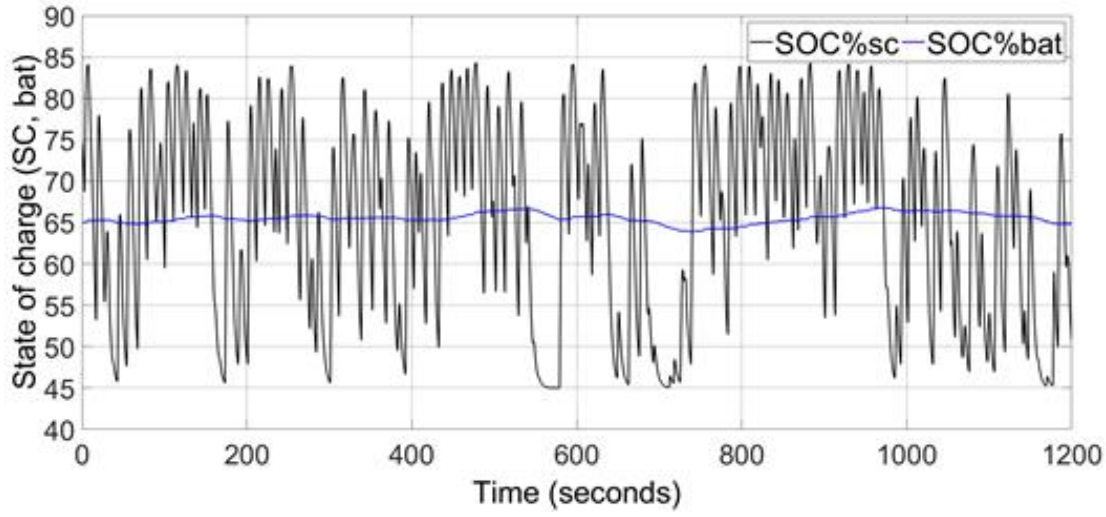

(i)

Figure 6. 3: First case study: a). VOWC chamber pressure head ΔP(kPa), b). air-turbine mechanical torque T_m(Nm), c). turbine-generator rotor angular speed ω_m(rad/sec), d).

power comparison of VOWC generator power P_s(W), grid power P_g(W), and supercapacitor power P_{sc}(W), e). Li-ion battery power P_{bat}(W), f). grid power P_{bat}(W), g). state of charge of the of the battery (SOC%$_{bat}$), h). DC-link Voltage v_{dc}(V), i). state of charge of the supercapacitor (SOC%$_{sc}$) and battery (SOC%$_{bat}$).

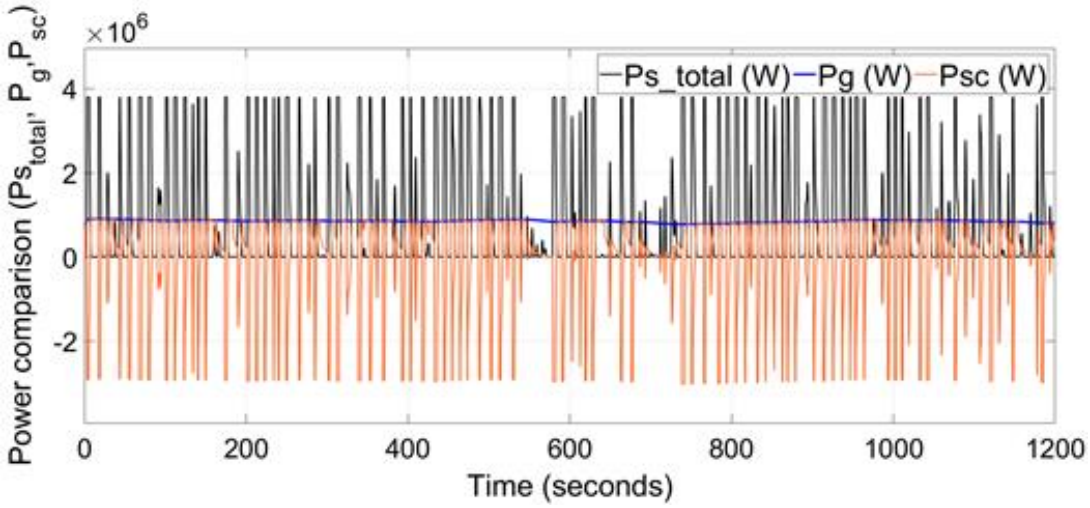

(a)

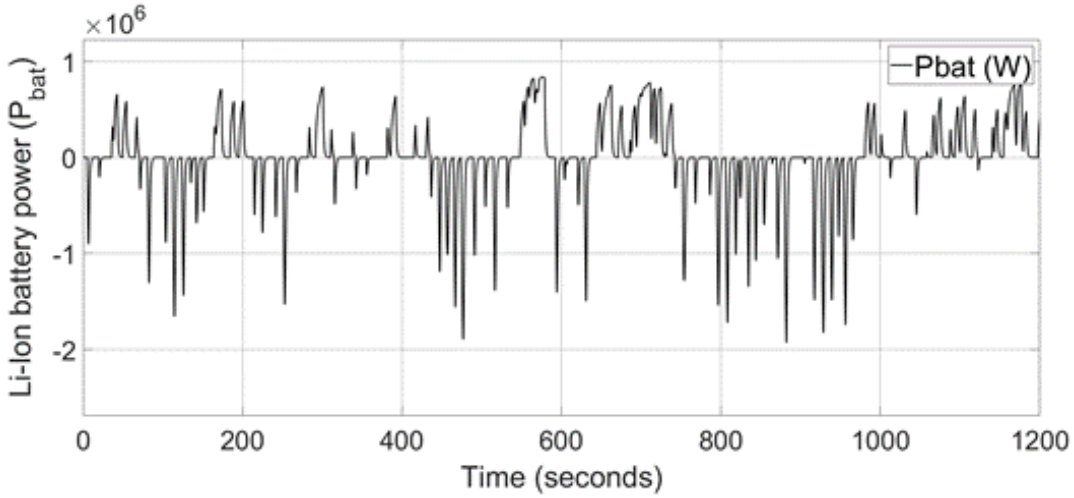

(b)

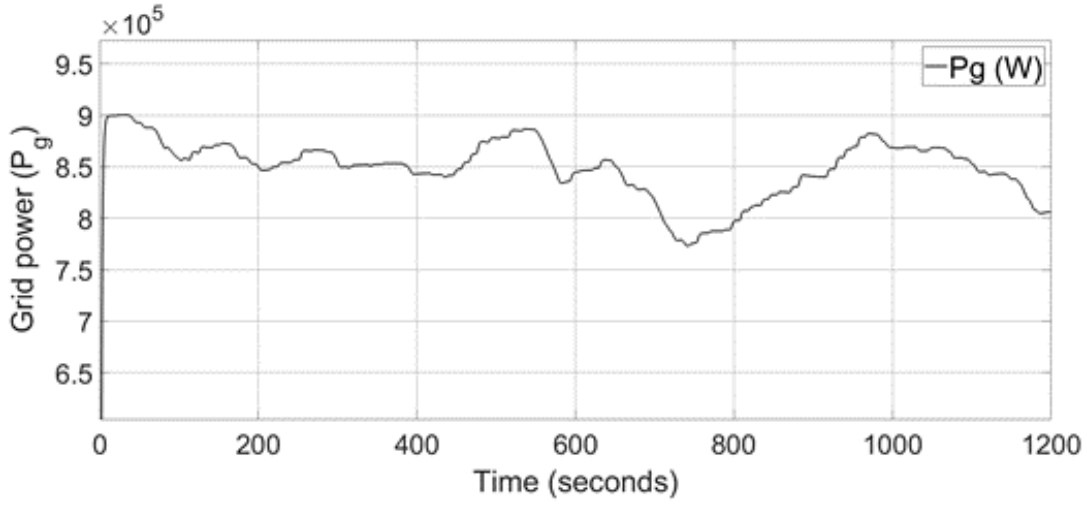

(c)

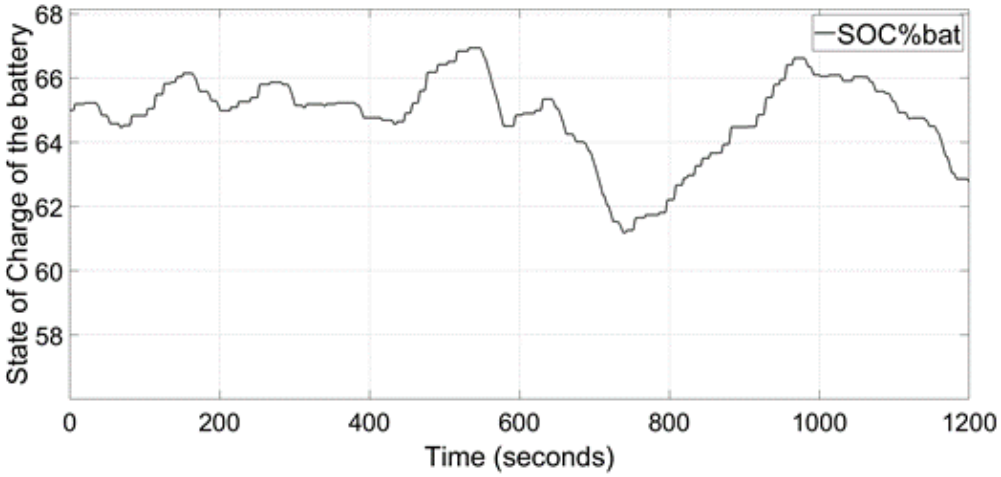

(d)

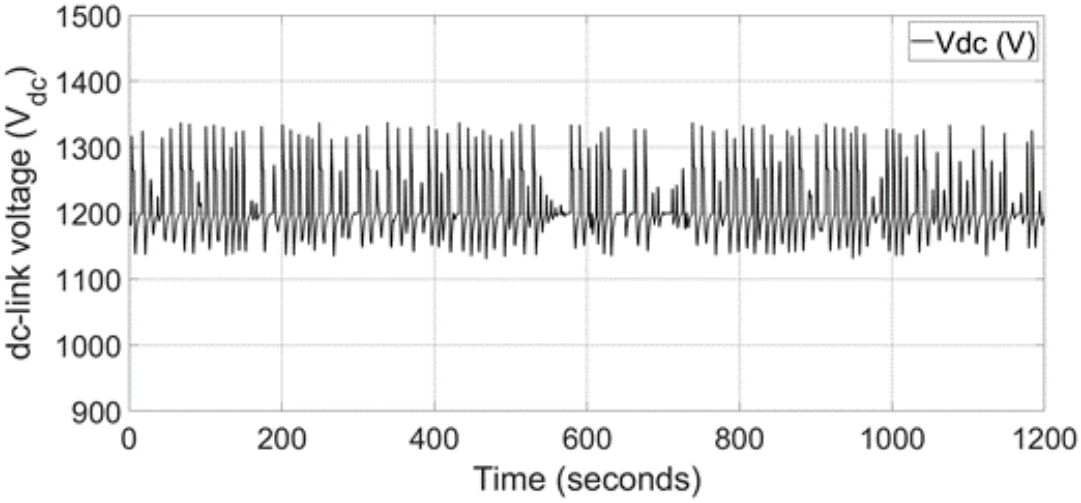

(e)

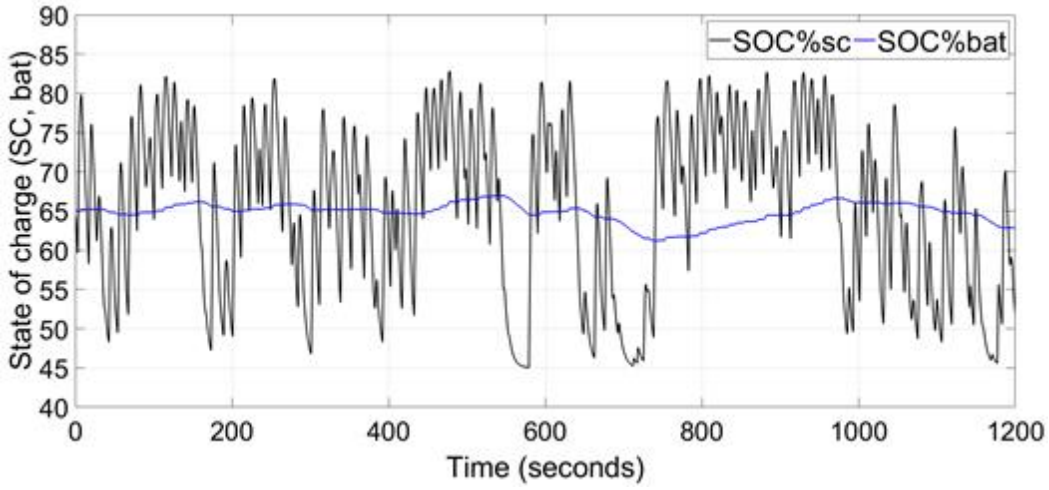

(f)

Figure 6. 4: Second case study: a). Power comparison of VOWC generators combined power P_{s_total}(W), grid power P_g(W), and supercapacitor power P_{sc}(W), b). Li-ion battery

power P_{bat}(W), c). grid power P_g(W), d). state of charge of the of the battery ($SOC\%_{bat}$), e). DC-link Voltage v_{dc}(V), f). state of charge of the supercapacitor ($SOC\%_{sc}$) and battery ($SOC\%_{bat}$).

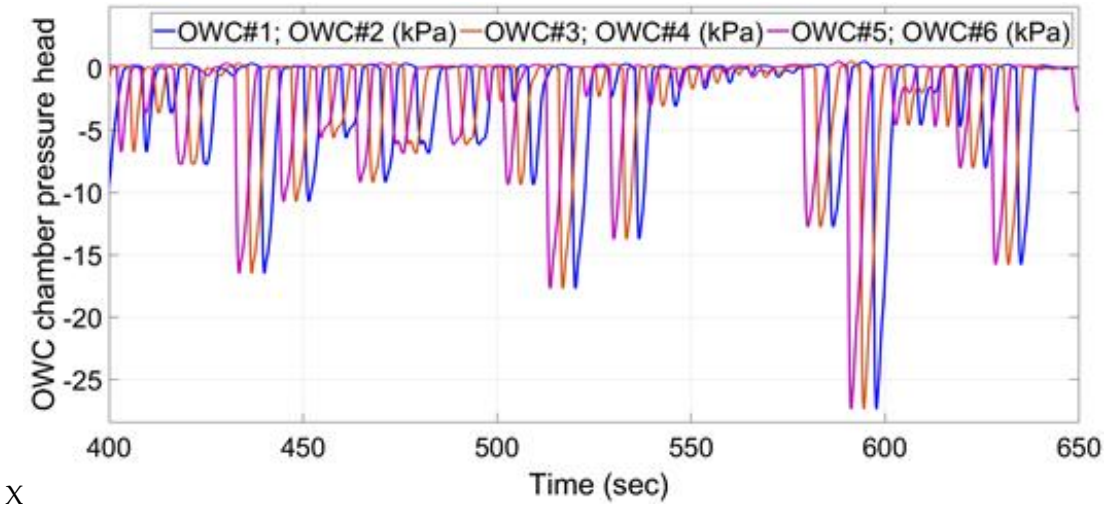

X

(a)

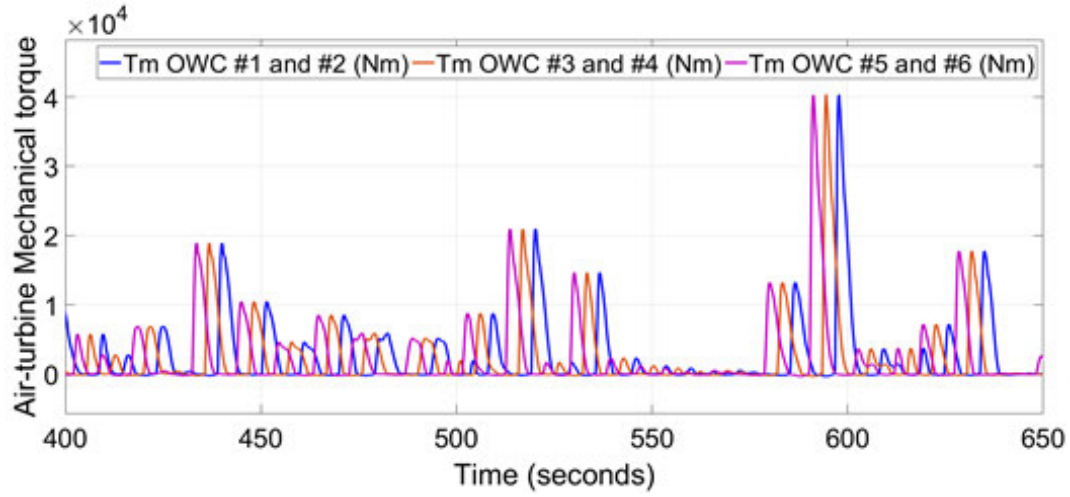

(b)

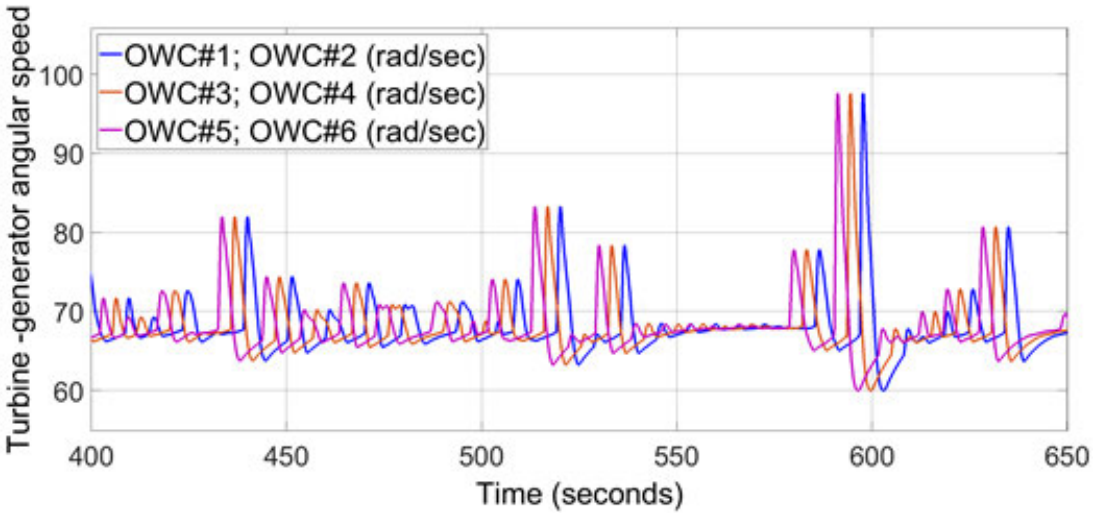

(c)

Figure 6. 5: Third case study: a). VOWC chamber pressure head ΔP(kPa) for #1, #3, and #5, b). air turbine #1, #3, and #5 mechanical torque T_m(Nm), c). turbine-generator #1, #3, and #5 rotor angular speed ω_m(rad/sec).

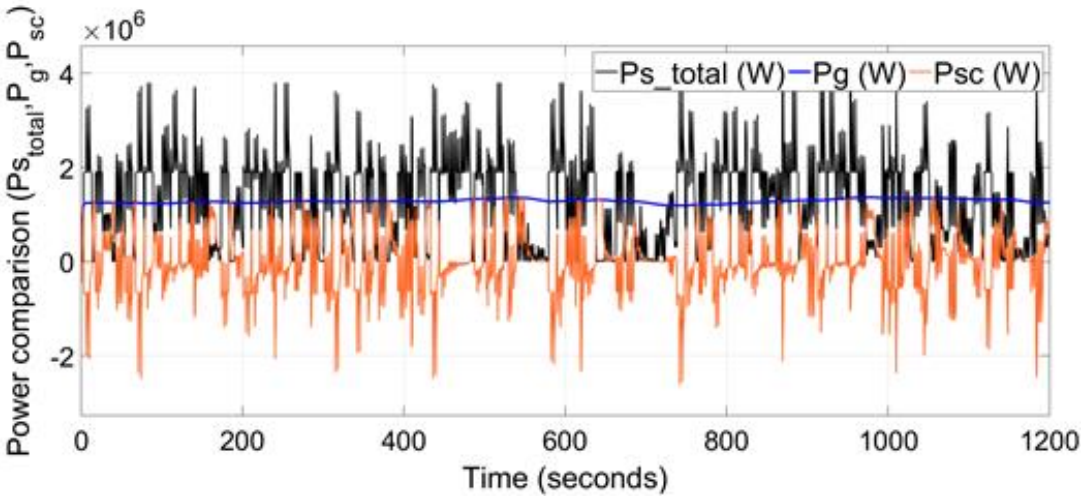

(a)

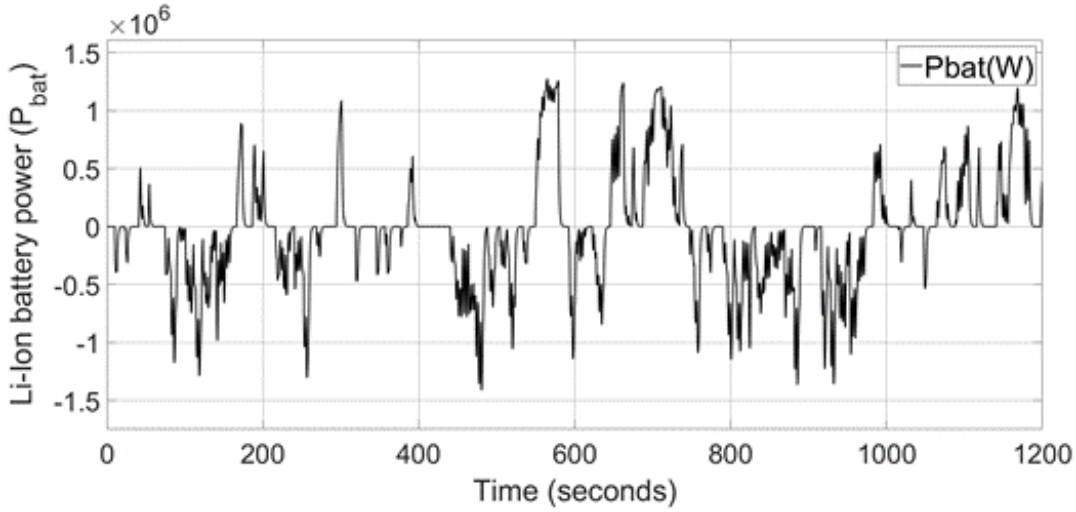

(b)

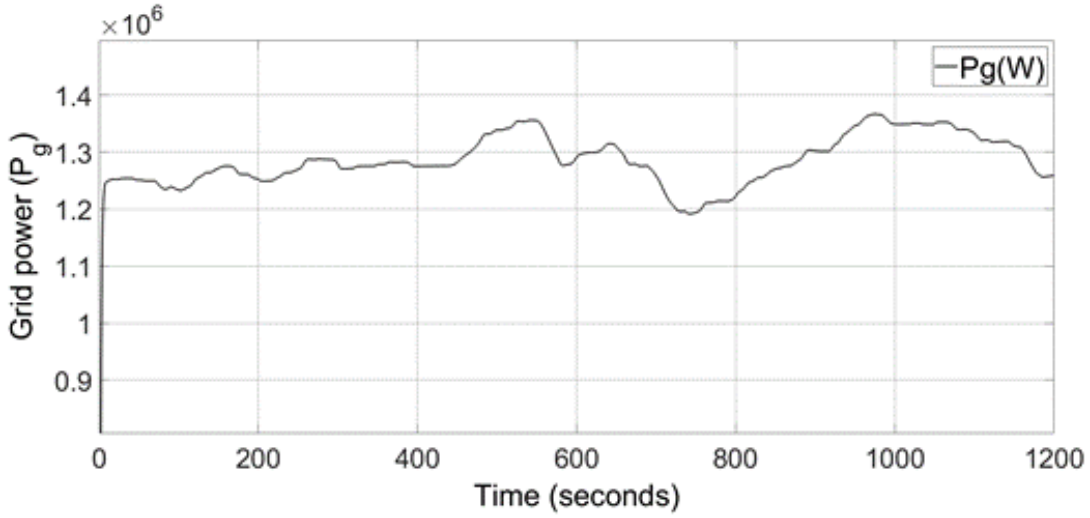
×10^6
Pg(W)
Grid power (P_g)
1.4
1.3
1.2
1.1
1
0.9
0
200
400
600
800
1000
1200
Time (seconds)

(c)

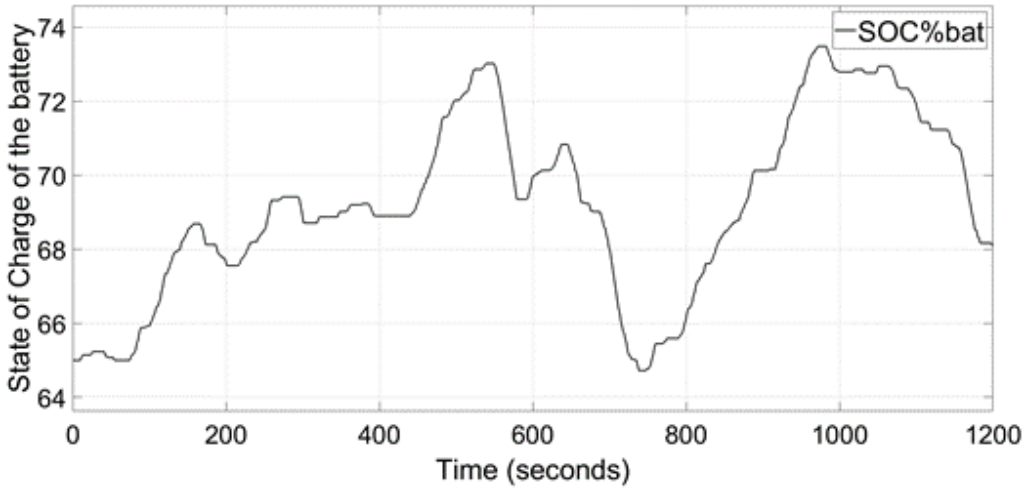
SOC%bat
State of Charge of the battery
74
72
70
68
66
64
0
200
400
600
800
1000
1200
Time (seconds)

(d)

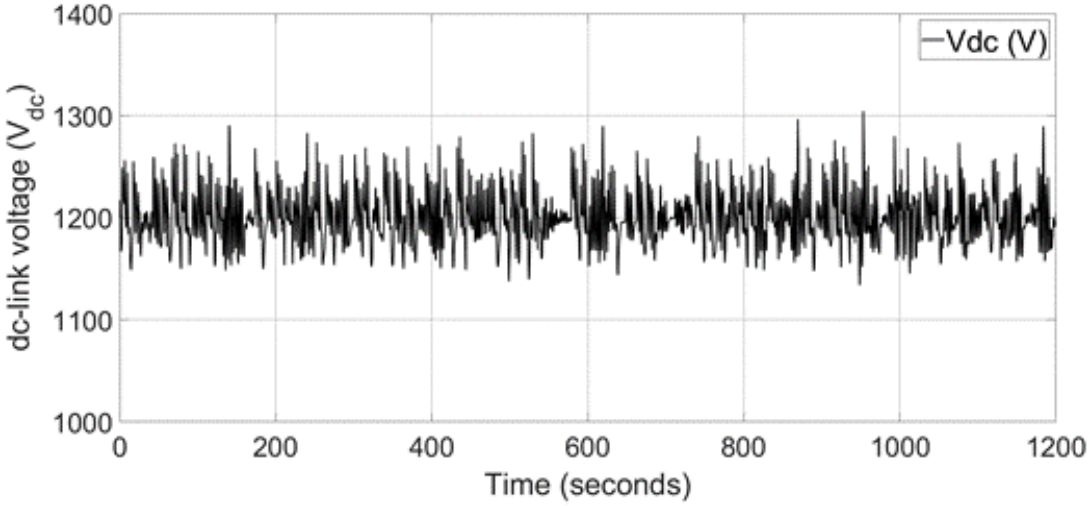
Vdc (V)
dc-link voltage (V_dc)
1400
1300
1200
1100
1000
0
200
400
600
800
1000
1200
Time (seconds)

(e)

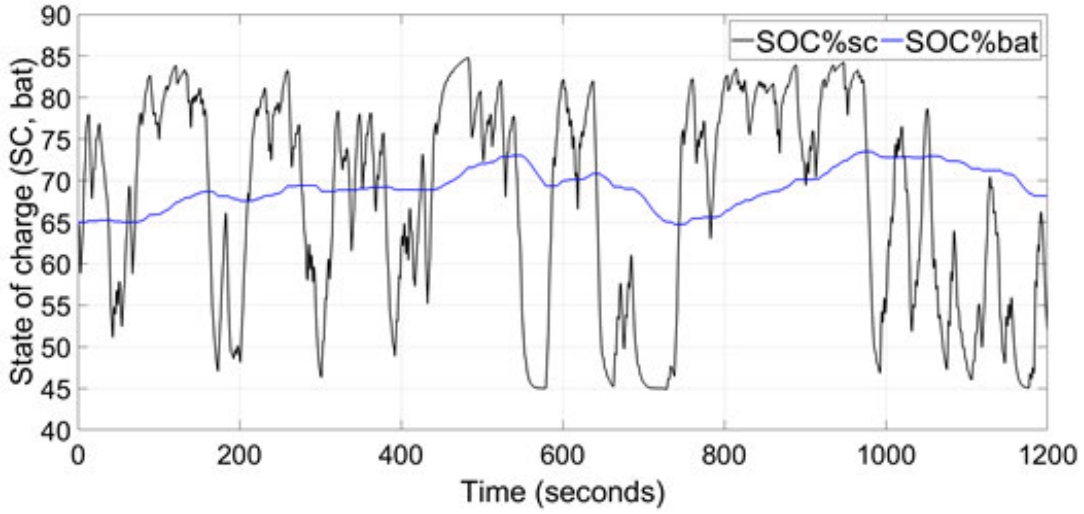

(f)

Figure 6. 6: Third case study: a). Power comparison of VOWC generators combined power P_{in_total}(W), grid power P_g(W), and supercapacitor power P_{sc}(W), b). Li-ion battery power P_{bat}(W), c). grid power P_g(W), d). state of charge of the battery (SOC%$_{bat}$), e). DC-link Voltage v_{dc}(V), f). state of charge of the supercapacitor (SOC%$_{sc}$) and battery (SOC%$_{bat}$)

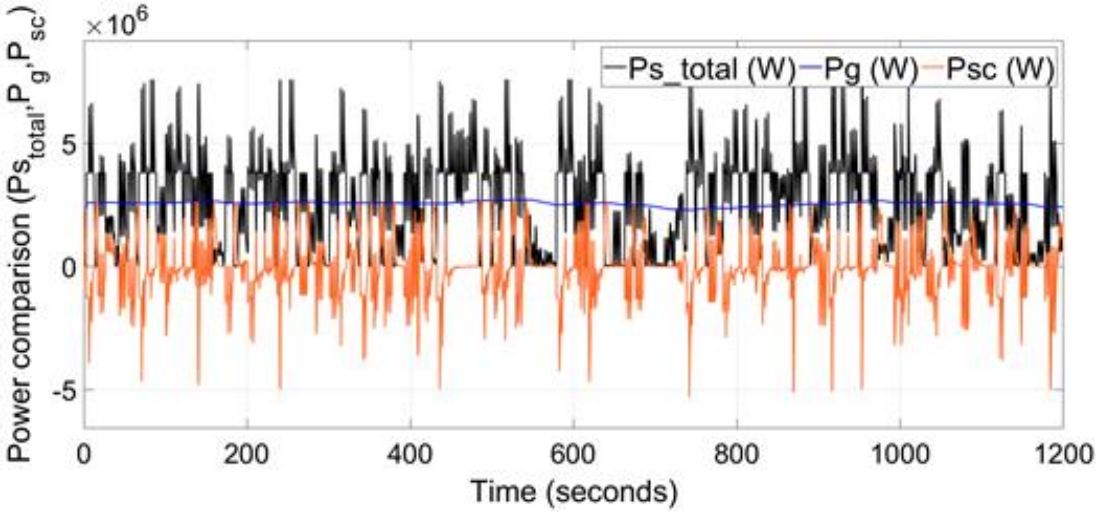

(a)

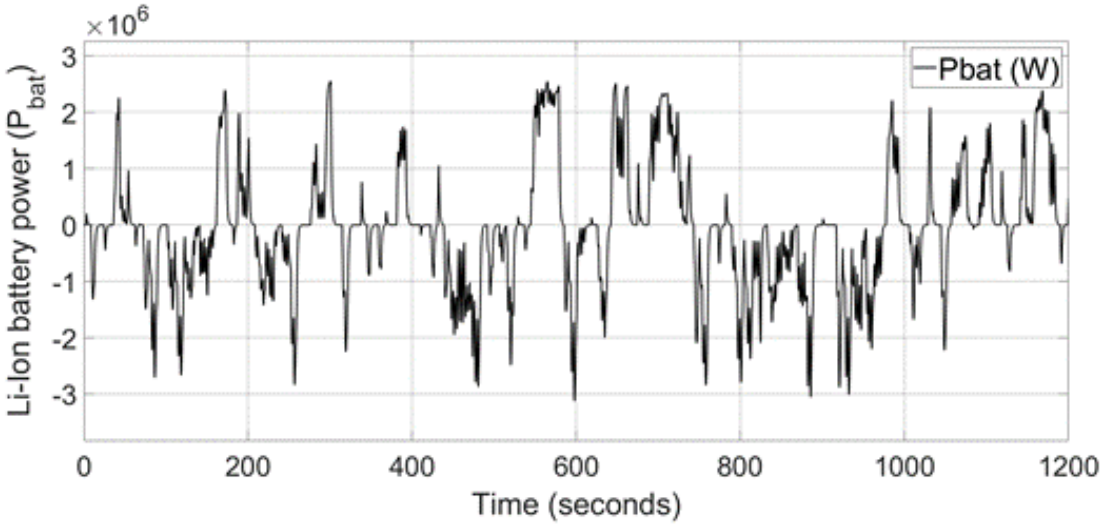
×10^6
Li-Ion battery power (P_bat)
Pbat (W)
Time (seconds)

(b)

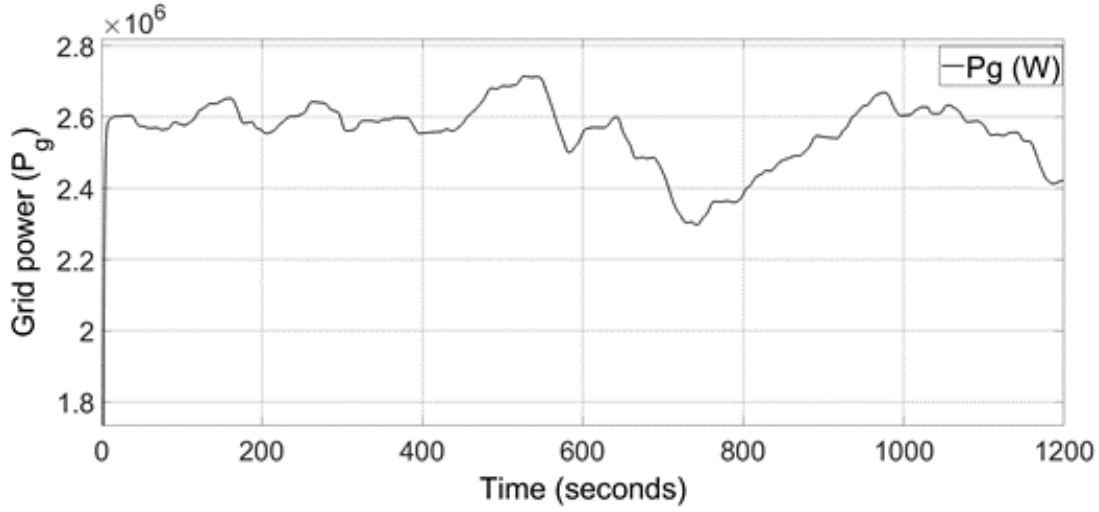
×10^6
Grid power (P_g)
Pg (W)
Time (seconds)

(c)

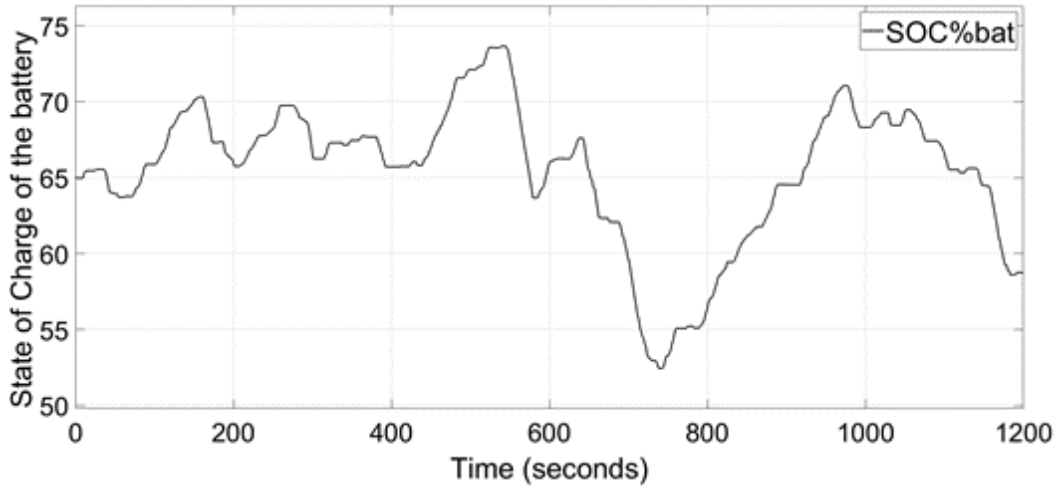
State of Charge of the battery
SOC%bat
Time (seconds)

(d)

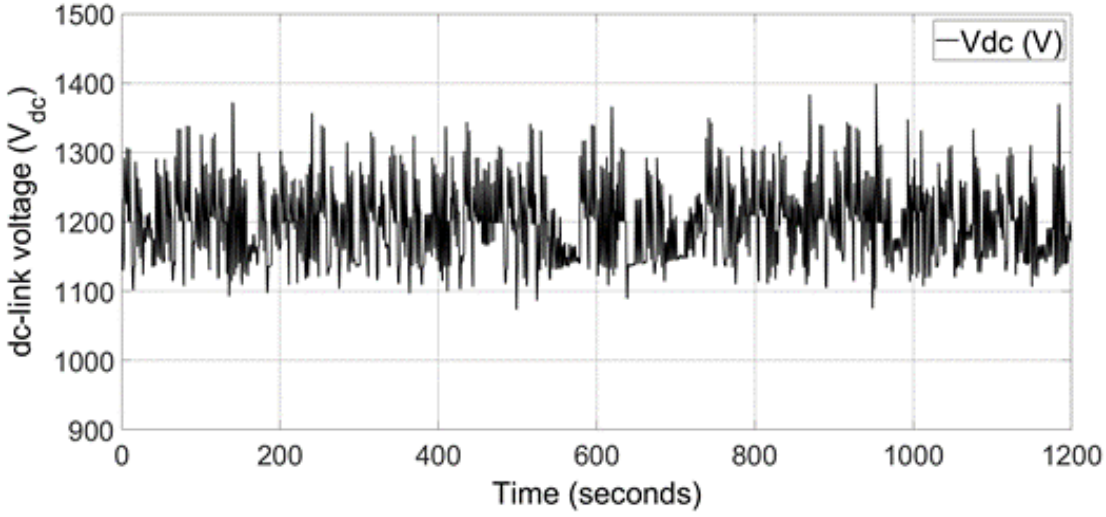

(e)

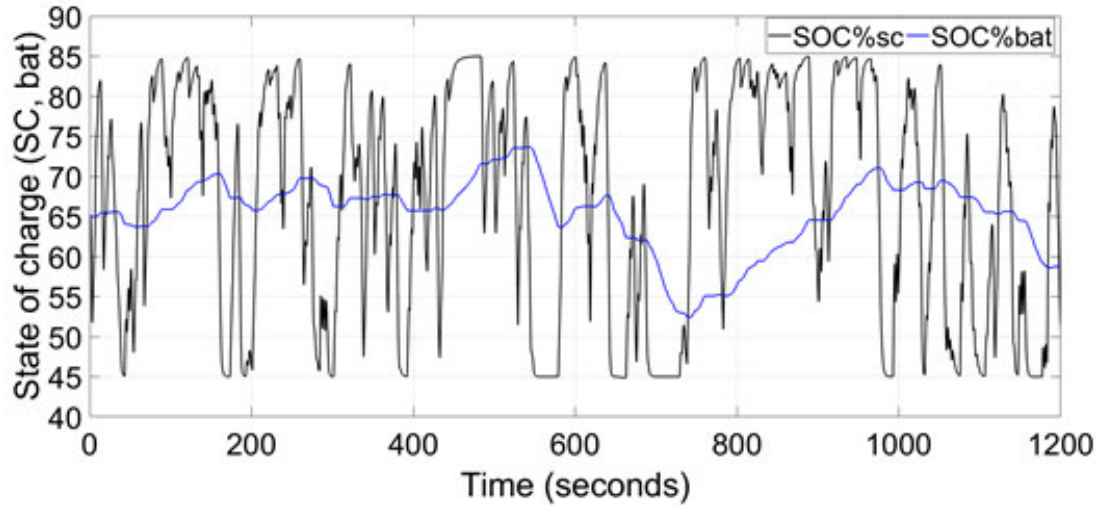

(f)

Figure 6. 7: Fourth case study: a). Power comparison of VOWC generators combined power P_{in_total}(W), grid power P_g(W), and supercapacitor power P_{sc}(W), b). Li-ion battery power P_{bat}(W), c). grid power P_g(W), d). state of charge of the battery ($SOC\%_{bat}$), e). DC-link Voltage v_{dc}(V), f). state of charge of the supercapacitor ($SOC\%_{sc}$) and battery ($SOC\%_{bat}$).

6.4.1 First Case Study: Isolated Single VOWC

In the first case study, an isolated VOWC was designed as in (Rajapakse et al., 2018a)

The pressure head of the VOWC chamber is shown in Figure 6. 3. a). Figure 6. 3. b) shows the air-turbine mechanical torque. The turbine-generator rotor angular speed is illustrated by Figure 6. 3. c). This was maintained between 20 and 157 rad/s throughout the simulation as predesigned. This variable rotational speed control approach enables the turbine to respond efficiently to a wider range of sea states and widen the response of the turbine to varying power levels of the waves (Rajapakse et al., 2018a).Operating the air-turbine speed at variable speed also helps to reduce the supercapacitor size (Rajapakse et al., 2018a). Figure 6. 3. d), illustrates the turbine-generator power output, grid power supply, and the supercapacitor power. The Li-ion battery power is shown in Figure 6. 3. e). The supply power to the grid is maintained closer to the reference with the 19.8 F supercapacitor. The power output is gradually varied between 380 to 453 kW, from start to the end, for 1200 s. This power fluctuation is considered acceptable by the Australian Energy Market (AEMO, 2019). The enlarged grid power output and the rate of change of the Li-ion battery SOC% are shown in Figure 6. 3. f), 6. 3. g), respectively. The output power reference is adjusted by the PMS throughout the simulation, maintaining the battery SOC% in desirable limits based on the deviation of the Li-ion battery SOC 65% and the rate of change of SOC. The DC-link voltage is regulated close to its reference within 9% deviation as shown in Figure 6. 3. h). Figure 6. 3. i), depicts the SOCs of the supercapacitor and Li-ion battery, which illustrate the energy transfer according to the PMS.

6.4.2 Second Case Study: VOWCDBW

The second case study was designed for VOWCDBW with two detached VOWCs in a breakwater. Both VOWCs' air-turbine torque and rotor angular speed represent similar characteristics because both are built into the same breakwater that experiences relatively the same differential air pressure that controls the air-flow through the turbines.

The simulation results of turbine-generator power output, grid power supply, and supercapacitor power are illustrated in Figure 6. 4. a). Figure 6. 4. b) depicts the Li-ion battery power. Figure 6. 4. c), 6. 4. d) shows the enlarged version of grid power and Li-

ion battery SOC%, respectively. The power is supplied to the grid following the reference, 900 kW with 39.6 F supercapacitor compared to case study 1. The power output is gradually varied between 700 to 900 kW, from start to the end, 1200 s. The DC-link voltage is regulated close to its reference within a 14% deviation as shown in Figure 6. 4. e). Figure 6. 4. f) shows the SOCs of the supercapacitor and Li-ion battery.

6.4.3 Third Case Study: Array of VOWC

The third case study was designed for an array of three isolated VOWCs.

The pressure heads of the VOWC chamber #1, #3, and #5 are shown in Figure 6. 5. a). The same pressure head that occurs in #1 occurs in #3 after 3.25 s and in #5 after 6.5 s. due to the configuration of the array. Figure 6. 5. b) depicts the VOWC #1, #3, and #5 air-turbine torques. Figure 6. 5. c) depicts the VOWC #1, #3, and #5 turbine-generator rotor angular speeds. The controllers have maintained the angular speeds of all the air turbines within the set range.

Figure 6. 6. a), shows the output power of the turbine-generator, supply power to the grid, and supercapacitor. The Li-ion battery power is illustrated in Figure 6. 6. b). Figure 6. 6. c) and 6. 6. d) depict the enlarged version of grid power and Li-ion battery SOC%. The supply power to the grid is maintained with a 39.6 F supercapacitor. The power output is gradually varied between 1250 to 1370 kW, from start to the end, 1200 s. The DC-link voltage is controlled close to its reference within 14% deviation as shown in Figure 6. 6. e). Figure 6. 6. f) depicts the SOCs of the supercapacitor and Li-ion battery.

6.4.4 Fourth Case Study: Array of VOWCDBW

The fourth case study was designed for an array of VOWCDBWs with two detached VOWCs in each breakwater. As in the third case study, the pressure heads of VOWCs in the VOWCDBW #1, #2, and #3 experience the same pressure head that occurs in VOWC #1 and #2, in VOWC #3 and #4 after 3.25 s, and in VOWC #5 and #6 after 6.5 s due to the configuration of the array.

The simulation results of powers, turbine-generator output power, supply power to the grid, and supercapacitor power are illustrated in Figure 6. 7. a). Figure 6. 7. b) depicts the Li-ion battery power. Figure 6. 7. c), 6. 7. d) show the enlarged version of grid power and

Li-ion battery SOC%, respectively. The supply power to the grid is maintained with a 39.6 F supercapacitor. The power output is gradually varied between 2300 to 2717 kW, from start to the end, for 1200 s. The DC-link voltage is regulated close to its reference within 14% deviation as shown in Figure 6. 7. e). The SOCs of the supercapacitor and Li-ion battery are depicted in Figure 6. 7. f).

Table 6. 2 summarises the results of the study and reveals that placing two VOWCs in the detached breakwater almost doubled the average generated power. Nevertheless, this approach increased the required SCES capacity. VOWCs in array configurations with correct layout effectively smoothed the generated power taking advantage of temporal and spatial distribution of waves. This approach not only increased the average generated power by the product of the number of devices but also allowed use the of same ESS capacity as a single detached breakwater with reduced power deviations. Although the results are obtained for VWOCs, the method can be applied for other OWC configurations as well.

Table 6. 2: Summary of the results.

Case Study	Power (kW)	Grid Power (kW) and Deviation from the Reference	Supercapacitor Energy Storage (SCES) Capacitance and Capacity
1 Isolated VOWC	425	380–453 −10.5–6.5%	19.8 F 300 AH
2 VOWCDBW	900	700–900 −22.2–0%	39.6 F 300 AH
3 Array of VOWC	1275	1250–1370 −1.9%–7.5%	39.6 F 300 AH
4 Array of VOWCDBWs	2700	2300–2717 −14.8–0.6%	39.6 F 300 AH

6.5 Conclusions

The paper presents four case studies of individual and array configurations of grid connected VOWC wave energy converters with battery/supercapacitor hybrid energy storage systems. Simulation results are used to determine the effect of different configurations on power quality and energy storage sizing. Results of the study reveal that placing two VOWCs in the detached breakwater doubles the average generated power with the cost of increased SCES capacity. In contrast, VOWCs in array configurations have effectively smoothed the generated power, reducing the required capacity of the energy storage system. This approach contributes towards cost reductions

to compete with other renewable energy technologies. Moreover, this study is adaptable into existing ocean structures or future developments such as breakwaters.

This study can be considered as a preliminary study, which compares effects on grid power and ESS sizing when the VOWCs are placed in different array configurations. Although the results obtained from software simulation are promising for air-turbine aerodynamic efficiency, generator efficiency, efficiency of power electronics, and efficiency reductions/fluctuations of VOWC array devices should be analysed to determine the best configuration.

7

CONCLUSIONS AND SUGGESTIONS FOR FUTURE RESEARCH

This chapter presents conclusions from the previous chapters and discusses the implications of the findings. Limitations of the proposed solutions and recommendations for future research are also presented at the end of the chapter.

7.1 Conclusions and Implications of the Research

This thesis has presented FCS-MPC for control of power converters of a grid connected unidirectional air-turbine OWC with energy storage systems. This control strategy satisfies relevant criterion in grid codes while maintaining the turbine speed within its optimum range. Moreover, this research has introduced a unique power management system for a single and/or an array of OWC wave energy conversion systems with energy storage systems (BESS/SCESS/HESS). These outcomes are based on an effort to answer the following questions,

1) How to develop controllers for power converters to maintain the turbine speed within optimum range and feed power to the grid while meeting grid code requirements?
2) What should be the power management strategy for a single generator system and multi-generator systems with energy storage?

The contributions and outcomes of this research can be summarised as,

1) MPC-based speed controller for a PMSG direct coupled to a single stage unidirectional air-turbine of an OWC system. Proposed controller extracts power from the air-turbine at varying input torque conditions maintaining the optimal speed range of the turbine under changing wave conditions.
2) Direct connection of a battery bank into the dc-link of the back-to-back power converter system and thereby smoothing the power delivered to the grid. This is to avoid instabilities in the power grid due to large variations present in the extracted power (power pulses ranging from 0 to 1 MW). MPC controllers are developed for the back-to-back power converter system to control the battery current (during charging and discharging).
3) Integration of SCES into the dc-link of the back-to-back power converter through a bidirectional dc-dc converter. FCS-MPC for the complex power converter arrangement to achieve the desired operation. The control algorithm can be applied to any type of ESS (SCES or BES) since it does not consider the ESS's parameters other than its voltage. Also, the PMS maintains the SOC of the ESS within predefined limits.
4) PMS for a grid connected OWC wave energy converter with a battery/supercapacitor HESS. PMS manages large power pulses present in the input to the energy storage

elements and thereby maintain smooth power delivery to the grid. In addition, maintaining SOC of the battery and supercapacitor within safe limits ensuring sufficient reserves. Power sharing between energy storage elements is determined based on the deviation of the supercapacitor SOC from the mid-point and its rate of change. The power commitment to the grid is adjusted based on the deviation of battery SOC from the mid-point and its rate of change. Simulation results have revealed that the variable speed operation of the WEC helps reduce the required capacity of the SCES to almost a half compared to the fixed speed operation. Therefore, variable speed operation of WEC within the optimal range is recommended to reduce the overall cost.

5) The same PMS is applied to an array of OWCs in different array configurations. Four case studies of individual and array configurations of grid connected VOWC wave energy converters with battery/supercapacitor hybrid energy storage systems were studied. Simulation results were used to determine the effect of different configurations on power quality and energy storage sizing. Results of the study have revealed that placing two VOWCs in the detached breakwater doubles the average generated power with the cost of increased SCES capacity. In contrast, VOWCs in array configurations have effectively smoothed the generated power, reducing the required capacity of the energy storage system. This approach contributes towards cost reductions to compete with other renewable energy technologies. Moreover, this study is adaptable into existing ocean structures or future developments such as breakwaters.

7.2 Future Research Work

The control system has a significant impact on technical performance of OWC. Also, it plays a big part in OWCs economic viability. The work presented in this thesis provides insight into the controllers and PMS for the particular WEC considering some realistic scenarios. Although, much work has been accomplished in this research, some areas such as nonlinearities and physical limitations of the device components require further investigations. The MPC algorithm was implemented in a Texas Instrument's Tiva microcontroller board and successfully verified by running an induction motor. Nevertheless, the combination of the MPC algorithm with the power management

algorithms is to be validated in an experimental setup. These could have significant impact on the device performance, the estimation of the final energy storages, results and conclusions. Including these nonlinearities and physical limitations would be interesting frontiers for future researchers to explore. Further research that can be expanded using the acquired knowledge is briefly described below.

1) Comparison of proposed controllers to classical control techniques (PID) to clarify the difference of controller performance and advantage of MPC over PID or vice versa.
2) Comparison of the proposed controllers to Fuzzy logic Control to clarify the differences of controller performances and advantage of MPC over Fuzzy logic or vice versa.
3) Application of proposed control strategies to the other power converter topologies such as multilevel converters, flying capacitor, novel power electronic converters, etc.
4) Application of proposed power management system to other types of renewable energy power conversion systems such as tidal energy.
5) Investigation of grid integrated OWC behaviour under unbalanced grid fault conditions.

8
BIBLIOGRAPHY

BPS Renewable Energy Company [Online]. Available: bps.energy/projects [Accessed 27/04 2017].

Carnegie Clean Energy [Online]. Available: http://carnegiewave.com/ [Accessed 27/04 2017].

2009. Modeling ofa Variable Speed Wind Turbine with a Permanent Magnet Synchronous Generator. *In* ROLAN, A., LUNA, A., VAZQUEZ, G. & AZEVEDO, G. (eds.) *EEE International Symposium on Industrial Electronics (ISlE 2009).* Seoul Olympic Parktel, Seoul, Korea.

2014. IEEE Recommended Practice and Requirements for Harmonic Control in Electric Power Systems. Revision of IEEE Std 519-1992.

2014 to present. *The King Island Renewable Energy Integration Project (KIREIP)* [Online]. hYDRO tASMANIA. Available: http://www.kingislandrenewableenergy.com.au/project-information/overview [Accessed 24/05 2017].

2015. *Power Module; Scalable and modular Lithium-Ion energy storage system* [Online]. PowerTech Systems. Available: https://www.powertechsystems.eu/wp-content/uploads/2016/05/Fiche-Produit-PowerModule_EN.pdf [Accessed 01/08 2017].

2017a. PBES Power and Energy Industrial Lithium Batteries. *In* STORAGE, P. B. E. (ed.) *PBES Specification Sheet System Specifications for the PBES Power & Energy Systems.* Vancouver • Trondheim • Barcelona • Copenhagen: Plan B Energy Storage.

2017b. PERMANENT MAGNET GENERATOR QUOTATION SHEET. *In* QINGDAO GREEF NEW ENERGY EQUIPMENT CO., L. (ed.). China: Greef Energy.

ABDELRAHEM, M., HACKL, C. & KENNEL, R. 2016. Model Predictive Control of Permanent Magnet Synchronous Generators in Variable-Speed Wind Turbine Systems. *Power and Energy Student Summit 2016 (PESS 2016).* ResearchGate.

ABDULLAH, M. A., YATIM, A. H. M , TAN, C. W. & SAMOSIR, A. S. 2013. Control of a Bidirectional Converter to Interface Ultracapacitor with Renewable Energy Sources. *IEEE International Conference on Industrial Technology (ICIT).* Cape Town: IEEEXplore.

ADERINTO, T. & LI, H. 2018. Ocean Wave Energy Converters: Status and Challenges. *Energies,* 11.

AEMO, A. E. M. O. 2019. Dispach - power system operating procedure *Generator Performance Standards.* Australia: Australian Energy Market Operator Ltd.

ANSARIFARD, N., FLEMING, A., HENDERSON, A. D., KIANEJAD, S., CHAI, S. & ORPHIN, J. 2019. Comparison of inflow and outflow radial air turbines in vented and bidirectional OWC wave energy converters. *Energy, ELSEVIER,* 182**,** 159-176.

ASHLIN, S. J., SANNASIRAJ, S. A. & SUNDAR, V. 2018. Performance of an array of oscillating water column devices integrated with an offshore detached breakwater. *Ocean Engineering, ELSEVIER,* 163**,** 518-532.

AUSTRALIAN MARITIME COLLAGE. 2017. [Accessed 27/03 2017].

BENELGHALI, S., BENBOUZID, M. E. H. & CHARPENTIER, J. F. 2007. Marine Tidal Current Electric Power Generation Technology: State of the Art and Current Status. IEEE IEMDC'07, 2007 Antalya, Turkey. IEEE, 1407-1412.

BENELGHALI, S , BENBOUZID, M. E. H. & CHARPENTIER, J. F. 2012. Generator Systems for Marine Current Turbine Applications: A Comparative Study. *IEEE Journal of Oceanic Engineering,* 37**,** 554-563.

BENNET, M., PENESIS, I., FLEMING, A., MACFARLANE, G. J. & NADER, J. R. Experimental Study into the Diffracted Wave Field Downstream of an Array of Wave Energy Converters in Irregular Waves. 12th European Wave and Tidal Energy Conference (EWTEC 2017), 2017 Cork, Ireland. University of Southampton, 1-10.

BERNAL, L. E. Z. 1997. *CHARACTERIZATION OF DOUBLE-LAYER CAPACITORS FOR POWER ELECTRONICS APPLICATIONS.* Master of Applied Science, University of Toronto.

BIMBHRA, P. S. 1992. *Generalized Theory Of Electrical Machines,* Delhi, India, Khanna Publishers.

BRKA, A., KOTHAPALLI, G. & ABDELI, Y. M. 2015. Predictive power management strategies for stand-alonehydrogen systems: Lab-scale validation. *International Journel of Hydrogen Energy Publications,* 40**,** 9907-9916.

CARDNO PTY LTD 2017. Structural Design and Planning - Wave Climate at WSE Site West Coast of King Island, Tasmania.

CARSON, L., BRADSHAW, M. & JAQUES, L. 2014. Australian Energy Resource Assessment 2014. 2 ed.

CARSON, L., BRADSHAW, M., JAQUES, L., CHE, N. & BALL, A. 2010. Australian Energy Resource Assessment 2010. Australia.

CEBALLOS, S., REA, J., LOPEZ, I., POU, J., ROBLES, E. & O'SULLIVAN, D. L. 2013. Efficiency optimization in low inertia wells turbine oscillating water column devices. *IEEE TRANSACTIONS ON ENERGY CONVERSION***,** 553-564.

CEBALLOS, S., REA, J., ROBLES, E., LOPEZ, I., POU, J. & O'SULLIVAN, D. L. 2015. Control strategies for combining local energy storage with wells turbine oscillating water column devices. *renewable Energy,* 83**,** 1097-1107.

CLEAN ENERGY COUNCIL 2016. Progress and Status of the Renewable Energy Target , Briefing Paper June 2016. Australia.

CLEANENERGYCOUNCIL. *Renewable Energy - Marine Energy* [Online]. Clean Energy Council. Available: https://www.cleanenergycouncil.org.au/technologies/marine-energy.html [Accessed 17/02 2017].

CLIMATE COUNCIL OF AUSTRALIA 2014. Australia's Electricity Sector: Ageing, Inefficient and Unprepared. Australia.

DE FONSECA, F. X., HENRIQUES, J. C. C., GATO, L. M. C. & FALCÃO, A. F. O. 2019. Oscillating Flow Ring for Air-Turbine Testing. *Renewable Energy, ELSEVIER,* 142**,** 373–382.

DE. CHOWDHURY, S., NADER, J. R., SANCHEZ, A. M., FLEMING, A., WINSHIP, B., ILLESINGHE, S., TOFFOLI, A., BABANIN, A., PENESIS, I. & MANASSEH, R. 2015. A review of hydrodynamic investigations into arrays of ocean wave energy converters.

DELMONTE, N., BARATER, D., GIULIANI, F., COVA, P. & BUTICCHI, G. 2016. Review of Oscillating Water Column Converters. *IEEE Transactions on Industry Applications,* 52**,** 1698 - 1710.

ENVIRONMENT AND COMMUNICATIONS REFERENCES COMMITTEE AUSTRALIA 2017. Retirement of coal fired power stations.

FALCAO, A. F. D. O. 2010. Wave energy utilization: A review of the technologies. *Renewable and Sustainable Energy Reviews,* 14.

FALCAO, A. F. O. & HENRIQUES, J. C. C. 2015. Oscillating-water-column wave energy converters and air turbines: A review. *Renewable Energy,* 85**,** 1391e1424.

FALCAO, A. F. O. & HENRIQUES, J. C. C. 2016. Oscillating-water-column wave energy converters and air turbines: A review. *Renewable Energy, ELSEVIER,* 85**,** 1391-1424.

FLEMING, A., MACFARLANE, G., HUNTER, S. & DENNISS, T. 2017. Power Performance Prediction for a Vented Oscillating Water Column Wave Energy Converter with a Unidirectional Air Turbine Power Take-off.

GUERRERO, J. M., VASQUEZ, J. C., MATAS, J., DE VICUÑA, L. G. & CASTILLA, M. 2011. Hierarchical Control of Droop-Controlled AC and DC Microgrids—A General Approach Toward Standardization. *IEEE Transactions on Industrial Electronics,* 58**,** 158-172.

HAMIDI, A., WEBER, L. & NASIRI, A. 2013. EV Chargeing Station Integrating Renewable Energy and Second Life Battery. *International cConference on Renewable Energy Research and Application.* Madrid, Spain.

HAMIDI, S. A., IONEL, D. M. & NASIRI, A. 2015. Modeling and Management of Batteries and Ultracapacitors for Renewable Energy Support in Electric Power Systems–An Overview. *Electrical Power Components and Systems,* 43**,** 1434-1452,.

HAMIDI, S. A., LONEL, D. M. & NASIRI, A. 2017. Modeling and Management of Batteries and Ultracapacitor for Renewable Energy Support in Electric Power Systems-An Overview. *Electric Power Components and systems,* 43**,** 1434-1452.

HANNAN, M. A., LIPU, M. S. H., HUSSAIN, A. & MOHAMED, A. 2017. A review of lithium-ion battery state of charge estimation and management system in electric vehicle applications: Challenges and recommendations. *Renewable and Sustainable Energy Reviews,* 78**,** 834–854.

HANNON, M., GRIFFITHS, J., VANTOCH-WOOD, A., CARCAS, M., BRADLEY, S., BOUD, R. & WYATT, S. 2016. World Energy Resources; Marine Energy 2016. *WORLD ENERGY COUNCIL; WORLD ENERGY RESOURCES.*

HANSEN, A., IOV, F., BLAABJERG, F. & HANSEN, L. 2011. Review of contemporary wind turbine concepts and their market penetration. *Journal of Wind Energy,* 58**,** 1081-1095.

HART, D. W. 2011. *Power Electronics,* New York, NY 10020, McGraw-Hill.

HEIER, S. 2014. *Grid Integration of Wind Energy,* United Kingdom, John Wiley & Sons Ltd.

HEMER, M. A., MANASSEH, R., MCINNES, K. L., PENESIS, I. & PITMAN, T. 2018. Perspectives on a way forward for ocean renewable energy in Australia. *Renewable Energy,* 127**,** 733-745.

HEMER, M. A., ZIEGER, S., DURRANT, T., O'GRADY, J., HOEKE, R. K., MCINNES, K. L. & ROSEBROCK, U. 2017. A revised assessment of Australia's national wave energy resource. *Renewable Energy,* 114**,** 85-107.

HONG, Y., WATERS, R., BOSTRÖM, C., ERIKSSON, M., ENGSTRÖM, J. & LEIJON, M. 2014. Review on electrical control strategies for wave energy converting system. *Renewable and Sustainable Energy Reviews***,** 329–342.

HUGHES, M. G. & HEAP, A. D. 2009. National-scale wave energy resource assessment for Australia. *Renewable Energy,* 35**,** 1783–1791.

ISLAM, M. S., HOSSAIN, M. B., HOSSAIN, M. N., ALAM, S. B. & CHOWDHURY, M. E. H. Modeling of a Double-Layer Capacitor with Individual Branch Response. World Congress on Engineering and Computer Science 2010 2010 San Francisco, USA.

JANSSON, E. 2016. *Multi-buoy Wave Energy Converter - Electrical Power Smoothening from Array Configuration.* Master Thesis, Uppsala University: Uppsala, Sweden.

KEMPENER, R. & BORDEN, E. 2015. Battery storage for renewables: market status and technology outlook.

KHIAREDDINE, A., SALAH, C. B., REKIOUA, D. & MIMOUNI, M. F. 2018. Sizing methodology for hybrid photovoltaic /wind/ hydrogen/battery integrated to energy management strategy for pumping system. *Energy,* 153**,** 743e762.

KIM, J., SUHARTO, Y. & DAIM, T. U. 2017a. Evaluation of Electrical Energy Storage (EES) technologies for renewable energy: A case from the US Pacific Northwest. *ELSEVIER, Journal of Energy Storage,* 11**,** 25-54.

KIM, J., SUHARTO, Y. & DAIM, T. U. 2017b. Evaluation of Electrical Energy Storage (EES) technologies for renewable energy: A case from the US Pacific Northwest. *Journal of Energy Storage***,** 25-54.

KRISHNAN, R. 2010. *Permanent magnet synchronous and brushless DC motor drives,* Taylor & Francis Group, London.

LEKUBE, J., GARRIDO, A. J. & GARRIDO, I. 2017. Rotational Speed Optimization in Oscillating Water Column Wave Power Plants Based on Maximum Power Point Tracking. *IEEE Transactions on Automation science and Engineering,* 14.

LEUCHTER, J. 2011. Bi-Directional DC - DC Converters for Battery Buffers with Supercapacitor. *Energy Storage in the Emerging Era of Smart Grids.* InTech.

LI, W., JOOS, G. & ABBEY, C. A parallel bidirectional dc/dc converter topology for energy storage systems in wind applications. Conference Record of the 2007 IEEE Industry Applications Conference, September 2007 New Orleans,USA. IEEE, 171-185.

LI, W., JOOS, G. & ABBEY, C. 2017. A Parallel Bidirectional DC/DC Converter Topology for Energy Storage Systems in Wind Applications.

LIU, Z., WANG, D. & PENG, Z. 2016. A Simplified Direct Finite-Control-Set Model Predictive Control for AFEs with DC-Link Voltage Dynamic Reference Design. *35th Chinese Control Conference (CCC).* Chengdu, China.

MAERCOS, V. M. M., MARTINEZ, M. A. G , GONZALEZ, F. B. & MONTERO, M. I. M. 2017. A Grid Connected Photovoltic Inverter with Battery-Supercapacitor Hybrid Energy Storage. *Sensors,* 17.

MANASSEH, R., DE CHOWDHURY, S , HASAN, M. K., PENESIS, I., FLEMING, A., MACFARLANE, G. & NADER, J. R. 2018. Towards an Australian capability in arrays of ocean wave-power machines. *Project overview and summary of final report - ARENA Emerging Renewables Program Funding Agreement number A00575.* Australia: Australian Maritime College, University of Tasmania and Swinburne University of Technology.

MAXWELL TECHNOLOGIES 2017. Maxwell_Supercapacitor_48v_DN 1009365 13.

MEHRASA, M., ADABI, M. E., POURESMAEIL, E. & ADABI, J. 2014. Passivity-based control technique for integration of DG resources into the power grid. *International Journal of Electrical Power & Energy Systems,* 58**,** 281-290.

MEHRASA, M., POURESMAEIL, E., AKOREDE, M. F , JØRGENSEN, B. N. & CATALAO, P. S. 2015. Multilevel converter control approach of active power filter for harmonics elimination in electric grids. *Energy,* 84**,** 722-731.

MEHRASA, M , REZANEJHAD, M., OURESMAEIL, E., CATALÃO, P. S. & ZABIHI, S. 2016. Analysis and control of single-phase converters for integration of small-scaled renewable energy sources into the power grid. *7th Power Electronics, Drive Systems & Technologies Conference (PEDSTC 2016).* Tehran, Iran: IEEE.

MURRAY, D., J., A., MULTON, B. & AHMED, H. B. 2013. *Electrical energy storage systems.*

MURRAY, D. B., HAYES, J. G , EGAN, M. G. & O'SULLIVAN, D. L. 2011. Supercapacitor Testing for Power Smoothing in a Variable Speed Offshore Wave Energy Converter. *IEEE Journal of Oceanic Engineering* 37**,** 301 - 308.

NADER, J. R., ZHU, S. P. & COOPER, P. 2014. Hydrodynamic and energetic properties of a finite array of fixed oscillating water column wave energy converters. *Ocean Engineering, ELSEVIER,* 88**,** 131–148.

NGUYEN, T. H. & KIM, K. H. 2017. Finite Control Set–Model Predictive Control with Modulation to Mitigate Harmonic Component in Output Current for a Grid-Connected Inverter under Distorted Grid Conditions. *Energies,* 10**,** 25.

NIMMA, K.S.; AL-FALAHI, M.D.A.; NGUYEN, H.D.; JAYASINGHE, S.D.G.; MAHMOUD, T.S.; NEGNAVITSKY, M. 2018. Grey Wolf Optimization-Based Optimum Energy-Management and Battery-Sizing Method for Grid-Connected Microgrids.. *Energies,* 11**,** 847.

O' SULLIVAN, K., MURPHY, J. & O' SULLIVAN, D. Power Output Performance and Smoothing Ability of an Oscillating Water Column Array Wave Energy Converter. 32nd International Conference on Ocean, Offshore and Arctic Engineering OMAE2013, 2013 Nantes, France. The American Society of Mechanical Engineers.

O'SULLIVAN, D. L. & LEWIS, A. W. 2011. Generator Selection and Comparative Performance in Offshore Oscillating Water Column Ocean Wave Energy Converters. *IEEE TRANSACTIONS ON ENERGY CONVERSION,* 26.

OCEANLINX. 2017. *Oceanlinx* [Online]. Australia: Oceanlinx. Available: http://www.oceanlinx.com/ [Accessed 27/03 2017].

PARVEZ, M., MEKHILEF, F., TAN, M. L. N. & AKAGI, H. 2016. A Robust Modified Model Predictive Control (MMPC) Based on Lyapunov Function for ThreePhase Active-Front-End (AFE) Rectifier.

PARVEZ, M., TAN, N. M. L. & AKAGI, H. 2015. An Improved Active-Front-End Rectifier Using Model Predictive Control. *IEEE Applied Power Electronics Conference and Exposition (APEC).*

PERAERO TURBINE DESIGN LLC. 2017. Turbine design report for Wave Swell Energy Ltd.

PIROOZ, A. & NOROOZIAN, R. 2016. Model Predictive Control of Classic Bidirectional DC-DC Converter for Battery Applications. *7th Power Electronics, Drive Systems & Technologies Conference (PEDSTC 2016).* Iran University of Science and Technology, Tehran, Iran: IEEE.

QUEVEDO, D. E., AGUILERA, R. P., P´EREZ, M. A , CORT´ES, P. & LIZANA, R. 2012. Model Predictive Control of an AFE Rectifier With Dynamic References. *IEEE Transactions on Power Electronics,* 7**,** 3128 - 3136.

RAHMOUN, A. & BIECHL, H. 2012. Modelling of Li-ion batteries using equivalent circuit diagrams. *PRZEGLĄD ELEKTROTECHNICZNY (Electrical Review),* 152-156.

RAJAPAKSE, G., JAYASINGHE, S. G. & FLEMING, A. Power Management of an Oscillating Water Column Wave Energy Converter with Battery/Supercapacitor Hybrid Energy Storage. 2018 8th International Conference on Power and Energy Systems (ICPES), 2018a Colombo, Sri Lanka. IEEE.

RAJAPAKSE, G., JAYASINGHE, S. G., FLEMING, A. & NEGNEVITSKY, M. 2018b. Model Predictive Control for Electrical Power Converters of a Grid Integrated Oscillating Water Column with Energy Storage. *Energies Special Issue "wave and Tidal Energy",* 11.

RAJAPAKSE, G., JAYASINGHE, S. G., FLEMING, A. & SHAHNIA, F. Model Predictive Control-based Power take-off Control of an Oscillating Water Column Wave Energy Conversion System. 2017 International Conference on Substantial Energy Engineering (ICSEE 2017), 2017a Perth, Australia. IOP science.

RAJAPAKSE, G., JAYASINGHE, S. G., NEGNEVITSKY, M. & FLEMING, A. 2017b. A Model Predictive Control-Based Power Converter System for Oscillating Water Column Wave Energy Converters. *Energies Special Issue "Marine Energy",* 10.

RODRIGUEZ, J. & CORT´ES, P. 2012. *Predictive Control Of Power Converters and Electrical Drives,* A John Wiley & Sons Ltd.

RODRIGUEZ, J., KAZMIERKOWSKI, M. P., ESPINOZA, J. R., ZANCHETTA, P., ABU-RUB, H., YOUNG, H. A. & ROJAS, C. A. 2013. State of the Art of Finite Control Set Model Predictive Control in Power Electronics. *IEEE Transactions on Industrial Informatics,* 9**,** 1003-1016.

ROY, A., AUGER, F., DUPRIEZ-ROBIN, F , BOURGUET, S. & TRAN, Q. T. 2018. Electrical Power Supply of Remote Maritime Areas: A Review of Hybrid Systems Based on Marine Renewable Energies. *Energies,* 11.

SAMOSIR, A. S. & YATIM, A. H. M. 2010. Implementation of Dynamic Evolution Control of Bidirectional DC–DC Converter for Interfacing Ultracapacitor Energy Storage to Fuel-Cell System. *IEEE Transactions on Industrial Electronics,* 57**,** 3468-3473.

SETOGUCHI, T., SANTHAKUMAR, S., MAEDA, H. & KANEKO, K. 2001. A review of impulse turbines for wave energy conversion. *Renewable Energy,* 23**,** 261–292.

STEGMAN, A., DE ANDRES, A., JEFFREY, H., JOHANNING, L. & BRADLEY, S. 2017. Exploring Marine Energy Potential in the UK Using a Whole Systems Modelling Approach. *Energies,* 10(9).

SULTANA, W. R., SAHOO, S. K , SUKCHAI, S., YAMUNA, S. & VENKATESH, D. 2017. A review on state of art development of model predictive control for renewable energy applications. *Renewable and Sustainable Energy Reviews,* 76**,** 391–406.

TAKAO, M. & SETOGUCHI, T. 2012. Review Article Air Turbines forWave Energy Conversion. *International Journal ofRotating Machinery*.

TANG, X., SUN, Y., ZHOU, G. & MIAO, F. 2017. Coordinated Control of Multi-Type Energy Storage for Wind Power Fluctuation Suppression. *Energies,* 10.

TARISCIOTTI, L., ZANCHETTA, P., WATSON, A., CLARE, J. C., DEGANO, M. & BIFARETTI, S. 2015. Modulated Model Predictive Control for a Three-Phase Active Rectifier. *IEEE Transactions on Industry Applications,* 51**,** 1610-1620.

TASNETWORKS 2016. TasNetworks Annual Planning Report 2016. Australia: Tasmanian Networks Pty Ltd (TasNetworks).

TEDESCHI, E., CARRARO, M., MOLINAS, M. & MATTAVELLI, P. 2011. Effect of Control Strategies and Power Take-Off Efficiency on the Power Capture From Sea Waves. *IEEE Transactions on Energy Conversion,* 26**,** 1088 - 1098.

TEXAS INSTRUMENTS 2017. TMS320F2837xS Delfino™ Microcontrollers. *In* TEXAS INSTRUMENTS (ed.) SPRS881D – AUGUST 2014–REVISED JULY 2017 ed.

THIRUGNANAM, K., JOY, E. R. T. P., SINGH, M. & KUMAR, P. 2014. Mathematical Modeling of Li-Ion Battery Using Genetic Algorithm Approach for V2G Applications. *IEEE Transactions on Energy Conversion,* 29**,** 332-343.

THOUNTHONG, P., SIKKABUT, S., MUNGPORN, P., MOBARAKEH, N., PIERFEDERICI, S. & DAVAT, B. 2014. Nonlinear Control Algorithm of Supercapacitor/Li-Ion Battery Energy Storage Devices for Fuel Cell Vehicle Applications. *Mecatronics-2014.* Tokyo, Japan: IEEE.

VAZQUEZ, S., LEON, J. I., FRANQUELO, L. G., RODRIGUEZ, J., YOUNG, H. A., MARQUEZ AND, A. & ZANCHETTA, P. 2014. Model Predictive Control: A Review of Its Applications in Power Electronics. *IEEE Industrial Electronics Magazine.* IEEE.

VICINANZA, D., DI LAURO, E., CONTESTABILE, P., GISONNI, C., LARA, J. L. & LOSADA, I. J. 2019. Review of innovative harbor breakwaters for wave-energy conversion. *Journal of Waterway, Port, Coastal, and Ocean Engineering, (American Society of Civil Engineers),* 145.

VILATHGAMUWA, M., NAYANASIRI, D. & GAMINI, S. 2015. *Power Electronics for Photovoltaic Power Systems,* Morgan & Claypool Publishers.

WAVE SWELL ENERGY. 2017. *Sustainable elecricity from the ocean* [Online]. Australia: Wave Swell Energy, Australia. Available: http://waveswellenergy.com.au/ [Accessed 27/03 2017].

WU, F., ZHANG, X. & JU, P. Application of the battery energy storage in wave energy conversion system. International Conference on Sustainable Generation and supply (SUPERGEN'09), 1-4 April 2009 Nanjing, China.

WU, Q., XU, Z. & ØSTERGAARD, J. 2010. Grid Integration Issues for Large Scale Wind Power Plants (WPPs). *Power and Energy Society General Meeting (IEEE PES GM 2010).* Providence, RI, USA: IEEE Conference Publications.

XIE, L. B. & TANG, T. H. 2012. Modeling and Control of a Small Marine Current Power Generation System. *2012 IEEE International Symposium on Industrial Electronics (Isie),* 1438-1443.

YARAMASU, V. N. R. 2014. *Predictive control of Multilevel Converters for MegaWatt Wind Energy Conversion Systems.* Doctor of Philosophy, Ryerson University.

ZHANG, L , PENG, H., NING, Z., MU, Z. & SUN, C. 2017. Comparative Research on RC Equivalent Circuit Models for Lithium-Ion Batteries of Electric Vehicles. *Applied Science, MDPI,* 7.

ZHI, L , PENG, Z., ZHIFU, W., QIANG, S. & YINAN, R. State of charge estimation for Li-ion battery based on extended Kalman filter. The 8th International Conference on Applied Energy – ICAE2016 2017. Energy Procedia, Elsevier Ltd, 3515 – 3520.

ZOU, Y. & CHENG, K. W. E. 2017. A Vertical Flux-Switching Permanent Magnet Based Oscillating Wave Power Generator with Energy Storage. *Energies,* 10 (7).

ZUBIETA, L. & BONERT, R. 2000. Characterization of Double-Layer Capacitors for Power Electronics Applications. *IEEE Transactions on Industry Applications,* 36**,** 199-205.

APPENDIX I:
SIMULATION SETUP

This appendix describes the MATLAB/Simulink models used in Chapters 2, 3, 4, 6 and 7 to obtain simulation results to confirm the validity of proposed control algorithms. In these models the air-turbine, PMSG and dc-link are common to all. Apart from that all other blocks, e.g. the machine side filter, AFE rectifier, 2L-VSI, grid side filter, dc-dc bidirectional converters, etc. are modelled.

AI.1 Air-Turbine

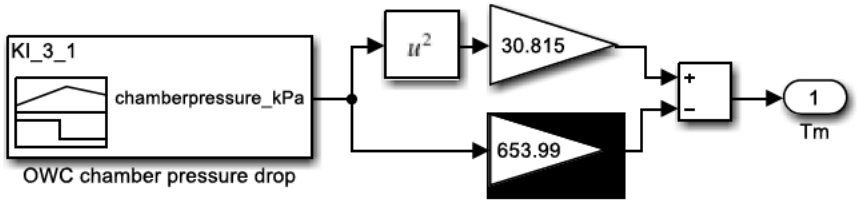

Figure AI. 1: Air-turbine model in Simulink (Chapter 2, 3 and 4)

AI.1 PMSG

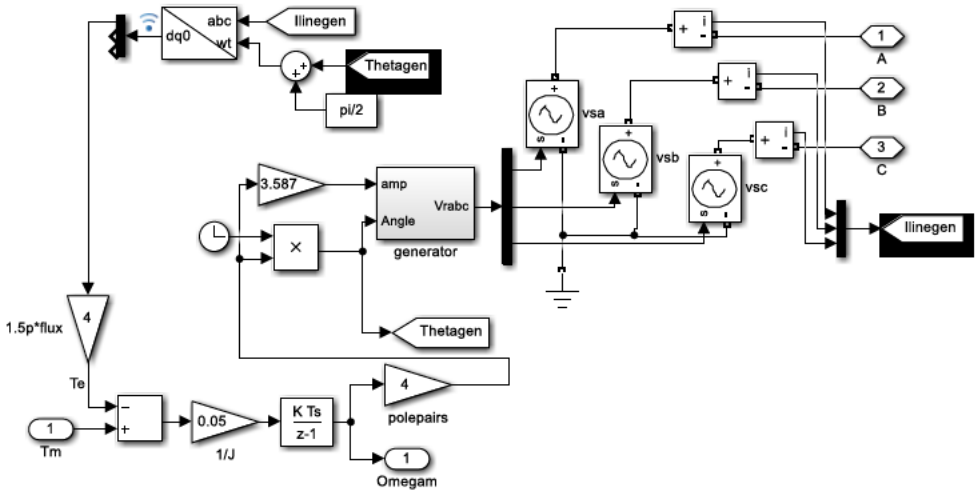

Figure AI. 2: PMSG model in Simulink

AI.3 AFE rectifier, dc-link, 2L-VSI, dc-dc converters, and filters

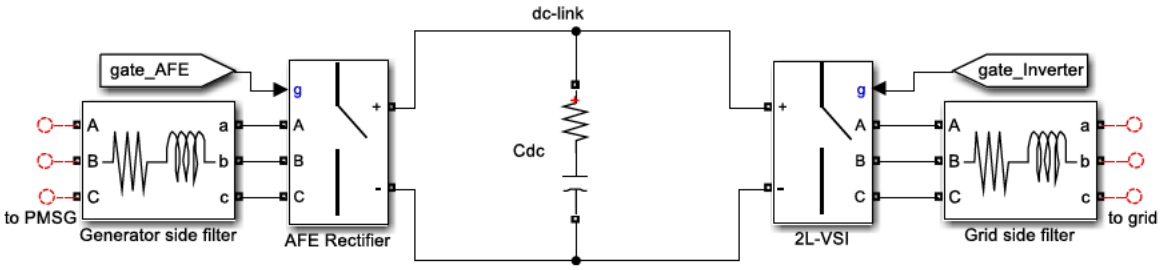

Figure AI. 3. 1: Power converters, filters and dc-link models in Simulink

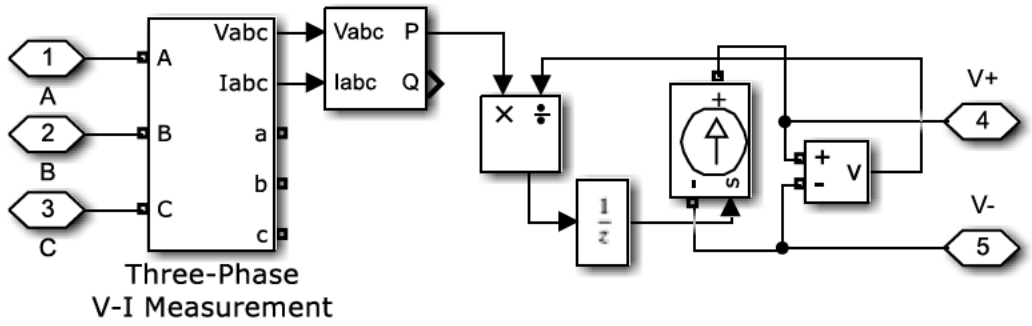

Figure AI. 3. 2: AC/DC converter model in Simulink (Chapter 6 and 7)

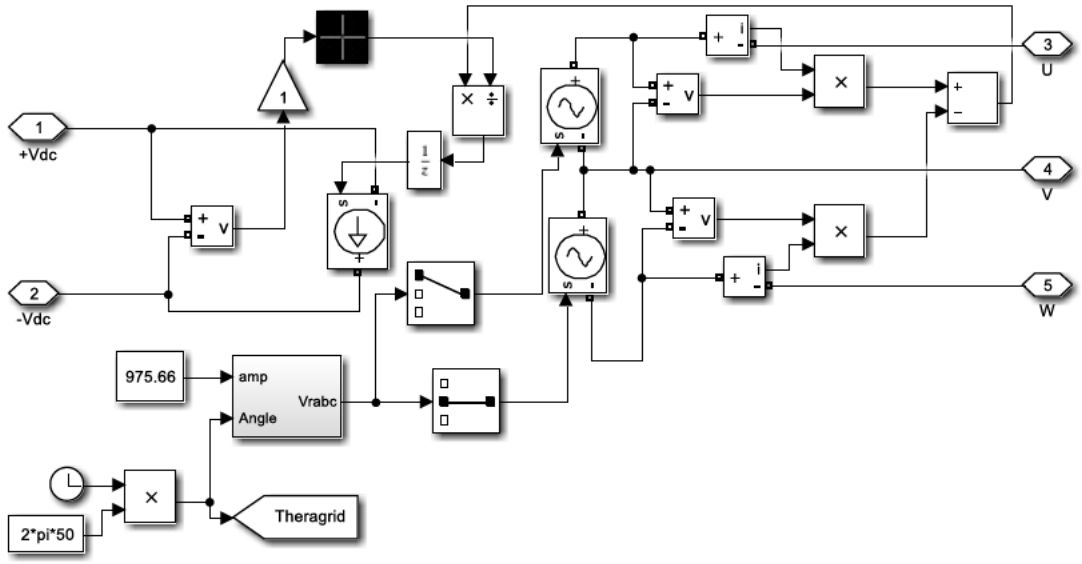

Figure AI. 3. 3: DC/AC converter model in Simulink (Chapter 6 and 7)

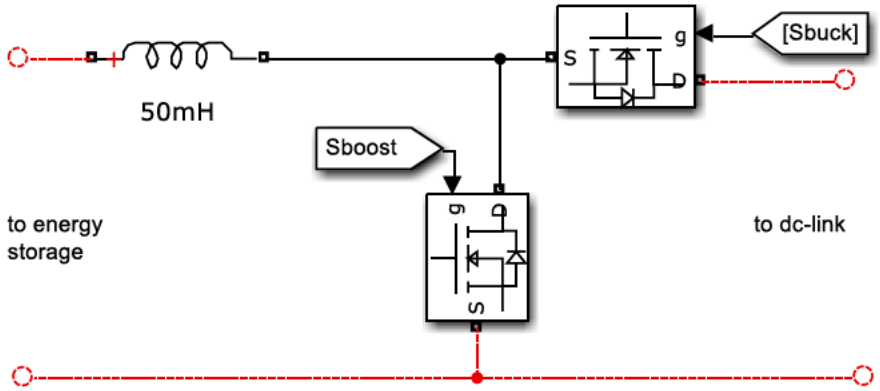

Figure AI. 3. 4: DC/DC converter model in Simulink

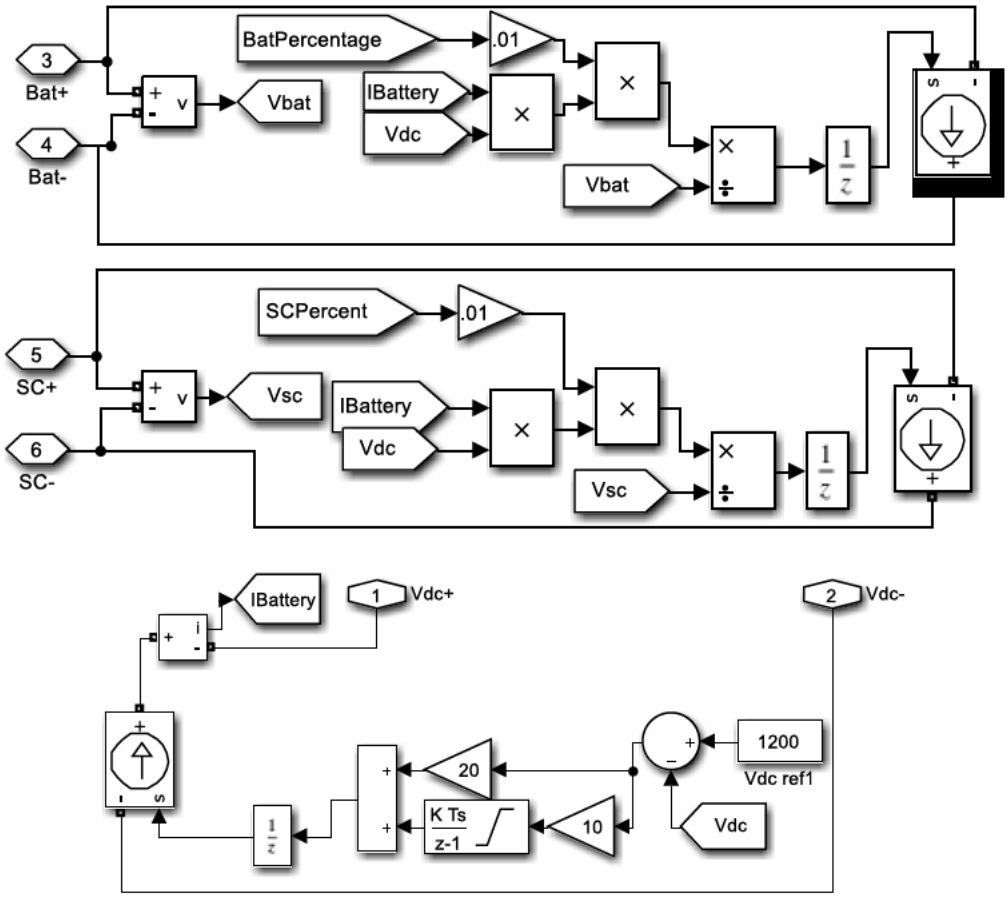

Figure AI. 3. 5: DC/DC converter model in Simulink (Chapter 6 and 7)

AI.4 Power grid

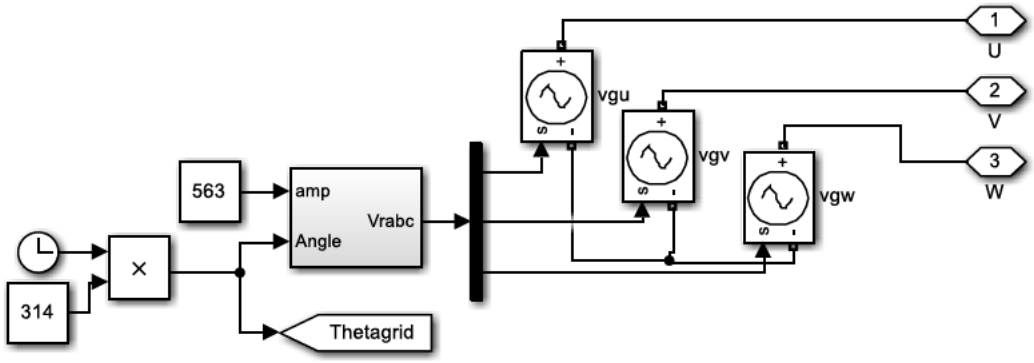

Figure AI. 4. 1: Power grid model in Simulink

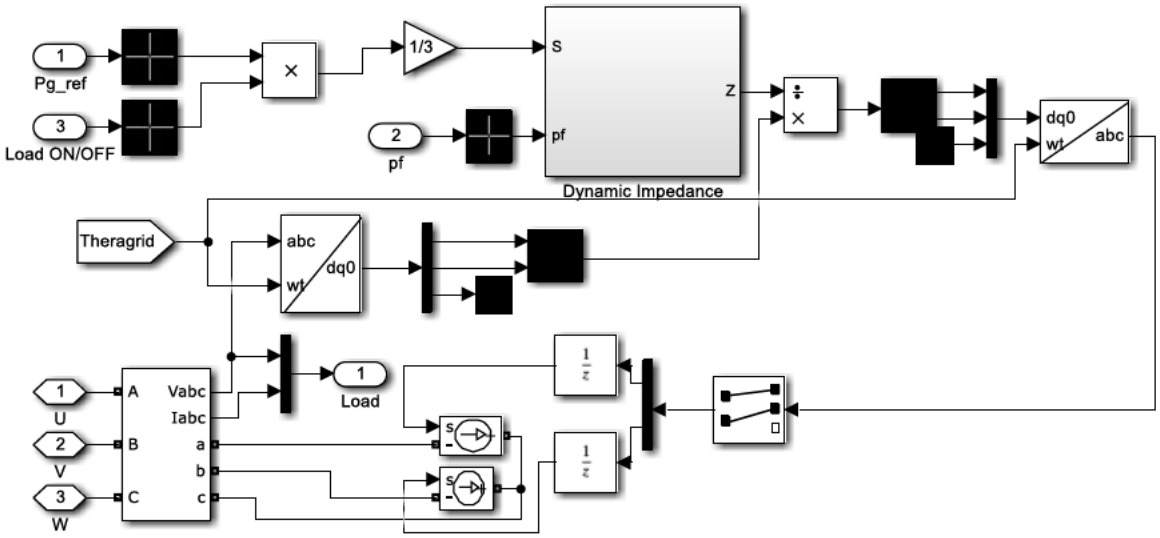

Figure AI. 4. 2: Power grid model in Simulink (Chapter 6 and 7)

APPENDIX II:
SYSTEM PARAMETERS AND FCS-MPCS USED IN CHAPTER 4

AII. 1 System parameters used in the design

Table II. 1: System parameters used in chapter 4 design

PMSG	
Rated Power	2MW
Rated rotate speed	650 rpm
Rated Voltage	690VAC
Rated current	1673.5A
Number of pole pairs	4
Resistance (R_s)	0.0024Ω
Inductances ($L_d = L_q$)	0.3552mH(line-phase)
Magnetic flux (Ψ_{pm})(0.119Wb X 6)	0.666Wb
Inertia (J)	20kgm^2
Grid side Filter	
Inductance	2mH
Resistance	0.01Ω
Rated charge/ discharge currents	1500A
Grid	
Voltage	690Vrms
Frequency	50Hz

Generator side Filter	
Inductance	1mH
Resistance	0.01 Ω
dc-link	
dc-link voltage (V_{dc})	1200V
dc-link current (I_{dc_max})	1000A
dc-link capacitor (C_{dc})	2.2mF
Supercapacitor	
Capacitance (C_{sc}) (83F; 21 in series; 4 parallel loop)	15.8F
Resistance (R_{sc})	52.5mΩ
Voltage Initial ($V_{initial}$) ($C_{sc\_nominal}$ 48V each)	900V
Reference Values	
Active Power	265kW
Reactive Power	0
Other	
Sample time (seconds) (Rec./Inv./bidirectional)	10^{-4} / 10^{-4} / $7x10^{-5}$
Simulator run time	20 seconds

AII. 2 FCS – MPC for Rectifier

```
function [Sa,Sb,Sc] = fcn(vdc, is, vs, Theta, omega, Torque)
% Sa,Sb,Sc: Switching signals for the rectifier; vdc: dc-link voltage; is: PMSG current;
vS: PMSG phase voltage; Theta: angle of the reference frame (rad/sec); omega: PMSG
rotational speed (rad/sec); Torque: air-turbine torque.
Ts = 1e-4; % Sample time [s]
% Load parameters
Rs = 0.01;      % Stator Resistance + generator side filter resistance [Ohm]
Ls = 1e-3;      % stator Inductance + Generator side filter inductance [H]
np =4;   %pole pairs
flux=0.66;      % PMSG flux
J=2;            % inertia
Omega_ref=68;           % 68 rad/sec
K = 2e-4;           % constant
id_ref = 0;

% Switching states
states = [0 0 0;1 0 0;1 1 0;0 1 0;0 1 1;0 0 1;1 0 1;1 1 1];
states2 = [0 0 0;2 -1 -1;1 1 -2;-1 2 -1;-2 1 1;-1 -1 2;1 -2 1;0 0 0];
vAFE = vdc*states2/3;
% is is derived from phase currents ia, ib and ic
%ia (k+1) = ik1a
%ib (k+1) = ik1b
%ic (k+1) = ik1c

g_opt = 1e10;
x_opt = 1;

for i = 1:8
    % Current prediction at instant k+1
    ik1a = (1 - Rs* Ts /Ls)*is(1) - Ts /Ls*( vAFE (i,1)-vs(1));
    ik1b = (1 - Rs* Ts /Ls)*is (2) - Ts /Ls*( vAFE (i,2)-vs (2));
```

```
    ik1c = (1 - Rs* Ts /Ls)*is(3) - Ts /Ls*( vAFE (i,3)-vs (3));
  % abc to dq conversion
  idk1 =2*(ik1a*sin(Theta)+ik1b*sin(Theta-2*pi/3)+ik1c*sin(Theta+2*pi/3))/3;
  iqk1 =2*(ik1a*cos(Theta)+ik1b*cos(Theta-2*pi/3)+ik1c*cos(Theta+2*pi/3))/3;

   Te = 1.5*flux* np*iqk1;  % Predicted torque
   omegak1 = omega + Ts *(Torque - Te)/J;  % Predicted speed
   g = abs(Omega_ref - omegak1)+ K*abs(id_ref - idk1);      % Cost function
    if (g<g_opt)    % Minimize cost function
      g_opt = g;
     x_opt = i;
    end
end
% Output switching states
Sa = states(x_opt,1);
Sb = states(x_opt,2);
Sc = states(x_opt,3);
```

AII. 3 FCS – MPC for Inverter

```
function [Su,Sv,Sw] = fcn(vdc, Pref, ig, vg)
% Su,Sv,Sw: Switching signals for the inverter; Pref: Active and reactive power
reference; vdc: dc-link voltage; ig: grid current;  vS: grid phase voltage.
Ts = 1e-4; % Sample time [s]
% Load parameters
Rg = 0.01;      % grid side filter Resistance [Ohm]
Lg = 1e-3;      % grid side filter Inductance [H]

% Voltage vectors
v0 = 0 + 1j*0;
v1 = 2/3*vdc + 1j*0;
v2 = 1/3*vdc + 1j*sqrt(3)/3*vdc;
v3 = -1/3*vdc + 1j*sqrt(3)/3*vdc;
```

```
v4 = -2/3*vdc + 1j*0;
v5 = -1/3*vdc - 1j*sqrt(3)/3*vdc;
v6 = 1/3*vdc - 1j*sqrt(3)/3*vdc;
v7 = 0 + 1j*0;
v = [v0 v1 v2 v3 v4 v5 v6 v7];
% Switching states
states = [0 0 0;1 0 0;1 1 0;0 1 0;0 1 1;0 0 1;1 0 1;1 1 1];

g_opt = 1e10;
x_opt = 1;

% Read power reference inputs at sampling instant k
Pkref = Pref(1) + 1j*Pref(2);
Pref(1) = 260e3;      % grid active power reference [w]
Pref(2)= 0;      % grid reactive power reference

% Read current and voltage measurements at sampling instant k
ik = (0.8165*(ig(1)- ig(2)/2 - i g(3)/2)) + 1j*(0.7071*(ig(2) – ig(3)));
vk = (0.8165*(vg(1)- vg(2)/2 - vg(3)/2)) + 1j*(0.7071*(vg(2) - vg(3)));

for i = 1:8
    % Current and power prediction at instant k+1
     ik1 = (1 - Rg* Ts /Lg)*ik + Ts /Lg*(v(i)- vk);
     Pk1 = (real(vk)*real(ik1) + imag(vk)*imag(ik1)) + 1j*(imag(vk)*real(ik1) -
real(vk)*imag(ik1));

     % Cost function
   g = (abs(real(Pkref - Pk1)))*(abs(real(Pkref - Pk1))) + (abs(imag(Pkref -
Pk1)))*(abs(imag(Pkref - Pk1)));

   % Selection of the optimal value
    if (g<g_opt)
```

```
        g_opt = g;
       x_opt = i;
    end
end
% Output switching states
Su = states(x_opt,1);
Sv = states(x_opt,2);
Sw = states(x_opt,3);
```

AII. 4 FCS – MPC for dc-dc bidirectional converter of energy storage

```
function [S1, S2]  = fcn(vdc, vESS, iL, vdcref, PPMSG, Pg)
% S1: buck switching; S2: Boost switching; vdc: dc-link voltage; vESS: energy storage system voltage; iL: inductor current; vdcref: dc-link reference (1200V); PPMSG: air-turbine generator power; Pgrid: grid power.
Ts = 1e-5;        % Sample time [s]
L = 5e-4;      % Inductance [H]
vdcref = 1200; % dc-link voltage reference [V]

g_opt = 1e10;
x_opt1 = 0;
x_opt2 = 0;

%Boost converter
 if (vdc < vdcref)    % Energy deficit condition. Boost converter should be selected
    iLref = ((Pg -PPMSG)+(vdcref-vdc)*100)/vESS;  % Inductor current reference.  '100' is an arbitrary gain to speed up.
   for i = 0:1
iLk1 = iL + (vESS + ((i-1)*vdc))* Ts /L; %Predicted inductor current
      g =abs(iLref-iLk1);              %Cost function for the boost converter
          if (g<g_opt)                %Search for the switching state which minimizes the cost function
              g_opt = g;
```

```
            x_opt1 = i;
            x_opt2 = 0;
          end
  end
end

 %Buck converter
 if (vdc > vdcref)                    % Energy excess condition. Buck converter should
be selected
iLref = ((Pg -PPMSG)+(vdcref-vdc)*100)/vESS;      % Inductor current reference. '100' is an
arbitrary gain to speed up.
   for i = 0:1
       iLk1 = iL - (i*vdc – vESS)* Ts /L;     %Inductor current prediction
       g =abs(iLref-iLk1);              %Cost function for the buck converter
          if (g<g_opt)                %Search for the switching state which minimizes the
cost function
             g_opt = g;
             x_opt1 = 0;
             x_opt2 = i;
          end
  end
end

% Set output signals
S1 = x_opt2;
S2 = x_opt1;
```